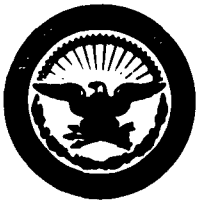

61-416

ELECTROSTATIC GENERATORS
(SELECTED PARTS)

295443

UNEDITED ROUGH DRAFT TRANSLATION

ELECTROSTATIC GENERATORS (SELECTED PARTS)

English Pages: 131

SOV/2746

THIS TRANSLATION IS A RENDITION OF THE ORIGINAL FOREIGN TEXT WITHOUT ANY ANALYTICAL OR EDITORIAL COMMENT. STATEMENTS OR THEORIES ADVOCATED OR IMPLIED ARE THOSE OF THE SOURCE AND DO NOT NECESSARILY REFLECT THE POSITION OR OPINION OF THE FOREIGN TECHNOLOGY DIVISION.	PREPARED BY: TRANSLATION SERVICES BRANCH FOREIGN TECHNOLOGY DIVISION WP-AFB, OHIO.

Fiziko-Tekhnicheskiy Institut
Akademii Nauk USSR

ELEKTROSTATICHESKIYE GENERATORY

Izdatel'stvo Glavnogo Upravleniya Po Ispol'zovaniyu
Atomnoy Energii Pri Sovete Ministrov SSSR
Moskva - 1959

Pages: 15-22
32-45
56-89
113-182

FTD-TT-61-416/1+2

TABLE OF CONTENTS

FORMATION OF A BEAM OF NEGATIVE HYDROGEN IONS BY RECHARGING OF POSITIVE IONS IN THE CATHODE CHANNEL OF A HIGH-FREQUENCY SOURCE

By A.G. Koval', L.I. Krupnik, A.D. Timofeyev, and Ya.M. Fogel'

INTRODUCTION

Reference [1] described a source of negative hydrogen ions based on the production of a beam of negative ions by recharging positive ions in a gas passing through a channel in the cathode of a high-frequency source. This method of producing negative ions represents a variety of the recently applied method of transforming a beam of positive ions into negative ions by passing them through a layer of matter known as a target [2, 3]. The current in the negative-ion beam depends on the number and energy of the positive ions striking the target, as well as on the thickness and atomic species of the target in which the transformation process takes place. The result is that for selection of the optimum operating conditions for a source based on the above method, it is desirable to have independent control firstly over the operation of the high-frequency source in order to obtain the highest possible positive-ion current, which requires selecting a definite pressure in the source tank and a definite extraction voltage, and, secondly, to find a target material and thickness that will give the highest possible $H^+ \rightarrow H^-$ transformation ratio, i.e., if the target is gaseous, to select the species of gas and its pressure in the target chamber. In the case of nega-

tive-ion formation in the channel of a high-frequency source, the transformation of the ions goes in the direction of gas molecules which flow from the source through the channel. As a result, the gas pressures in the source and in the target are found to be mutually dependent, and only the gas used in the source tank can be used as a target material.

The energy of the ions passing through the channel is determined by the extracting potential difference applied between the source anode and cathode.

A shortcoming of this method consists in the fact that the optimum conditions for producing the highest positive-ion current and the maximum transformation ratio in the gaseous target do not coincide; this limits the negative-ion current that can be obtained by this method (in Reference [1], a H_1^--ion current of 2.2 μamp was obtained). In References [2] and [3], therefore, the positive-ion source and the target chamber were spatially separated, and the gas was fed independently into the target chamber. Considering the simplicity of the method for producing negative ions proposed in Reference [1] and the small dimensions of the source based on this method, it is desirable to evaluate the possibilities of this source from the viewpoint of producing the highest possible negative-hydrogen current, as well as to compute the optimum conditions for its operation. Such an evaluation has become possible due to recently conducted measurements of the effective capture sections and electron losses of the hydrogen particles when they collide with hydrogen molecules, inasmuch as these sections determine the composition of the hydrogen beam that has passed through the target.

COMPUTATION OF THE NUMBER OF NEGATIVE HYDROGEN IONS IN A BEAM THAT HAS PASSED THROUGH A CHANNEL IN THE CATHODE OF A HIGH-FREQUENCY SOURCE

Let us denote by I_0^+ the current of positive ions that enters the channel of the high-frequency source, and by I^+ and I^- the currents of positive and negative ions in the beam that has emerged from the channel. The quantity I_0^+ depends on $\underline{p}$, the gas pressure in the source, on U_v, the extracting potential difference, and on a number of other parameters that determine the geometry of the ion-beam scavenging system, as well as on the power absorbed by the high-frequency discharge, and so forth. All of these parameters with the exception of $\underline{p}$ and U_v will henceforth be regarded as nonvarying.

The quantities I^+ and I^- depend on I_0^+, on the target thickness nL ($\underline{n}$ is the number of atoms in 1 cm^3; L is the channel length), the target being a gas flowing through the channel, on the energy E of the beam entering the channel, and on the geometrical characteristics of the channel, i.e., on its diameter D and length L.

In work with ion sources, we usually measure I_2^+, U_v, and Q (the gas flow into the source tank). It should henceforth be borne in mind that the energy of the ions entering the channel is determined by the relationship

$$E = eU_v, \tag{1}$$

while the target thickness nL is given by the relationship

$$nL = \frac{Q(1{,}61\,L + 2{,}14\,D)}{3{,}45 \cdot 10^3 D^2} \frac{L}{2kT}. \tag{2}$$

It is assumed in the derivation of Formula (2) that a linear decline in pressure prevails in the channel, from the value $\underline{p}$ at the entry into the channel to zero at the exit from it.

The quantities I^+ and I^- can be determined by the formulas

$$I^+ = I_0^+ \frac{I^+}{I_0^+}, \tag{3a}$$

$$I^- = I_0^+ \frac{I_0^-}{I_0^+}. \qquad (3b)$$

As will be seen from Formula (3b), the quantity I^- is determined by two factors, of which the first, I^+, depends only on the properties of the source, while the second, I^-/I_0^+, which is the relative content of negative ions in the beam leaving the channel, depends only on the properties of the target and the energy of the beam. As will be seen from Formulas (1) and (2), however, the parameters U_v and Q, on which I_0^+ depends, simultaneously determine the quantities E and nL, on which the quantity I^-/I_0^+ depends.

This circumstance, which was noted earlier, prevents us from regulating the quantities I_0^+ and I^-/I_0^+ independently.

Excluding the quantity I_0^+ from Formulas (3a) and (3b), we obtain the following formula for the quantity I^-:

$$I^- = I^+ \frac{\frac{I_0^-}{I_0^+}}{\frac{I_0^-}{I_0^+}} \qquad (4)$$

The quantity I^+, which is determined directly by experiment, and the quantities I^+/I_0^+ and I^-/I_0^+, which can be computed if we know the effective capture sections and electron losses that determine the composition of the hydrogen beam, appear in Formula (4).

As we know, the composition of a hydrogen beam that has traversed a layer of matter with a thickness nL is described [4] by the following differential equations:

$$\frac{dI^+}{d(nL)} = -(\sigma_{10} + \sigma_{1-1})I^+ + \sigma_{01}I^0 + \sigma_{-11}I^-, \qquad (5a)$$

$$\frac{dI^0}{d(nL)} = \sigma_{10}I^+ - (\sigma_{01} + \sigma_{0-1})I^0 + \sigma_{-10}I^-, \qquad (5b)$$

$$\frac{dI^-}{d(nL)} = \sigma_{1-1}I^+ + \sigma_{0-1}I^0 - (\sigma_{-11} + \sigma_{-10})I^-, \qquad (5c)$$

where σ_{ik} is the effective section for transition of particles from charge state "ie" to charge state "ke."

Solution of Eqs. (5) gives the following formulas for the quantities of interest to us, I^+/I_0^+ and I^-/I_0^+:

$$\frac{I^-}{I_0^+} = \frac{1}{\beta}\left(a_0 + a_1 e^{r_1 nL} + a_2 e^{r_2 nL}\right), \tag{6a}$$

$$\frac{I^+}{I_0^+} = \frac{1}{\beta}\left(b_0 + b_1 e^{r_1 nL} + b_2 e^{r_2 nL}\right), \tag{6b}$$

where

$$r_{1,2} = \frac{-\alpha \pm \sqrt{\alpha^2 - 4\beta}}{2};\quad \alpha = \sigma_{10} + \sigma_{01} + \sigma_{0-1} + \sigma_{-10}\sigma_{1-1} + \sigma_{-11};$$

$$\beta = (\sigma_{01} + \sigma_{10} + \sigma_{11})(\sigma_{01} + \sigma_{-10} + \sigma_{-11}) - (\sigma_{01} + \sigma_{-11})(\sigma_{0-1} - \sigma_{1-1});$$

$$a_0 = \sigma_{10}\sigma_{0-1} + \sigma_{1-1}\sigma_{01} + \sigma_{1-1} + \sigma_{0-1};$$

$$a_1 = \frac{r_2}{r_1 - r_2}(\sigma_{1-1}r_1 + a_0);\quad a_2 = \frac{r_1}{r_2 - r_1}(\sigma_{1-1}r_2 + a_0);$$

$$b_0 = \sigma_{01} - \sigma_{-10} + \sigma_{-11}\sigma_{01} + \sigma_{-11}\sigma_{01};$$

$$b_1 = \frac{r_2}{r_1 - r_2}[b_0 - \beta - r_1(\sigma_{10} + \sigma_{1-1})];$$

$$b_2 = \frac{r_1}{r_2 - r_1}[b_0 - \beta - r_2(\sigma_{10} + \sigma_{1-1})].$$

To compute the ratios I^+/I_0^+ and I^-/I_0^+ for different target-thickness values, we employed the values available in the literature for all sections σ_{ik}. These values are listed in Table 1 for ion energies of 4 and 6 kev.

TABLE 1

Values of Section σ_{ik} for Ion Energies of 4 and 6 kev

σ_{ik}	1) Значение сечения, см², при 2) E = 4 кэв	3) E = 6 кэв	4) Литературный источник
σ_{1-1}	$1{,}3\cdot10^{-18}$	$3{,}4\cdot10^{-18}$	[8]
σ_{10}	$7{,}4\cdot10^{-16}$	$8\cdot10^{-16}$	[5]
σ_{0-1}	$1{,}41\cdot10^{-17}$	$1{,}7\cdot10^{-17}$	[11]
σ_{01}	$3{,}4\cdot10^{-17}$	$4{,}35\cdot10^{-17}$	[11]
σ_{-10}	$1{,}26\cdot10^{-15}$	$1{,}31\cdot10^{-15}$	[6]
σ_{-11}	$3{,}76\cdot10^{-17}$	$4{,}05\cdot10^{-17}$	[7]

1) Section in cm^2 for; 2) E = 4 kev; 3) E = 6 kev; 4) literature source.

Substituting the section values from the table in Eqs. (6a) and (6b), we compute the ratios I^+/I_0^+ and I^-/I_0^+ for various target thicknesses.

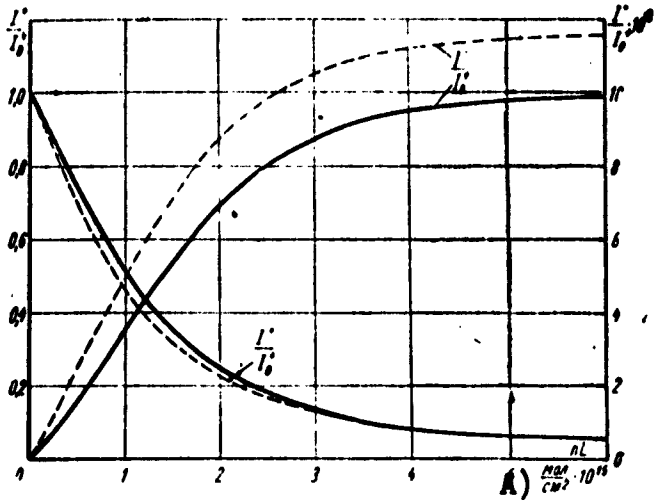

Fig. 1. Ratios I^+/I_0^+ and I^-/I_0^+ as functions of target thickness; – – – E = = 6 kev; ——— E = 4 kev. A) Mol/cm^2.

Figure 1 presents curves of the ratios I^+/I_0^+ and I^-/I_0^+ as functions of target thickness for ion energies of 4 and 6 kev.

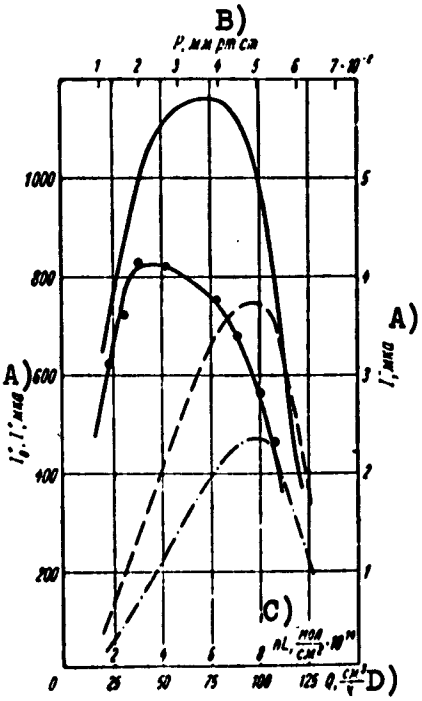

Fig. 2. Relationships I^+, I_0^+, and $I^- = f(Q)$ for a Reifenschweiler high-frequency source: . . . $I^+ = f(Q)$; ——— $I_0^+ = f(Q)$; – · – · – $I^- = f(Q)$ for $E = 4$ kev; – – – $I^- = f(Q)$, $E = 6$ kev.

A) μamp; B) mm Hg; C) nL mol/cm^2.10^{14}; D) cm^3/hr.

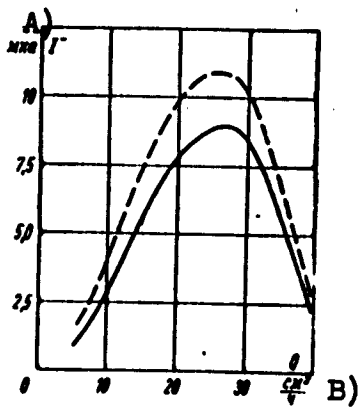

Fig. 3. Relationship $I^- = f(Q)$ for ion energies of 4 and 6 kev and L = 40 mm: – – – E = 6 kev; ——— E = 4 kev. A) μamp; B) cm^3/hr.

To compute the current I^- in the beam leaving the channel, it is necessary to know, in addition to the computed values of I^+/I_0^+ and I^-/I_0^+, the value of I^+.

We made a detailed study of the quantity I^+ as a function of various parameters, including the quantities U_v and Q [9].

Figure 2 shows the relationship $I^+ = f(Q)$ as obtained for a Reifenschweiler high-frequency source [10]. The measurements were made with the optimal $U_v = 4$ kev and the channel parameters D = 2.3 mm and L = 10 mm. Applying Formulas (3a) and (4), we computed values of I_0^+ and I^- for various values of Q and plotted the corresponding curves of $I_0^+ = f(Q)$ and $I^- = f(Q)$ in Fig. 2. As will be seen from Fig. 2, the maximum negative-ion-current value does not exceed 2.5 μamp and is attained at Q = 100 cm^3/hr, i.e., at a flow rate that is not optimal for the quantity I_0^+. A somewhat larger negative-ion current may be obtained by applying a 6-kev extracting voltage to the source. The curve of the relationship $I^- = f(Q)$ for an ion energy of 6 kev is plotted with a broken line on Fig. 2. In computing the value of I^- for this curve, it was assumed that the relationship $I^+ = f(Q)$ for $U_v = 6$ kev is the same as the corresponding relationship for $U_v = 4$ kev.

The relatively low value of the negative-ion current in the beam emerging from the channel of the high-frequency source is the result of the fact that the calculation was carried out for a short channel with L = 10 mm, as is ordinarily used in high-frequency sources. Use of the short channel has as its consequence that at the flow rates that are optimal from the viewpoint of obtaining a large I_0^+, the value of nL for the channel is found to be small, and we find ourselves at the very beginning of the curve of $I^-/I_0^+ = f(nL)$, where the quantity I^-/I_0^+ is still far from its maximum, which is obtained at large values of nL. It is clear from these considerations that we may hope to obtain large negative-ion currents by the use of long channels in the cathode of the high-frequency source.

We computed the relationship $I^- = f(Q)$ for a channel with L = = 40 mm; in this calculation, it was assumed that the relationship $I_0^+ = f(p)$ is the same for channels with L = 10 mm and L = 40 mm.

Curves of $I^- = f(Q)$ for ion energies of 4 and 6 kev and L = = 40 mm are presented in Fig. 3. As follows from these curves, negative-ion currents larger than 10 μamp may be obtained for the longer channel. However, it must be remembered that such currents can be obtained for long channels and high extracting voltages, i.e., that the corresponding high-frequency source must be adjusted to operate in a mode that is unusual for it, and that this may, among other things, result in a considerable shortening of its lifetime due to the increased rate of attrition of the cathode at the high extraction voltages.

The calculations carried out indicate that the method of obtaining negative hydrogen ions under consideration here cannot produce beams of high intensity, although in cases where a H_1^--ion current of the order of 10 μamp is adequate, use of this method is expedient. If it is necessary to produce a bundle of negative ions that are heavier than hydrogen ions, the present method gives even poorer results due to the difficulty of focusing a beam of heavy ions into a relatively long and narrow channel.

BIBLIOGRAPHY

1. J.A. Phillips and I.L. Tuck. Rev. Sci. Instr., 27, 97 (1956).
2. J.A. Weinman, and J.R. Cameron. Rev. Sci. Instr., 27, 288 (1956).
3. Ya.M. Fogel', L.I. Krupnik, and V.A. Ankudinov. ZhTF (J. Tech. Phys.), XXVI, 1208, 1956.
4. Ya.M. Fogel' and R.V. Mitin. ZhETF (J. Exp. Theor. Phys.), 30, 450 (1956).
5. M. Stier and C.F. Barnett. Phys. Rev., 103, 896 (1956)

6. A.C. Whittier. Can. J. Phys., 32, 275 (1954).
7. Ya.M. Fogel', V.A. Ankudinov, and R.P. Slabospitskiy. ZhETF, 32, 453 (1957).
8. Ya.M. Fogel', R.V. Mitin, V.F. Kozlov, and N.D. Romashko, ZhETF, 35, 565 (1958).
9. Ya.M. Fogel', L.I. Krupnik, A.G. Koval', and A.D. Timofeyev. Trudy soveshchaniya po elektrostaticheskim generatoram (Trans. Conf. Electrostatic Generators).
10. O. Reifenschweiler. Ann. der Phys. (Annals of Physics), 14, 33 (1954).
11. Ya.M. Fogel', V.A. Ankudinov, D.V. Pilipenko, and N.V. Topolya. ZhETF, 34, 579 (1958).

FORMATION OF NEGATIVE HELIUM, CARBON, OXYGEN, AND CHLORINE IONS ON PASSAGE OF POSITIVE IONS THROUGH A SUPERSONIC JET OF MERCURY VAPOR

By Ya.M. Fogel', R.P. Slabospitskiy, and I.T. Guzhovskiy

INTRODUCTION

At the present time, by virtue of a whole series of studies [1]-[3], the problem of producing a source of negative hydrogen ions for recharging electrostatic generators may be regarded as solved. However, a recharging generator can be used not only to produce protons or deuterons with energies of 2U ev (U is the potential of the recharging-generator guide), but also heavier ions with energies of (k + 1) eU ev and a charge ke. The possibility of accelerating multiply charged positive ions involves the construction of a source of negative ions heavier than hydrogen ions. The development of such a source may be based on the phenomenon exploited for the creation of the negative-hydrogen-ion source, i.e., on the phenomenon of electron capture by positive ions passing through matter. Preliminary experiments to study the transformation of positive oxygen and helium ions into negative ions on their passage through a vapor-stream target were described in the dissertation of L.I. Krupnik. A source of negative helium ions based on the transformation $He^+ \rightarrow He^-$ in a gaseous target is reported in an abstract of a report given before a session of the American Physical Society [4]. The authors of this report obtained a He^--ion current of $3.5.10^{-9}$ amp.

It was the purpose of the present study to examine in detail the transformation of positive helium, carbon, oxygen, and chlorine ions into negative ions as they passed through a mercury-vapor target and ascertain the possibility of building a source of heavy negative ions for a recharging generator.

EXPERIMENTAL APPARATUS AND TECHNIQUE

We studied the transformation of positive helium, carbon, oxygen, and chlorine ions in a mercury-vapor target, using the apparatus described in detail in the first part of Reference [7]. Since this apparatus was designed for study of the $H^+ \rightarrow H^-$ transformation, the magnetic lens that focuses the ions after passage through the stream was designed for negative hydrogen ions with energies of 30 kev. Quite naturally, this lens was practically incapable of focusing the heavier negative ions with which we were dealing in the present study. This means that the values given below for the transformation coefficients and the absolute negative-ion current values are somewhat lower than their true values. As will be seen from the data of Reference [1], these values may be increased by no more than a factor of two by means of focusing the heavy negative ions.

A high-frequency source was employed to produce the beam of positive ions; here, to produce the He^+, C^+, O^+, and Cl^+ ions, the source cylinder was filled with helium, carbon dioxide, oxygen, and freon CCl_2F_2, respectively. In study of the transformation $Cl^+ \rightarrow Cl^-$, we took into account the circumstance that the beam of Cl_{35}^+ ions might contain an impurity of ClF^+ e [sic] CCl^+ ions formed on dissociation of $CClF_2^+$ and $CClF^+$ ions in the mercury-vapor jet. Since the "apparent" mass of these ions is near 35, the magnetic analyzer in the apparatus could not separate them from the beam of Cl^+ ions. Since the energy of these ions is smaller than the energy of the Cl^+

ions, they may be separated from the beam of Cl^+ ions by means of an electric field. Such energy-based separation of ions was effected by the use of the electric field set up by a plate capacitor placed before the entry into the magnetic analyzer.

We studied the transformation coefficients as functions of the primary-beam energy and the boiler temperature, which determines the thickness of the jet. Further, using a Faraday cylinder with a variable diaphragm (the diaphragm diameter could be varied from 2 to 22.5 mm) mounted at the magnetic-analyzer output, we studied the current and current-density distribution over the section of the negative-ion beam. The results of these experiments are presented below.

THE $He^+ \rightarrow He^-$ TRANSFORMATION

The possibility of the existence of metastable negative helium ions proceeds from theoretical calculations [5]. The appearance of negative helium ions on collisions between positive helium ions and atoms of inert gases was first reported in Reference [6]. Preliminary results of study of the $He^+ \rightarrow He^-$ transformation in a mercury-vapor target were reported by L.I. Krupnik in his dissertation. The American study [4] devoted to the source of negative helium ions has already been mentioned in the introduction to the present article.

Figure 1 shows the mass spectrum of the beam of positive ions produced from the high-frequency source* operating on helium and the mass spectrum of the negative-ion beam that emerged from the mercury-vapor target. As will be seen from this figure, only He^+ ions are present in the positive-ion spectrum in any significant quantity, and only He^- ions from the $He^+ \rightarrow He^-$ transformation are present in the negative-ion spectrum in significant numbers.

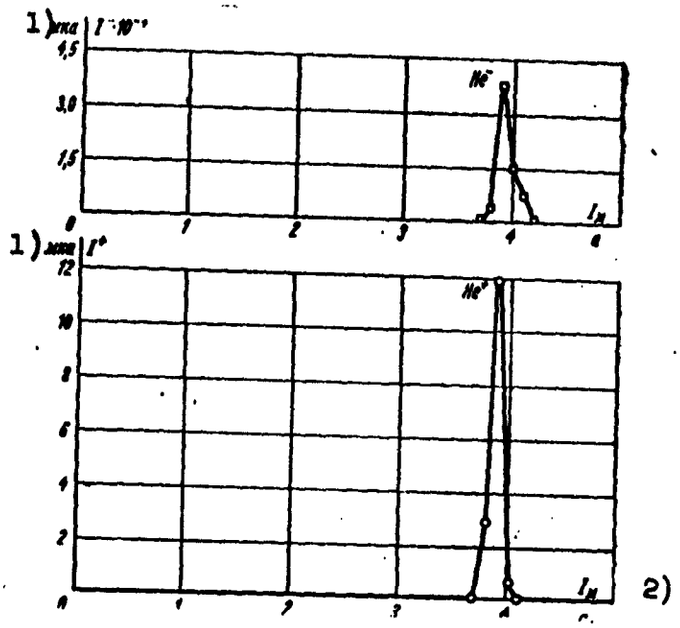

Fig. 1. Mass spectra of positive-ion beam from high-frequency source and negative-ion beam from mercury-vapor target. 1) μamp; 2) I_m.

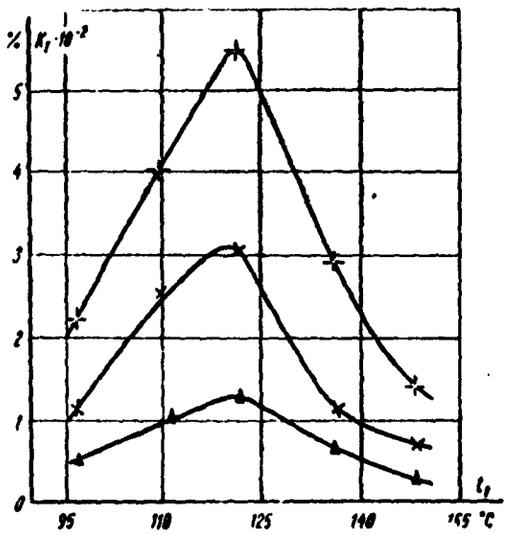

Fig. 2. Transformation coefficient of $He^+ \rightarrow He^-$ as a function of boiler temperature: ▲▲▲E = 22.2 kev; XXX – E = = 32.2 kev; +++ – E = 42.4 kev.

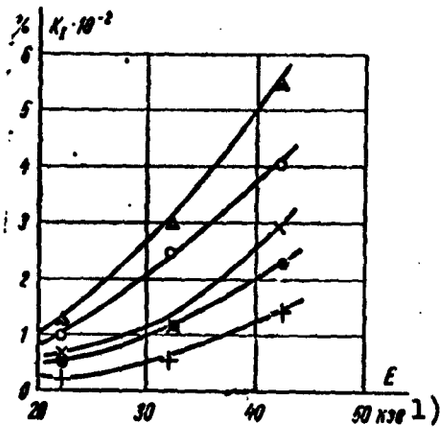

Fig. 3. Transformation coefficient of $He^+ \rightarrow He^-$ as a function of ion energy: ●● – t = 95°C; 000 – t = 110°C; ▲▲▲ – t = 123°C; XXX – t = 135°C; +++ – t = 147°C. 1) Kev.

Figures 2 and 3 show curves of the transformation coefficient of $He^+ \rightarrow He^-$ as a function of boiler temperature and ion energy.

The small value of the transformation coefficient is a characteristic property of the $He^+ \rightarrow He^-$ transformation. The highest value obtained for this coefficient in our measurements was $6 \cdot 10^{-4}$. Because the dependence of transformation coefficient on energy is a monotonically rising curve (Fig. 3), the possibility that a considerably higher transformation coefficient may be obtained with He^+-ion energies in excess of 40 kev is not excluded. The largest He^--ion current obtained in the experiments described above was $2.9 \cdot 10^{-9}$ amp.

THE $C^+ \rightarrow C^-$ TRANSFORMATION

Figure 4 shows the mass spectrum of the positive-ion beam striking the mercury-vapor target and the mass spectrum of the negative-ion beam emerging from the mercury-vapor target. C^- ions from the processes $C^+ \rightarrow C^-$, $CO^+ \rightarrow C^-$, and $CO_2^+ \rightarrow C^-$ were detected in the negative-ion spectrum. The number of C^- ions from the $CO_2^+ \rightarrow C^-$ process was so small that no transformation-coefficient measurements were made for this process. CO^- and CO_2^- ions were not detected in the negative-ion spectrum, from which we may conclude that the transformation coefficients of the processes $CO^+ \rightarrow CO^-$ and $CO_2^+ \rightarrow CO_2^-$ were respectively smaller than $1.25 \cdot 10^{-3}$ and $5 \cdot 10^{-3}$.

Figures 5 and 6 show curves of the transformation coefficients of the processes $C^+ \rightarrow C^-$ and $CO^+ \rightarrow C^-$ as functions of boiler temperature and ion energy. As will be seen from these figures, the coefficient K_I ($C^+ \rightarrow C^-$ transformation) is considerably larger than the coefficient K_{II} ($CO^+ \rightarrow C^-$ transformation), so that only the process $C^+ \rightarrow C^-$ is of practical significance from the standpoint of producing intense C^--ion beams. In view of this, it would be desirable to find the optimum operating conditions for the high-frequency source, which would give the highest content of C^+ ions in the positive-ion beam.

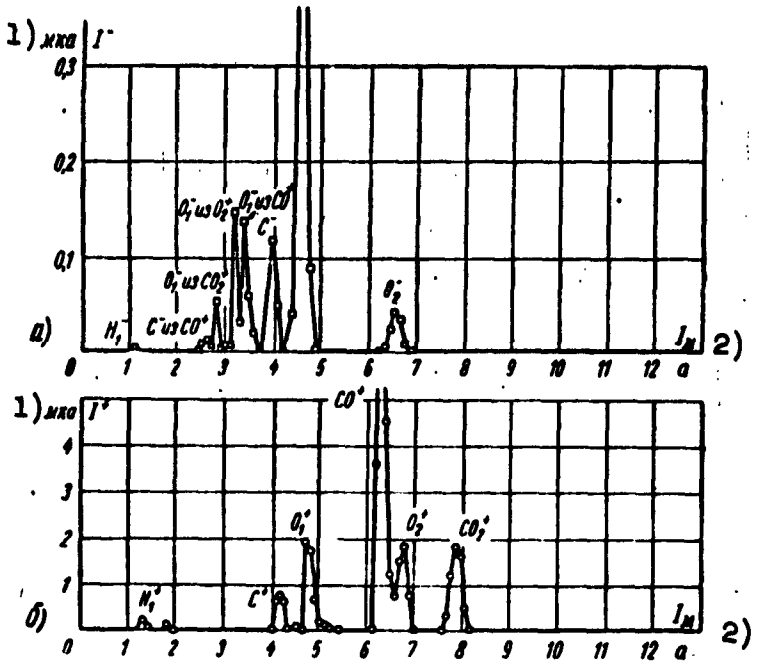

Fig. 4. Mass spectra of beam of positive ions incident on mercury-vapor target and beam of negative ions emerging from mercury-vapor target: a) $I_{O_1^-\ max}$ = 0.41 μamp; b) $I_{CO^+_{max}}$ = = 7.8 μamp. 1) μamp; 2) I_m.

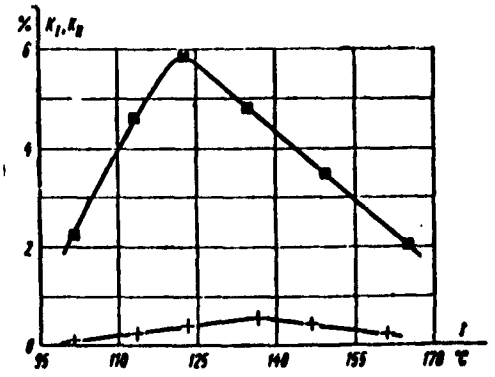

Fig. 5. Transformation coefficient of processes $C^+ \rightarrow C^-$ and $CO^+ \rightarrow C^-$ as function of boiler temperature. E = = 42.4 kev. ■■■ $C^+ \rightarrow C^-$, +++ $CO^+ \rightarrow C^-$.

On the other hand, since we observe a monotonic rise in the coefficient K_I with ion energy, it would be advisable to measure it at energies greater than 40 kev.*

Figure 7 shows curves of the current and current density of C^- ions with energies of 32.2 kev obtained from the transformation $C^+ \rightarrow C^-$ as functions of the variable-diaphragm diameter. It is curious that a current of $4.5 \cdot 10^{-9}$ amp can still be obtained through a diaphragm 2 mm in diameter. The maximum current through a diaphragm 22.5 mm in diameter

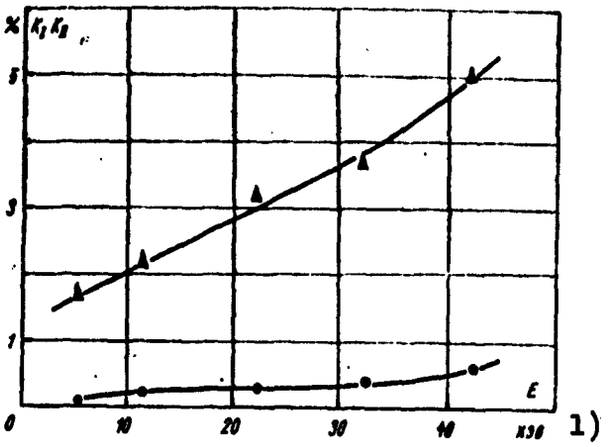

Fig. 6. Transformation coefficient of processes $C^+ \rightarrow C^-$ and $CO^+ \rightarrow C^-$ as a function of ion energy: ▲▲▲ – t = 123°C; $C^+ \rightarrow C^-$; ●●● – t = 136°C; $CO^+ \rightarrow C^-$; 1) kev.

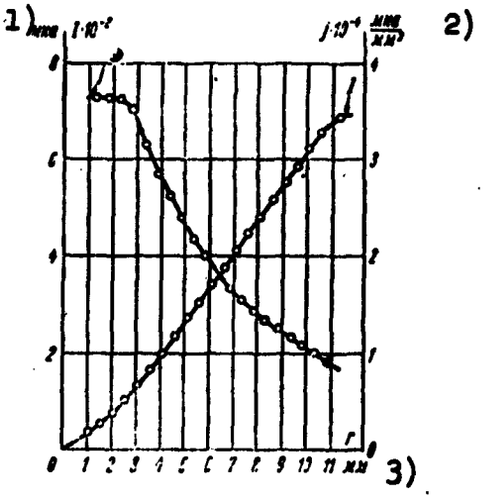

Fig. 7. Current and current density of C^- ions with energy E = = 32.2 kev obtained from transformation $C^+ \rightarrow C^-$ as functions of variable-diaphragm diameter. 1) μamp; 2) μamp/mm^2; 3) mm.

reached 0.1 μamp.

THE $O^+ \rightarrow O^-$ TRANSFORMATION

Figure 8 presents the mass spectra of the positive and negative oxygen ions. Monotonic oxygen ions from the transformations $O_1^+ \rightarrow O_1^-$; $O_2^+ \rightarrow O_1^-$; and $O_3^+ \rightarrow O_1^-$ and molecular oxygen ions from the transformation $O_2^+ + O_2^-$ were observed in the negative-ion spectrum. The $O_3^+ \rightarrow O_1^-$ transformation was not studied because of the very small content of O_3^+ ions in the positive-ion beam.

Figures 9 and 10 give curves of the transformation coefficients K_I, K_{II}, and K_{III} (the $O_1^+ \rightarrow O_1^-$; $O_2^+ \rightarrow O_2^-$; $O_2^+ \rightarrow O_2^-$ transformations, respectively) as functions of boiler temperature and ion energy. As will be seen from these figures, the coefficient K_{II} is smaller than K_I for the oxygen ions, in contrast to the transformations $H_1^+ \rightarrow H_1^-$ and $H_2^+ \rightarrow H_1^-$, so that it is expedient to employ the transformation $O_1^+ \rightarrow O_1^-$ to obtain higher-intensity beams of O^- ions.

Figure 11 presents curves of current and current density of O_1^- ions with an energy of 32.2 kev obtained from the transformation

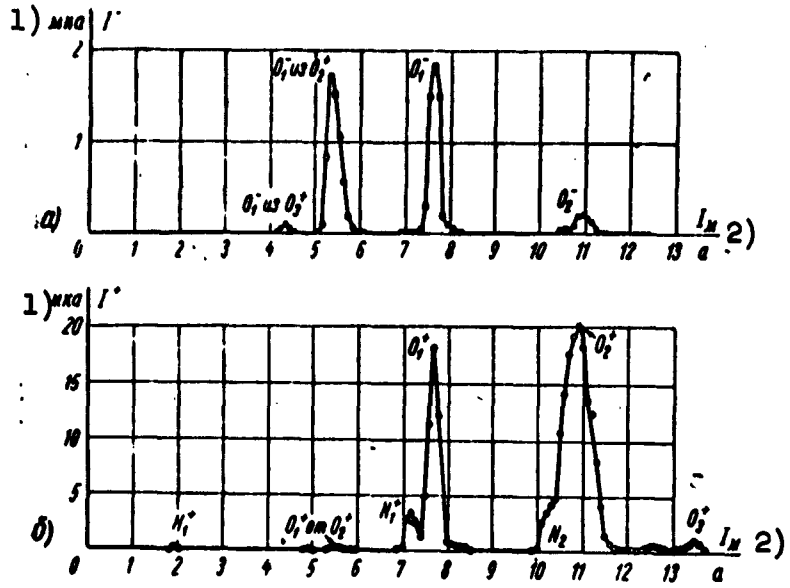

Fig. 8. Mass spectra of positive and negative oxygen ions. 1) μamp; 2) I_m.

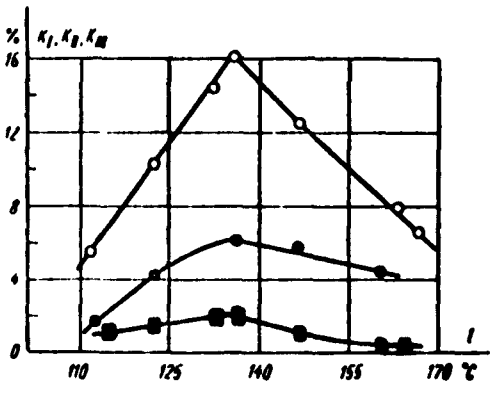

Fig. 9. Transformation coefficients K_I, K_{II}, and K_{III} as functions of boiler temperature: E = 11.6 kev; 000 – $- O^+ \rightarrow O^-$; ●●● – $O_2^+ \rightarrow O_1^-$; ■■■ – $O_2^+ \rightarrow O_2^-$

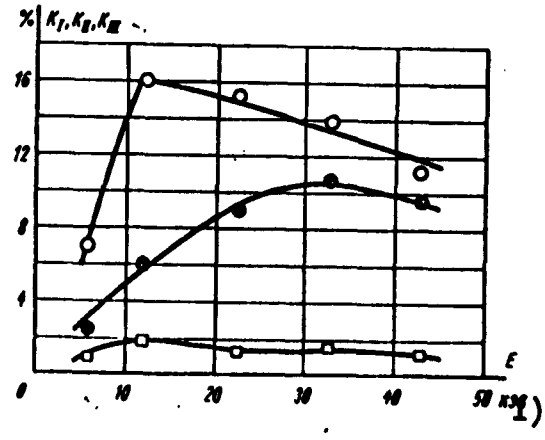

Fig. 10. Transformation coefficients K_I, K_{II}, and K_{III} as functions of ion energy. t = = 136°C. 000 – $O_1^+ \rightarrow O_1^-$; 000 – $O_2^+ \rightarrow O_1^-$; – $O_2^+ \rightarrow$ $\rightarrow O_2^-$. 1) kev.

$O_1^+ \rightarrow O_1^-$ as functions of variable-diaphragm diameter.

In the experiments with oxygen ions, we produced O_1^--ion currents up to 2.5 μamp at an unseparated-beam current of 150 μamp and with the Faraday-cylinder diaphragm fully opened (d = 22.5 mm). A current of 0.1 μamp was obtained through a diaphragm with d = 2 mm. In view of the fact that the transformation coefficient of $O_1^+ \rightarrow O_1^-$

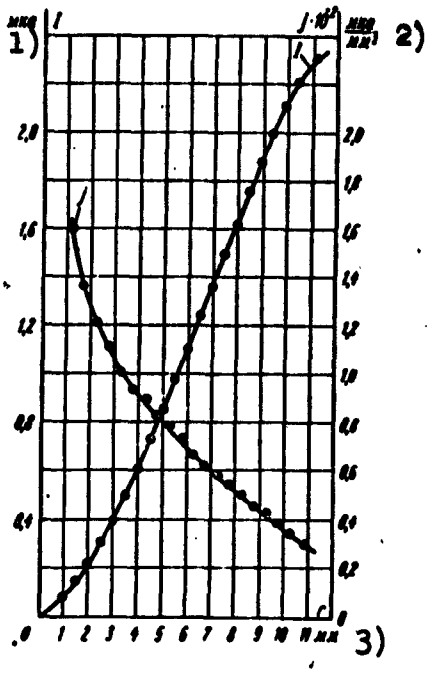

Fig. 11. Current and current density of O_1^- ions with energy of 32.2 kev obtained from the transformation $O_1^+ \rightarrow O_1^-$ as functions of variable-diaphragm diameter. 1) μamp; 2) μamp/mm^2; 3) mm.

is very large, we may hope to obtain O_1^--ion beams of considerably greater intensity provided that the intensity of the positive-ion beam is increased and improvements are made in focusing it and the negative ions formed in the vapor-stream target.

THE $Cl^+ \rightarrow Cl$ [sic] TRANSFORMATION

The mass spectrum of the positive-ion beam striking the mercury-vapor target and the mass spectrum of the beam of negative ions emerging from it are shown in Fig. 12. As will be seen from Fig. 12, the spectrum of negative ions having an energy equal to the energy of the positive ions shows Cl_1^- ions from the $Cl_1^+ \rightarrow Cl_1^-$ transformation and a very small number of CCl^- and CF_2^- ions from the transformations $CCl^+ \rightarrow CCl^-$ and $CF_2^+ \rightarrow CF_2^-$. No Cl_2^- ions were observed in the spectrum of the full-energy negative ions, from which it follows that the transformation coefficient of the process $Cl_2^+ \rightarrow Cl_2^-$ is below $2 \cdot 10^{-3}$. On adjusting the strengths of the electric and magnetic fields of the electrostatic and magnetic analyzers, we observed Cl^- ions from the transformations $CCl^+ \rightarrow Cl^-$, $CCl_2F^+ \rightarrow Cl_1^-$, and $Cl_2^+ \rightarrow Cl_1^-$. The number of negative chlorine ions from these processes was insignificant, so that we did not study the transformation coefficients in this case.

Figures 13 and 14 show curves of the coefficient K_I for the

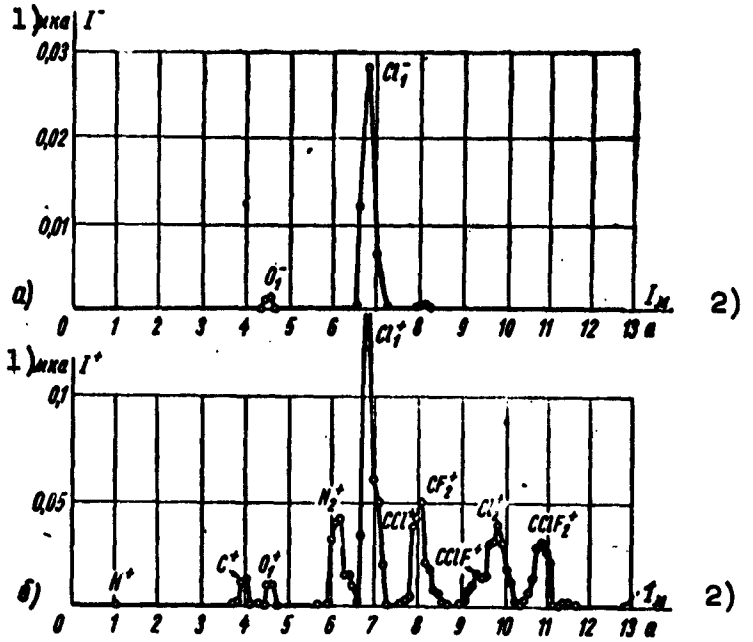

Fig. 12. Mass spectra of positive ions striking mercury-vapor target and of negative ions emerging from it. 1) μamp; 2) I_m.

transformations $Cl_1^+ \rightarrow Cl_1^-$ as a function of boiler temperature and ion energy. Comparison with the transformation processes for other ions indicates that the transformation coefficient for $Cl_1^+ \rightarrow Cl_1^-$ is largest and reaches values of about 20%.

Figure 15 shows curves of current and current density of the Cl_1^- ions with energies of 32.2 kev as functions of the variable diaphragm diameter. The maximum current of Cl_1^- ions in the Faraday cylinder with diaphragm fully opened was 0.85 μamp with a current of 62.5 μamp in the current of mass-unresolved positive ions. Apparently, the current of Cl_1^- ions might be increased considerably with observance of the above conditions.

As a conclusion to the present paper, Fig. 16 presents a comparison of the curves of $K_I = f(E)$ for all of the transformations that we investigated, as well as that for $H_1^+ \rightarrow H_1^-$, which was studied in [7].

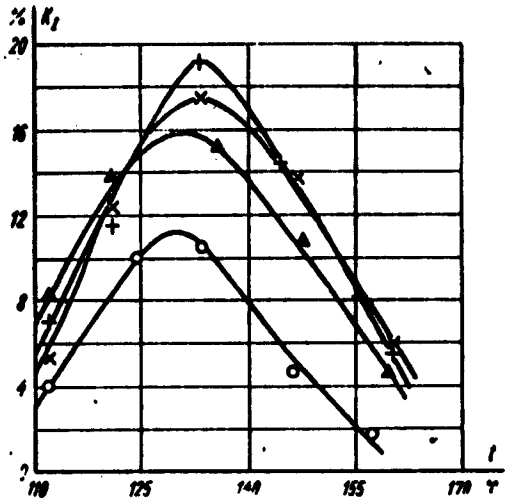

Fig. 13. Coefficient K_I for transformation $Cl^+ \rightarrow Cl^-$ as a function of boiler temperature: 000 – E = 11.6 kev; ΔΔΔ – E = 22.2 kev; XXX – E = 32.2 kev; +++ – E = 42.4 kev.

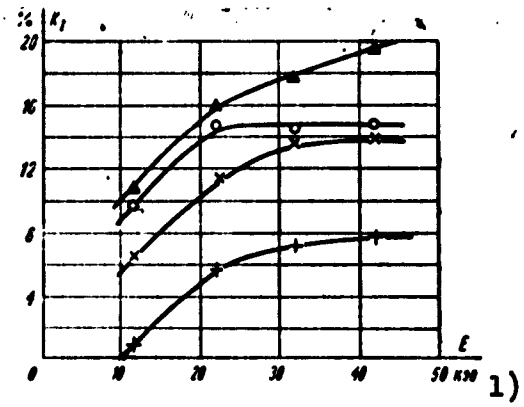

Fig. 14. Coefficient K_I for transformation $Cl^+ \rightarrow Cl^-$ as a function of ion energy: XXX – t = 118°C; 000 – t = 125°C; ΔΔΔ – t = 135°C; +++ – t = 157°C. 1) Kev.

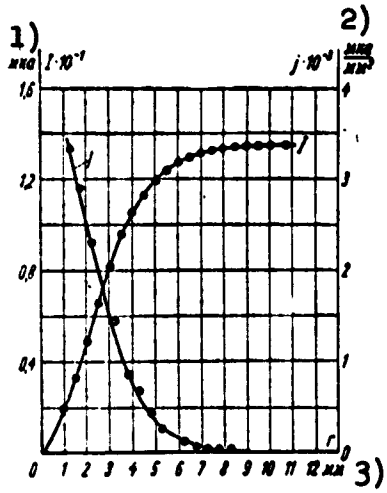

Fig. 15. Current and current density of Cl_1^- ions with energy of 32.2 kev as a function of variable-diaphragm diameter. 1) μamp; 2) μamp/mm^2; 3) mm.

We suggest that the experiments described in the present paper may be used as a basis for development of a source of heavy negative ions for a overcharging generator to transform positive into negative ions in a mercury-vapor target. As regards production of intense He^- beams, solution of this problem can be guaranteed only by the use of an ion source that creates a very-high-intensity beam of positive helium ions.

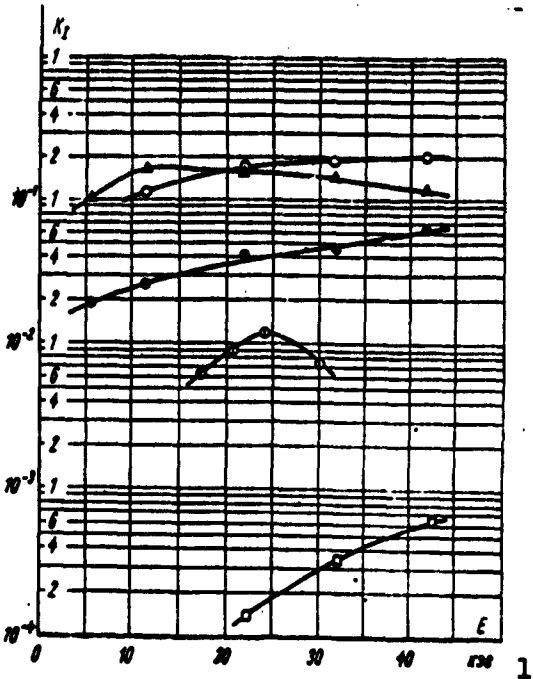

Fig. 16. Comparison of curves of $K_I = f(E)$ for all transformations investigated and the transformation $H_1^+ \rightarrow H^-$ after Reference [7]: □□□ – $He^+ \rightarrow He^-$; ●●● – $H_1^+ \rightarrow H_1^-$; ●●● – $C_1^+ \rightarrow C_1^-$; ▲▲▲ – $O_1^+ \rightarrow O_1^-$; ooo – $Cl_1^+ \rightarrow Cl_1^-$. 1) kev.

BIBLIOGRAPHY

1. Ya.M. Fogel', L.I. Krupnik, and V.A. Ankudinov. ZhTF (J. Tech. Phys.), XXVI, 1208, (1956).

2. J.A. Phillips and I.L. Tuck. Rev. Sci. Instr., 27, 97, (1956).

3. J.A. Weinman and J.R. Cameron. Rev. Sci. Instr., 27, 288 (1956).

4. P.M. Windham, P.J. Joseph, J.A. Weinman, and R.G. Herb. Bull. Amer. Phys. Soc., 2, No. 1, II, (1957).

5. E. Holfien and J. Midtal. Proc. Phys. Soc., A 68, 815, (1955).

6. V.M. Dukel'skiy, V.V. Afrosimov, and N.V. Fedorenko. ZhETF (J. Exp. Theor. Phys.), 30, 792 (1956).

7. Ya.M. Fogel', L.I. Krupnik, A.G. Koval', and A.D. Timofeyev. Trudy soveshchaniya po elektrostaticheskim generatoram (Trans. Conf. Electrostatic Generators), page 141.

[Footnotes]

Manuscript Page No.

12 *This spectrum was reported in the presence of a supersonic mercury-vapor jet.

15 *This could not be done in the present study because the ion-beam accelerating tube did not withstand voltages above 40 kev.

INVESTIGATION OF THE DIELECTRIC STRENGTH OF CERTAIN COMPRESSED GASES AND GASEOUS MIXTURES BY MEANS OF AN ELECTROSTATIC GENERATOR

By L.I. Pivovar and V M. Tubayev

GENERAL PROPOSITIONS

Very-high-voltage electrostatic generators are of considerable interest both from the standpoint of particle acceleration for precision nuclear research and from the standpoint of their extensive application in a number of scientific and engineering fields. Consequently, research into the factors that limit the voltages and currents of electrostatic generators is of great importance. As we know, the voltages of contemporary electrostatic generators are primarily limited by the dielectric strength of the accelerating tubes and then further by the dielectric strength of the compressed gases that serve to insulate the generator. Development of electrostatic generators should proceed in the direction of increased currents and voltages and high compactness. Successful solution of these problems may be achieved only on the basis of systematic study of the dielectric strength of the vacuum and the compressed gases, as well as the superficial sparkover strength of the dielectrics in a vacuum and in compressed gases at high voltages, Until recently, only a small number of studies had been devoted to these problems. Only recently did reports appear describing studies of the dielectric strength of certain compressed gases (N_2, CO_2, air) in homogeneous steady-voltage fields up to 900-1000 kv [1], [2].

In the majority of electrostatic-generator designs described in the literature, nitrogen has been used as the insulating gaseous medium [3], [4]; only in isolated cases do we find nitrogen being used in mixture with freon [5], [6] or "elegaz" [7], or nitrogen mixed with carbon dioxide [8], or, finally, pure carbon dioxide [9].

Comparison of the sparkover voltages in compressed gases for various electrostatic generators indicates that there is a wide scattering in the value of the maximum sparkover potential gradient attained in these designs. This fact suggests that it is necessary to conduct systematic investigations of the dielectric strengths of compressed gases and gaseous mixtures for selection of the most suitable gaseous insulation for electrostatic generators and other high-voltage apparatus operating in compressed gases.

The present paper describes a compact electrostatic generator and comparisons made on it between the dielectric strengths of certain practically important compressed gases and gaseous mixtures in the weakly nonhomogeneous electric fields characteristic for the majority of operational electrostatic-generator designs.

DESCRIPTION OF EXPERIMENTS

The apparatus that we designed and built for the investigations is a compact electrostatic generator that operates in a compressed gas. The generator was mounted inside a vertical steel cylindrical tank 65 cm in diameter and 140 cm long; this tank was designed for operating pressures as high as 19 atmospheres. Provision was made in the generator design for installation of interchangeable electrodes on the guide and the cover of the tank for investigation of the dielectric strengths of gases in homogeneous fields. The general configuration of the generator is shown in Fig. 1.

The generator's insulating column was built up from two sections

and has a total length of 80 cm. The bottom of the column consists of 23 aluminum divider disks, each 375 mm in diameter, and the top of the column consists of 17 aluminum divider disks 300 mm in diameter. The divider disks were fabricated from sheet aluminum 1 mm thick and wrapped at the periphery with aluminum tubing 12 mm in diameter. The insulating column was assembled with organic-glass insulators threaded together in such a way that a divider disk was clamped between each pair of insulators. The cylindrical insulators, which were 30 mm in diameter, have smooth polished surfaces. Threaded together, the insulators from a cylindrical column. There are four such columns at the bottom of the generator and three at the top. This insulating-column design guarantees the necessary mechanical strength as well as excellent contact between the metallic disks and the insulator faces. The generator voltage is distributed uniformly along the insulating column by means of resistance blocks that connect successive disks. Each block is composed of ten 100-megohm type KLV resistors, so that the total resistance of each block is 1000 Megohms. The resistance blocks are assembled into a separate column with a total length of 80 cm. In assembled form, this column is inserted into the generator's insulating column, and electrical contact between the blocks and the equipotential disks is provided by flat springs. The electric field is distributed along the charge conveyor belt by means of cylindrical duralumin rods 12 mm in diameter. These rods are screwed to the equipotential disks and their position relative to the belt can be adjusted between 6 and 8 mm.

A high-voltage electrode with a maximum diameter of 330 mm was made in the form of a hemisphere terminating in a radius of curvature of 100 mm where it joins the insulating column.

We prepared two electrodes of the same type – one from aluminum and the other from copper. At the top of the copper electrode, we drilled and tapped a centered hole to accept the mount of one of the Rogovskiy electrodes. When the copper electrode was used to study

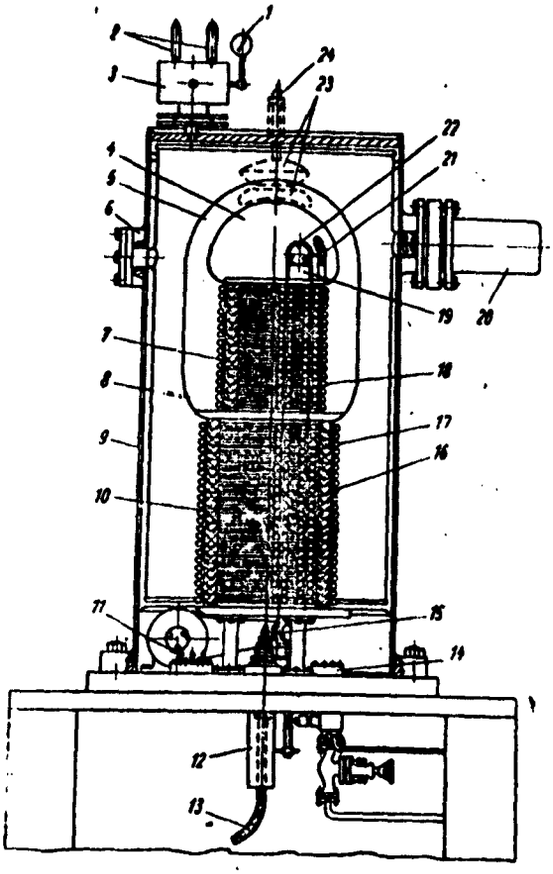

Fig. 1. Diagram of apparatus: 1) manometer; 2, 3) safety valves; 4) high-voltage guide 330 mm in diameter; 5) intermediate screen 460 mm in diameter; 6) inspection windows; 7, 10) column sections; 8) protective screen; 9) tank; 11) motor; 12) high-voltage input; 15, 22) conveyor-belt sheaths; 19) charge conveyor belt; 20) rotor voltmeter.

sparkover in a weakly nonhomogeneous field, a plug that provided a smooth electrode surface was screwed into the hole.

To ascertain the part played by the intermediate electrostatic screens (since the data on this point in the literature are contradictory), we made provision for installing a single intermediate screen. This 460-mm-diameter intermediate screen was made from aluminum and is a combination of a hemisphere with a cylinder with a marginal radius of curvature of 160 mm where it meets the insulating column.

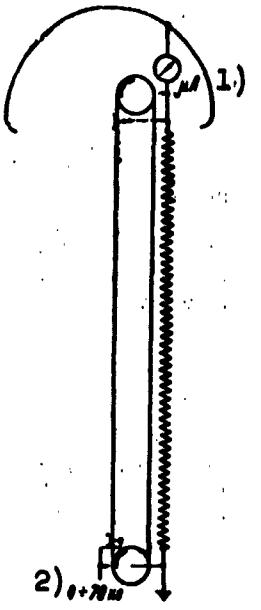

Fig. 2. Diagram of generator charging. 1) μamp; 2) 0 to 70 kv.

The generator tank was made from a steel tube which had roughness of the order of 1-1.5 mm in depth on its internal surface as a result of corrosion. Consequently, a cylindrical polished aluminum screen 630 mm in diameter was mounted inside the tank to screen this roughness. The generator's charging belt, which was 125 mm wide, was made from four-ply rubber-impregnated percale and moves at a rate of 15 m/sec. The charges are fed onto the belt by means of corona brushes.

As a result of tests made on a number of systems for charging the belt, we settled on a system that combines the highest generator short-circuit current with stability of its voltage within a few tens of percent. This system for charging the generator is illustrated in Fig. 2. The lower brush, which is mounted on the inner surface of the belt, serves to pick off the surface charge of the opposite sign that has appeared as a result of friction between the belt and the sheaves and "parasitic" discharging in the wedge of gas between the sheave and the belt. This device delivers high natural stability of the generator voltage. Charging of the belt, on the other hand, is effected by a brush mounted at the roller on the outside of the belt.

The belt tension is regulated by means of two rods that pass through the lower bulkhead of the boiler. The rods are pivot-connected to the sheave frame and are tensioned by means of a manual screw feed. Inspection windows were cut into the bottom of the boiler to

permit visual inspection of the belt movement and reading the thermometer.

TECHNIQUE OF MEASUREMENT

All experiments with the electrostatic generator were carried out with the positive guide polarity. The generator voltage was measured by a compensation-type rotor voltmeter mounted in a sidearm of the tank. The generating plate of the rotor voltmeter was sunk far enough into the hole in the protective screen so that it would "see" only the high-voltage guide of the generator.

We calibrated the rotor voltmeter prior to each measurement; for this purpose, we fed the high potential from the rectifier apparatus to the guide or to the intermediate screen as needed. The applied voltage was measured to an accuracy of $\pm$ 1.5% by a kilovoltmeter. As we know, the reading of a rotor voltmeter can be severely distorted by corona currents, so that we used a microammeter to monitor the data obtained, inserting it between the interchangeable brushes, which were insulated from the top plate of the generator, and the guide (Fig. 2). The appearance of corona currents from the conductor is registered by this microammeter, thus making it possible to exclude doubtful data from analysis. To estimate the error with which the generator-voltage values measured by the rotor voltmeter had been determined, we compared the rotor-voltmeter reading with the current readings of a potentiometer. These comparisons were made at various pressures of the gases in the tank and for the voltage interval ranging from 200 kv to the sparkover voltage. It was found in all cases that the discrepancy between the readings of the rotor voltmeter and the potentiometer in carbon dioxide, in hydrogen, and in mixture of carbon dioxide with "elegaz" and nitrogen did not exceed $\pm$ 2%, while the divergence for technical nitrogen was $\pm$ 6%.

Apart from the comparisons, we verified the correctness of the rotor-voltmeter readings over the entire range of measured voltages by setting up screen grids directly in front of the rotor voltmeter. These checks indicated that under our conditions, the readings of the rotor voltmeter were undistorted, since the agreement between the readings of the rotor voltmeter with and without the grids was within 1.5-2%.

The high-voltage guide, the intermediate screen, and the protective screen were polished to an excellent mirror finish. Prior to each experiment, the guide, screen, and generator were rinsed with ether. The gases under investigation were injected into the tank through a purifying battery containing alumina gel and a number of cotton filters.

Prior to filling with gas, the generator was dried under a vacuum of the order of 0.5 mm Hg for 15-20 hours. In the majority of cases, such drying of the gas and the generator provided a relative humidity of 0.2-0.5% at tank gas pressures of 10-15 atm abs. To ascertain the influence of the residual humidity on the dielectric strength of the gases, we placed a copper coil in the tank and passed a coolant through it, thereby establishing the water-vapor pressure in the tank at the level corresponding to the coil temperature.

The "elegaz" used in the experiments was subjected to thorough purification. For this purpose, the gas was frozen out at a temperature of -85°C and the uncondensed fractions were released into the atmosphere. This operation was repeated twice, after which the liquefied fraction was passed through a number of absorbers to purify the "elegaz" of condensed impurities.

The puncture voltage of the gas gap was measured by raising the applied potential difference by small steps to the sparkover value

through the voltage interval 3-5% below the sparkover value. The guide potential was varied by fine adjustment of the belt-charging voltage. The time of sparkover was registered visually through the inspection windows, and by an oscillograph which served as a compensation indicator in the measurement circuit of the rotor voltmeter. From 10 to 20 readings were taken at each point for averaging purposes. As a rule, the limiting sparkover voltage was not reached at once; instead, the voltage rose slowly to a constant value after a number of repeated triggerings of the discharge. The longest "training period" was required in technical nitrogen at elevated pressures. In these cases, the final puncture voltage was reached after several hundreds and sometimes even thousands of discharge triggerings, with the final voltage 35 to 40% above the original voltage. Running-water cooling was employed to hold the temperature in the tank between 20 and 25°C during the experiment. The temperature in the tank was monitored by a thermometer mounted in it.

In studying dielectric puncture between the 330-mm-diameter high-voltage guide and the protective screen, the shoulder of the generator's lower section was screened by a steel ring having a 60-mm radius of curvature.

RESULTS OF MEASUREMENTS AND DISCUSSION OF RESULTS

a) Carbon Dioxide*

Figure 3 shows curves of the puncture voltage as a function of pressure for carbon dioxide in the pressure region from 1 to 11 atm abs. Curve I corresponds to sparkover between the 440-mm-diameter intermediate screen and the protective screen. We used the intermediate screen as a guide by short-circuiting that part of the generator which was situated inside it. As will be seen from the figure, the puncture voltage rises linearly with increasing pressure and has

reached 1140 kv at 8 atm. Discharges along the belt interfered with further elevation of the voltage.

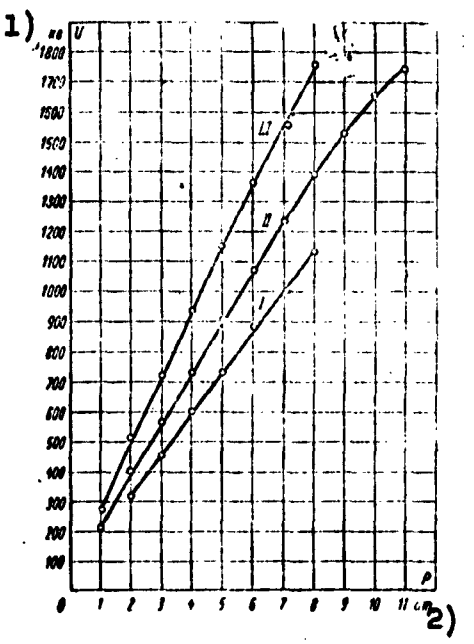

Fig. 3. Puncture voltage as a function of pressure in carbon dioxide. 1) kv; 2) atmospheres.

Curve II corresponds to sparkover between the 330-mm-diameter guide and the protective screen. In this case, the puncture voltage rises linearly to 7 atm abs, after which its increase with pressure becomes slightly slower. At 11 atm, the puncture voltage reaches 1750 kv. Again, sparkover along the belt prevented further increase in the potential of the high-voltage guide with increasing pressure. As a rule, these sparkovers put the belt out of service as a result of carbonization of the percale.

The data given here represent averages from several independent measurements. The puncture-voltage measurements were made with copper and aluminum guides having the same shape and dimensions. Comparison of the puncture-voltage values obtained with the copper and aluminum guides indicates that no differences in the puncture-voltage values are observed within the limits of experimental error.

Curve III illustrates the puncture voltage in carbon dioxide as a function of pressure in the presence of a 460-mm-diameter intermediate screen. In this case, given the same pressures, the puncture voltage increases over the value obtained with the conductor alone by about 25%, thus showing rather good agreement with the calculated value. The puncture voltage at 8 atm abs was 1760 kv, after which any further increase in the voltage was restricted by sparkover along

the belt.

Excellent reproducibility of the results was observed with carbon dioxide gas, together with very narrow scattering of the sparkover voltage value over the entire range of pressures that we investigated.

b) Nitrogen

Figure 4 shows sparkover voltage as a function of pressure for nitrogen in the pressure region from 1 to 12 atm abs.

Curve I shows the puncture voltage as a function of pressure exerted by nitrogen containing 8% of oxygen and corresponds to sparkover between the 330-mm-high-voltage copper guide and the protective screen. As will be seen from the figure, the puncture voltage rises linearly with pressure only to 5 atm abs, after which its increase with pressure proceeds at a sharply reduced rate. Here, in addition to being retarded, the puncture-voltage curve splits, so to speak, into two branches, forming a region (cross-hatched on the figure) in which puncture may take place at any voltage value between the upper and lower boundaries of this region. The upper sparkover-voltage limit at a pressure of 12 atm abs is 1700 kv. Spark discharges along the belt prevented any further increase in voltage with pressure.

Curve II presents the puncture voltage as a function of pressure exerted by nitrogen containing 0.03% oxygen. This curve was registered under the same geometrical conditions and with the same electrodes as curve I. As we see, the scattering in the sparkover-voltage values for pure nitrogen is greater than that for technical nitrogen.

Curve III corresponds to puncture between the 460-mm guide and the protective screen in nitrogen containing 8% of oxygen. Discharge anomalies in technical nitrogen took place in all of the cases considered, in approximately the same pressure region (the cross-hatched

regions on Fig. 4). These anomalies were observed in all experiments without exception, and cannot be accounted for as accidental effects. There are oblique references to scattering of the puncture-voltage values in the report by Fortesque and Gall [6]. Felici [10] also makes reference to the instability of the pure-nitrogen discharge voltage in a nonhomogeneous field at large spark lengths. Consequently, one possible reason for the discharge anomalies in nitrogen would be the existence of large local electric-field nonhomogeneities that make their appearance at elevated pressures.

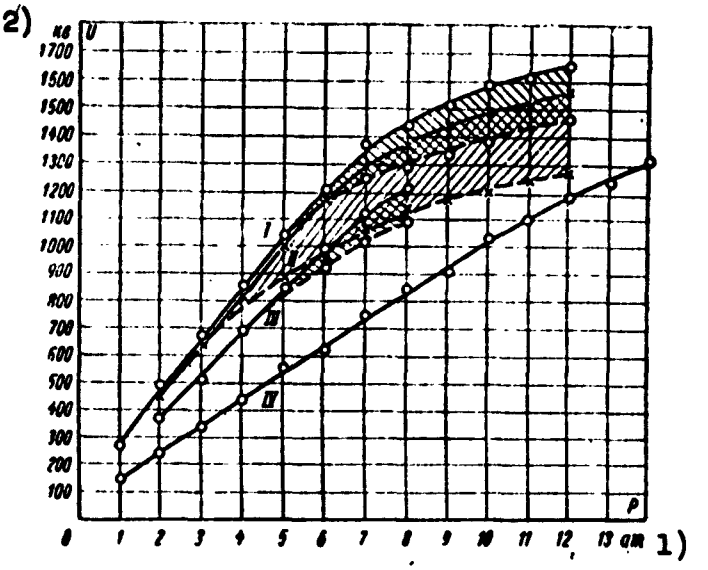

Fig. 4. Puncture voltage as a function of pressure in nitrogen and hydrogen. 1) Atmospheres; 2) kv.

The dependence of sparkover voltage in nitrogen on pressure has been investigated by a number of authors, including V.S. Akshanov, who used an electrostatic generator that he built himself. The curve that he obtained differs from those obtained by us, but this may be accounted for by differences in the "training period" and possibly in the lengths of the gas gaps.

As in the case of carbon dioxide, we carried out the puncture-voltage measurements in technical nitrogen using the copper and

aluminum guides. In this case, it was established, in contrast to that of carbon dioxide, that the limiting sparkover-voltage values in the pressure region above 7-8 atm abs was slightly lower for the aluminum electrode than for the copper electrode. This difference is a consequence of the fact that the maximum puncture voltages in technical nitrogen at elevated pressures were, as a rule, attained only after a large number of discharges, which formed craters on the aluminum surface. It is at these craters that the elevated potential gradients localize, apparently with the result that the sparkover voltages show a slight decrease. Craters are also formed on the copper guide, but they were much less distinctly expressed on the copper than on the aluminum.

We also studied the influence of residual humidity on the electrical properties of technical nitrogen. For this purpose, we passed a stream of liquid nitrogen through a coil passing through the lower tank bulkhead for 8 to 10 hours, so that a very low water vapor pressure in the tank was guaranteed. The curves then obtained for sparkover voltage as a function of the pressure exerted by nitrogen containing 8% of oxygen were virtually coincident with curve I in Fig. 4. This suggests that a relative moisture content of less than 0.5% in nitrogen no longer exerts a noticeable influence on its electrical properties.

c) Hydrogen

In a recently published note [10], Felici refers to the advantages of using compressed hydrogen as insulation in rigid-rotor electrostatic generators. The basic advantages consist in the relatively high efficiency and high surface density of the transferred charge together with relatively high dielectric strength in nonhomogeneous fields with long gas gaps. Felici employed compressed hydrogen as

insulation in rigid-rotor machines at voltages up to 250 kv. In view of the above special properties of hydrogen, it was regarded as worthwhile to investigate the possibility of using compressed hydrogen as insulation for belt-conveyor electrostatic generators. Consequently, we investigated the dielectric strength of pure hydrogen (99.9%) in the pressure region up to 14 atm abs.

Figure 4 (curve IV) shows the sparkover voltage as a function of pressure for hydrogen in the pressure region from 1 to 14 atm abs. The curve corresponds to sparkover between the 330-mm copper high-voltage guide and the protective screen. As will be seen from the figure, the sparkover voltage increases almost linearly to 11 atm abs, after which its increase with pressure is slightly slower. The sparkover voltage at 14 atm abs is 1375 kv. Further elevation of the voltage was restricted by discharge along the belt.

Simultaneously with the above measurements, we evaluated the magnitude of the aerodynamic losses in motion of the belt in hydrogen on the basis of the power change. It was found that they amounted to only a few percent of the electric power of the generator at 14 atm abs. Together with the low aerodynamic losses, we found that the charging voltage of the belt was approximately 1/2 to 1/3 that observed in nitrogen or carbon dioxide.

In the pressure region that we investigated, the sparkover field strengths in hydrogen remained even lower than those in nitrogen or carbon dioxide. However, the shape of the curve of discharge voltage as a function of pressure in hydrogen justifies the conclusion that at pressures of the order of 15-20 atm abs, the dielectric strength of hydrogen will not be inferior to that of nitrogen.

In cases where efficiency and a high density of the transferred charge are of great importance, the use of compressed hydrogen as

insulation for electrostatic generators with belt conveyors may be found expedient.

d) Mixtures of Technical Nitrogen with Carbon Dioxide

Comparison of the discharge voltages in nitrogen and carbon dioxide indicates that in the pressure region below 7-8 atm abs, technical nitrogen possesses a dielectric strength higher than that of carbon dioxide. In the region of pressures above 7-8 atm abs, however, carbon dioxide has the higher dielectric strength. It was therefore regarded as interesting to investigate the dielectric strength of mixtures of technical nitrogen with carbon dioxide at elevated pressures. For this purpose, we made a study of the dielectric strength of mixtures of technical nitrogen containing 8% of oxygen with pure carbon dioxide. The mixtures investigated contained 9, 18, 30, and 50% of carbon dioxide gas by volume.

Figure 5 presents the results of the corresponding measurements of the sparkover voltage between the 330-mm guide and the protective screen as a function of pressure. The curves illustrate the dependence of sparkover voltage on pressure for mixtures containing 18 and 50% of carbon dioxide. For purposes of comparison, Fig. 5 also shows curves of the sparkover voltages as functions of pressure for pure carbon dioxide and technical nitrogen as taken from Figs. 3 and 4. As will be seen from Fig. 5, the sparkover voltages of the mixtures below 6-7 atm abs have values close to those for nitrogen. At pressures above 7 atm abs, however, the dielectric strength of the mixtures is higher than that of either of the components. As the carbon-dioxide content in the mixture is varied from 9% to 50%, its dielectric strength varies only very slightly over the entire range of pressures investigated. Some scattering in the sparkover-voltage value appears in mixtures containing 9 and 18% carbon dioxide; this

scattering lies in the pressure region above 7 atm abs for the 9% mixture and in the pressure region above 10 atm abs for the 18% mixture (region hatched on figure).

e) Mixtures of Carbon Dioxide with "Elegaz"

As we know from experience in the use of certain electrostatic

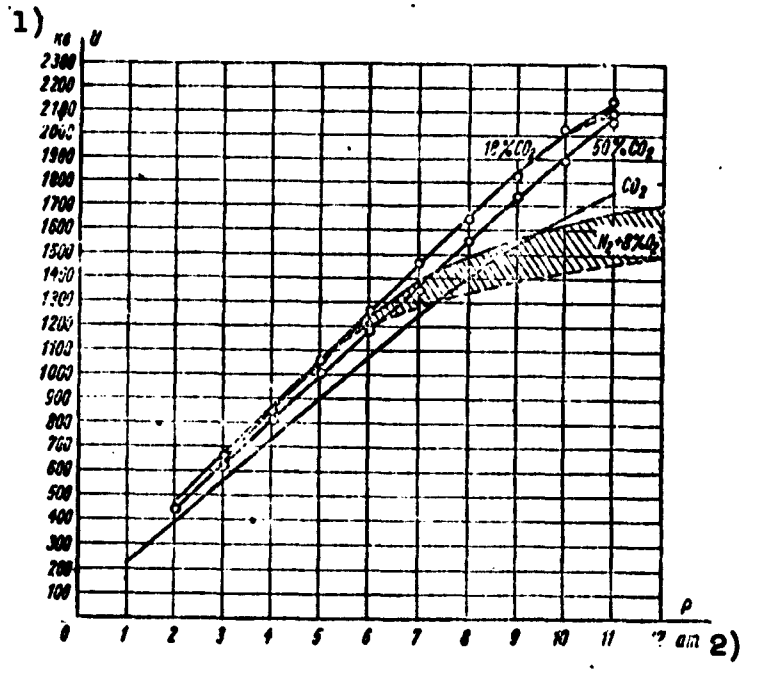

Fig 5. Sparkover voltage as a function of pressure in mixtures of nitrogen and carbon dioxide. 1) kv; 2) atmospheres.

generators [7], [12], the addition of small quantities of electrically negative gases to nitrogen or air raises the discharge voltage considerably. As an illustration, we might cite the recently described electrostatic generator developed by Gokhberg et al. [7]. By adding 3.5% of "elegaz" to nitrogen, the authors succeeded in increasing the electric strength of the design markedly. For proper selection of the components and composition from the economy and technical standpoints, study of the influence exerted by additives, including "elegaz" to certain practically important gases is of high importance.

Thus we carried out the first investigations of the dielectric strength of mixtures of carbon dioxide with "elegaz" as a function of the "elegaz" content in the mixture, and also made certain measurements in mixtures of nitrogen with "elegaz" in the pressure interval from 1 to 10 atm abs.

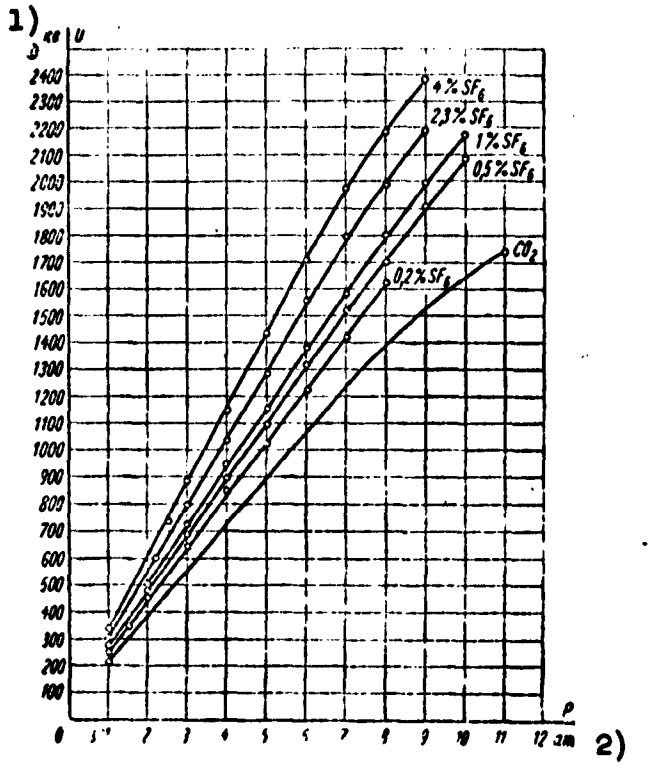

Fig. 6. Sparkover voltage as a function of pressure in mixtures of carbon dioxide and "elegaz." 1) kv; 2) atmospheres.

Figure 6 presents curves of the sparkover voltage as a function of pressure in mixtures of carbon dioxide with "elegaz" for various volume contents of the latter. The percentage content of "elegaz" was determined by weighing the "elegaz" tank before and after admission of the "elegaz" into the generator tank. The curves correspond to sparkover between the high-voltage 330-mm guide and the protective screen.

As will be seen from the curves, a sharp rise in the sparkover

voltages of the mixture takes place even at very low "elegaz" contents as compared with carbon dioxide; here, an almost linear variation of sparkover voltage with pressure is retained over the entire range of pressures investigated.

Figure 7 shows the sparkover voltages of the mixtures as functions of "elegaz" content in carbon dioxide for various pressures.

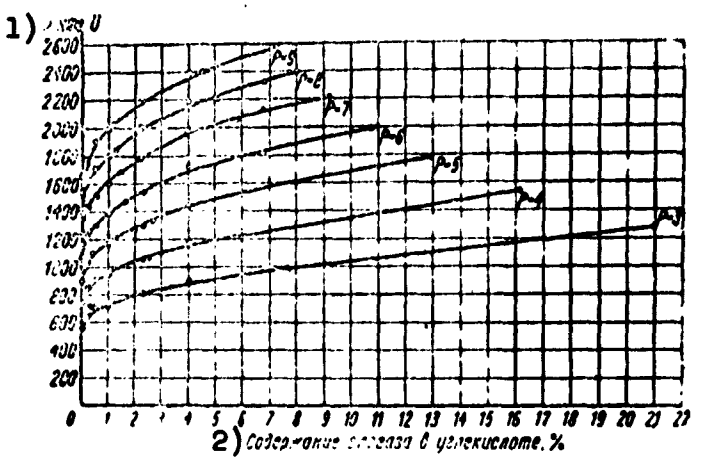

Fig. 7. Sparkover voltage as a function of "elegaz" content in mixtures of carbon dioxide with "elegaz". 1) [kv]; 2) content of "elegaz" in carbon dioxide, %.

A characteristic property of these curves is the very sharp increase in sparkover voltage with increasing content of "elegaz" when very small quantities of it are added to the carbon dioxide. With a further increase in the "elegaz" content, the rise in sparkover voltage is slower. The degree of this retardation for various pressures is excellently illustrated in Fig. 8, which shows the relative increase in the mixture sparkover voltages as compared with pure carbon dioxide as a function of the "elegaz" content in the mixture. A special property of these curves is the extremely rapid drop in their slopes with increasing "elegaz" content, with the slope diminishing more rapidly the higher the pressure of the mixture. Discovery of these properties of mixtures of carbon dioxide with

"elegaz" suggests the expediency of using compressed mixtures with small "elegaz" contents from both the economical and technical standpoints, since there are indications of a certain chemical instability of "elegaz" in the corona and spark discharges [12].

In conclusion, we note that the maximum sparkover voltage in a mixture of carbon dioxide with "elegaz" (2580 kv) was obtained by the present authors at 7.3% SF_6 and 9 atm abs. An average field strength of about 3200 kv/m along the support corresponds to this voltage. Spark discharges along the belt limited any further increase in the generator voltage. It should be noted that with certain individual belts, the limiting sparkover intervened at voltages as low as about 2000 kv. The highest electric-field strengths achieved in the present study are considerably higher than the strengths obtained on the better contemporary electrostatic generators.

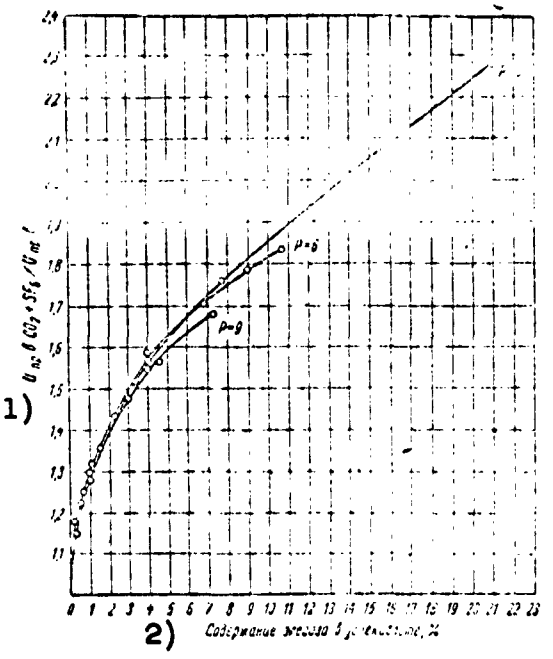

Fig. 8. Relative increase in dielectric strength as a function of "elegaz" content in mixtures of carbon dioxide with "elegaz." 1) U_{pr} in CO_2 + SF_6/U_{pr} in CO_2; 2) content of "elegaz" in carbon dioxide, %.

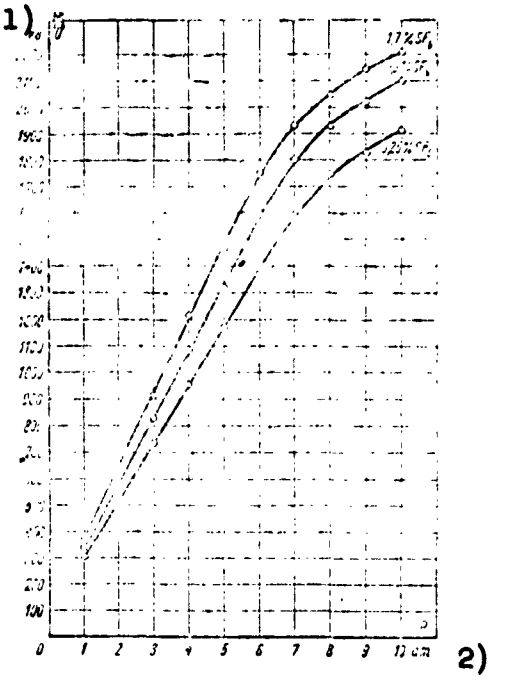

Fig. 9. Sparkover voltage as a function of pressure in mixtures of nitrogen with "elegaz." 1) kv; 2) atmospheres.

f) Mixtures of Technical Nitrogen with "Elegaz"

Figure 9 shows the changes in the sparkover voltage of a mixture of technical gas (N_2 + 8% O_2) with "elegaz" as a function of pressure for various "elegaz" contents. The curves correspond to sparkover between the 330-mm guide and the protective screen. As will be seen from the figure, the addition of a small quantity of "elegaz" to the nitrogen (0.25, 0.9 and 1.7% by volume) sharply raises the sparkover voltage, and even eliminates scattering in the sparkover-voltage value. However, a sharp deviation from linearity in the pressure region above 6 atm abs is also characteristic for these curves. Comparison of the sparkover voltages of mixtures of nitrogen with "elegaz" indicates that the advantage lies with the carbon-dioxide-"elegaz" mixtures at elevated pressures and that these advantages become increasingly marked as the pressure is raised further, since the deviations from linearity of the sparkover voltages of mixtures of carbon dioxide gas with "elegaz" are small at the highest pressures that we studied.

CONCLUSIONS

1. A mixture of nitrogen with "elegaz" may be regarded as the most suitable gaseous insulation for electrostatic generators at pressures below 8 atm abs, and mixtures of carbon dioxide with "elegaz" for higher pressures. It is fully sufficient to add "elegaz" in volumes of 2-10%.

2. In mixtures, nitrogen and carbon dioxide gas possess higher dielectric strength at pressures above 7-8 atm abs than either of the components taken alone. The content of CO_2 in the mixture should not be below 20-25%.

3. It is not advisable to use nitrogen to insulate electrostatic generators.

4. In certain cases, it is possible and expedient to employ pure hydrogen to insulate electrostatic generators.

REFERENCES

1. Trump, J.G., Safford, F.J., Cloud, R.W., A.I.E.E. Trans., 60, 132 (1941).

2. Tramp, J.G., Cloud, R.W., Mann, T.G., Hanson, E.P. Electr. Eng., 69, 961, (1950).

3. Jennings, B., Swartz, C., Rossy, H.H. Rev. Sci., 15, 64 (1944).

4. Buechner, W.W., Van de Graaf, R.J., Sperduto, A., McIntosh, L.R. and Burrill, E.A. Rev. Sc. Instr., 18, 754 (1947).

5. Turner, C., Corc, B., Ballam, J. and Gordon, H. Phys. Rev., 73, 534 (1948).

6. Fortescue, R.L., Gall, P.D., Proc. Instr. El. Eng., part I, 96 (1949).

7. Gorlov, G.V., Gokhberg, B.M., Morozov, V.M., and Otroshenko, G.A. Dokl. AN SSSR (Proc. Acad. Sci. USSR), 102, 237 (1955).

8. Rogers, E.J., Turner, C.R. Rev. Sci. Instr., 24, 805 (1953).

9. Lampfer, R.W., Robinson, G.P. Nucleonics, 10, No. 10, 28, 1952.

10. Noel, J., Felici. Comptes Rendues (Proceedings), 237, 979 (1953).

11. Parkinson, D.B., Herb, R.G., Bernet, E.J., and McKibben, J.L. Phys. Rev., 53, 642 (1938).

12. Schumb, W.C., Tramp, J.G., Priest, G.L. Ind. and Engineering Chemistry, 41, 1348 (1949).

[Footnote]

Manuscript Page No.

29 *Chemical analysis of the commercial foods-grade carbon

Manu-
script
Page
No.

dioxide that we used indicated that its impurity content did not exceed 0.3%.

[List of Transliterated Symbols]

39 пр = pr = probivnyy = puncture, sparkover

B.S. Novikovskiy

VOLTAGE STABILIZATION OF HIGH-CURRENT DIRECT-ACTION ACCELERATORS

Solution of a number of problems posed by contemporary physics requires one-shot accelerators that produce beams of accelerated particles that are admittedly of not particularly great energy (less than 2.5 Mev), but are nevertheless of high intensity. At the present time, construction of such an accelerator with a working current of the order of 10 ma is a pressing problem. What type of accelerator this will be — one based on an electrostatic generator or on a multiplication scheme — is unimportant. What is important is that voltage stabilization be effected in it by a method differing from those presently in use in low-current generators. The use of an electron gun or a controlled corona can hardly be justified in attempts to stabilize a high-current high-voltage source.

Dependable voltage stabilization of an electrostatic generator requires that the stabilizing current amount to approximately 10% of the total current. For an accelerator with a 10-ma output, this means 1 ma. Consequently, several kilowatts of the power developed by the generator will be expended on stabilization, not to mention the other inconveniences associated with the use of an electron gun or an intense controllable corona.

The capacitance method of voltage stabilization is likewise little suited to the present case, since with the small internal resist-

ance (which is an inherent property of the high-current generator), the "liner" system fails to compensate not only protracted, but also relatively rapid oscillations of the generator voltage.

If the high-current accelerator is based on the multiplication system, these stabilization methods become totally useless, since the voltage-multiplication systems respond weakly to changes in load.

A new voltage-stabilization system that makes it possible to stabilize the output of a high-current accelerator has been proposed and tested in principle in our laboratory. The system can be used in accelerators based on the electrostatic generator and the voltage-multiplication system.

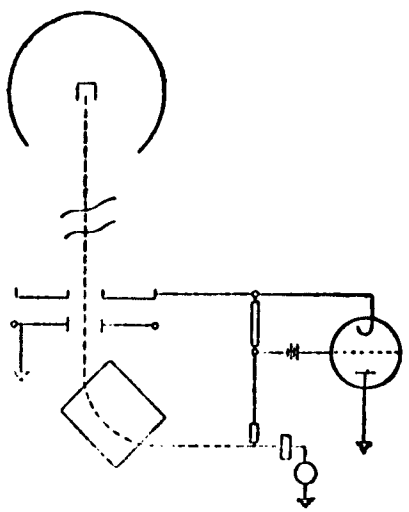

Fig. 1. Schematic diagram of accelerator stabilization using controllable deceleration voltage.

The circuit (Fig. 1) works as follows. The low side of the high-voltage installation (in our case, a voltage-multiplication circuit) was grounded not directly, as is usually the case, but through a high-voltage triode (in our case a GMI-30) whose grid was controlled from the upper plate of the slit diaphragm. (By using a balancing circuit,

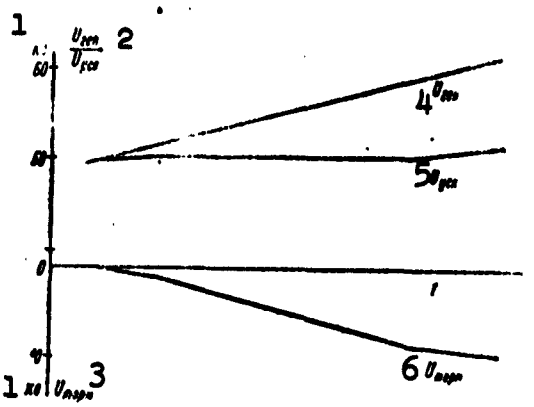

Fig. 2. U_{torm} and U_{usk} as functions of U_{gen}. 1) kv; 2) U_{gen}/U_{usk}; 3) U_{torm}; 4) U_{gen}; 5) U_{usk}; 6) U_{torm}.

it is possible to control the triode from either plate of the slot diaphragm; this increases the precision of stabilization, but we investigated only the principle of this method.) The result is creation of an accelerator-to-ground capacitance system. If we now place the accelerator in oscillation (supply a beam), the accelerator-to-ground capacitance begins to charge and a potential difference arises between the generator zero and the ground; this will increase to a value determined by the grid bias of the triode. The voltage that has arisen between the bottom of the generator and the ground exerts a decelerating influence on the particles of the beam and is therefore known as U_{torm}.

If we were now to proceed in such a way that when the voltage across the generator increases, U_{torm} will increase proportionally and vice versa, we would obtain at the target an energy-stabilized beam of accelerated particles. For this purpose, the beam was rotated in a magnetic analyzer and directed at the target in such a way that part of it settled on the upper half of the slit diaphragm and went to change the triode bias. If now for any reason the voltage on the gen-

erator drops by a certain amount, this will result in an increase in the current through the diaphragm plate, and the triode will begin to block until U_{torm} has been reduced to the same value. The reverse effect occurs when the voltage is raised. Thus, the energy of the particles that leave the target remains almost constant, particularly when the beam is well filtered and the triode has a large gain.

Testing of the circuit on a small accelerator gave the following results (Fig. 2). The variation of the generator voltage within certain limits does not result in any change in the resultant accelerating voltage. The system compensates slow and fast fluctuations of generator voltages quite well; here, the larger the beam current, the more rapidly does the stabilization system respond.

In stabilization by a corona or by means of an electron gun, restoration of a collapsed generator voltage takes place more slowly than depression of a suddenly increased generator voltage, since the stabilization system can respond to a drop in accelerator voltage only by reducing the electron-gun current (or the corona current). But this current is small (15-20 μa), so that when the capacitance of the generator's high-voltage electrode with respect to ground is of the order of a few hundred micromicrofarads, about 0.1 sec is required for restoration of the generator voltage when it is suddenly depressed by several kilovolts. Consequently, a system of this type may prove inadequate to compensate frequent voltage drops, and the voltage drop is the principal deviation that must be corrected in the stabilization system.

In the methods described here, the stabilization system responds rapidly precisely when it is necessary to increase the accelerating voltage, since the depression of U_{torm} takes place in a very short time.

The decelerating voltage U_{torm} not only stabilizes the energy of

the beam, but simultaneously and dependably blocks access of secondary electrons to the tube.

An electron gun or, even better, an ion gun may be used in this stabilization method (instead of the high-voltage triode). We may regulate U_{torm} by regulating the gun current. Use of the gun considerably broadens the range of effectiveness of the system.

Manuscript Page No.

[List of Transliterated Symbols]

44 торм = torm = tormozyashchiy = decelerating

44 уск = usk = uskoryayushchey = accelerating

44 ген = gen = generator = generator

HIGH-FREQUENCY SOURCES FOR ELECTROSTATIC GENERATORS

A. N. Serbinov

The basic advantage of high-frequency ion sources, and that which is responsible for their widespread application, consists in the possibility of producing a high percentage content of monatomic ions with small powers supplied to the discharge chamber of the source. From this standpoint, high-frequency sources have no competition in the region of ion currents below 1 ma.

From 1953 through 1955, we investigated the high-frequency ion source with the object of obtaining a satisfactory design for laboratory accelerators, including an electrostatic generator.

The study was begun with an investigation of the conditions that influence an annular discharge in hydrogen in a transverse magnetic field and the percentage composition of the ions in the frequency range from 10 to 50 Mc and initial pressures in the discharge chamber from 1 to $4 \cdot 10^{-2}$ mm Hg. Then we investigated the properties of the probe scavenging system. Below we discuss the basic results of the studies, which may be useful in designing and building high-frequency sources for electrostatic generators.

Let us pause to consider the conditions of self-initiation of the source discharge. As we know, self-initiation of an annular discharge is possible only in cases where it is preceded by some process that produces a large number of electrons in the discharge chamber.

In our case, this process was the linear discharge that arises under the influence of a high-frequency electric field between the edges of the coils in the tank circuit.

As was shown by the studies of Gill and Engel [1], and later by Hatch and Williams [2], the appearance of a linear discharge and low pressures depend heavily on the ability of the elctrodes to emit secondary electrons and on the interelectrode distance. A discharge may arise in cases where the time required for a group of electrons to cross the gap and for secondary electrons to appear at the surface of the electrode is slightly longer than one-half of a period, and the number of electrons increases from period to period until it is adequate to ionize the gas. If the emission of secondary electrons ceases before the sign of the field is reversed, the process ceases, and even very high field strengths of the order of 300 v/cm are incapable of initiating the discharge, i.e., there exists a "frequency boundary" for the discharge gap below which it is extremely difficult or impossible to initiate discharge.

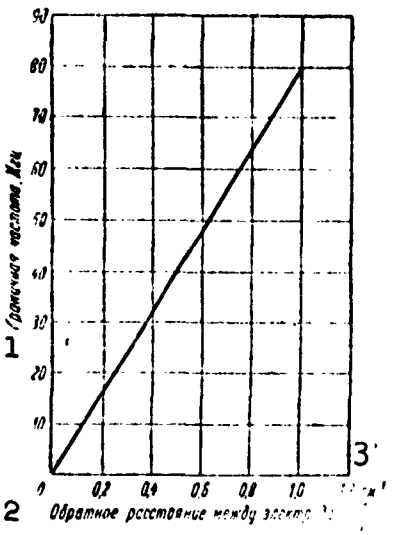

Fig. 1. Variation of "boundary frequency" (Mc) as a function of reciprocal of distance between electrodes. 1) Frequency boundary, Mc; 2) reciprocal of interelectrode distance, 1/d; 3) cm^{-1}.

In the case of an ion source, this gap is the height of the discharge chamber, and the electrodes from which emission of secondary electrons takes place are its walls. Consequently, in designing the source, we must make sure that the "boundary frequency" of the chamber will be lower than the generator frequency. The minimum height of the chamber may be determined from a diagram showing the "boundary

frequency" as a function of the reciprocal of the interelectrode gap (Fig. 1), which we have borrowed from the work of Hatch and Williams.

Experiments have shown that contaminating organic films on the surfaces of quartz or pyrex possess lower secondary-electron emissions than clean surfaces, so that initiation of the discharge becomes difficult when the chamber is dirty.

Thus, independent initiation of the source discharge is ensured only in cases where the generator frequency is higher than the chamber's "boundary frequency," and the wall surfaces are clean.

Let us now consider the conditions determining the behavior of the power in the source discharge chamber.

In the presence of a transverse magnetic field, we observe resonance absorption of the discharge power, this absorption depending on the amplitude and frequency of the high-frequency field, the gas pressure, and the strength of the transverse magnetic field. The resonance value of the magnetic field depends basically on the diameter of the discharge chamber and intervenes for chambers 30 to 50 mm in diameter at the magnetic-field strength at which the electron cyclotron frequency ω_v is 2 – 3 times the frequency ω of the high-frequency field. A larger frequency ratio corresponds to larger diameters. Since

$$\omega_v = \frac{eH}{m}, \text{ and } \omega_v/\omega = 2 \div 3$$

then, expressing the generator frequency in Mc, we obtain the resonance value of the magnetic-field strength in oersteds:

$$H = (0{,}7 \div 1{,}1) f, \text{ oersteds.}$$

The nature of power absorption by the discharge may be illustrated by a diagram (Fig. 2) on which the power absorption by the discharge is plotted as a function of the transverse magnetic-field strength for a frequency of 30 Mc and a pressure of $6 \cdot 10^{-2}$ mm Hg. The parameter is the anode voltage of the high-frequency generator, which

was proportional in this case to the amplitude of the high-frequency field strength. Similar patterns are also observed for other frequencies and pressures, but the power-absorption maximum always corresponds to a definite ratio.

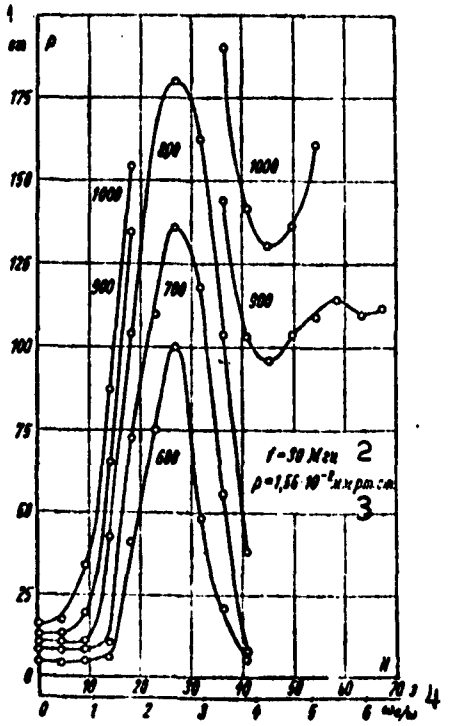

Fig. 2. Power absorption by an annular discharge as a function of transverse magnetic-field strength with a frequency of 30 Mc and an initial gas pressure of $1.5 \cdot 10^{-2}$ mm Hg. The parameter is the anode voltage of the high-frequency generator. The discharge chamber diameter is 50 mm. 1) Watts; 2) f = 30 Mc; 3) p = $1.56 \cdot 10^{-2}$ mm Hg; 4) ω_v/ω.

Figure 3 shows the variation of the high-frequency generator's anode voltage as a function of magnetic field for this same frequency with the condition that the power absorbed by the discharge remains constant. As will be seen from the diagram, the smallest high-frequency field-strength amplitude that maintains a given power level is required at resonance. The results obtained confirm those of Kuch and Neuert [3] as regards the resonance field value. To ascertain the advantages of using an annular discharge in a transverse magnetic field, let us examine a diagram (Fig. 4) on which the power absorbed by the discharge is plotted as a function of pressure for various frequencies. In one case, the annular discharge was excited without the magnetic field, while in the other case it was excited in a transverse magnetic field. It follows from the diagram that the transverse magnetic field increases the power absorbed by the discharge and shifts the burning boundary of the discharge into a region of lower pressures.

If for some frequency we examine diagrams analogous to Fig. 3 for various pressures, the smallest high-frequency field-strength amplitude that provides for maintenance of constant discharge power will correspond to the optimum value for the frequency in question. Figure 5 represents graphically the variation of optimum pressure as a function of frequency. Unlike the no-field annular-discharge optimum chamber pressure, the transverse-field optimum diminishes with increasing frequency.

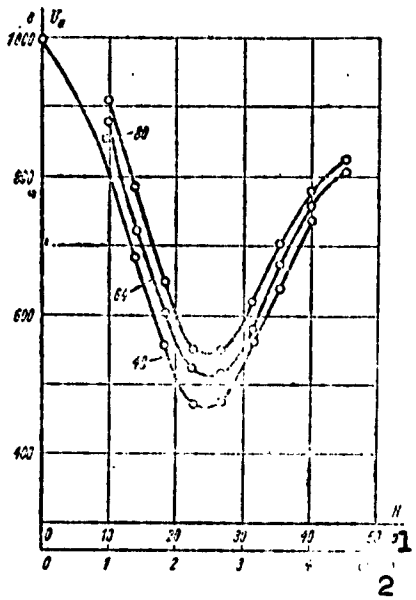

Fig. 3. Variation of anode voltage of high-frequency generator as a function of transverse-magnetic field strength for constant values of the power absorbed by the discharge (48, 64, 80 watts). Frequency was 30 Mc. 1) Oersteds; 2) ω_v/ω.

Thus, when an annular discharge is used in a transverse magnetic field, it is necessary to increase the frequency and amplitude of the field to increase the power absorbed by the discharge in a discharge chamber with a given set of dimensions.

Let us consider the influence of certain factors on the composition of the ion beam.

The content of monatomic ions in the beam is determined by the specific power absorbed by the discharge and by recombination of atomic hydrogen at the walls of the discharge chamber. It increases with increasing specific power and decreases as the recombination coefficient of atomic hydrogen at the discharge-chamber walls rises. Examination of the possible elementary processes enables us to assume that the basic process in formation of monatomic ions in a high-frequency source is apparantly dissociation of hydrogen molecules by electron impact with subsequent progressive ionization of the atomic hydrogen.

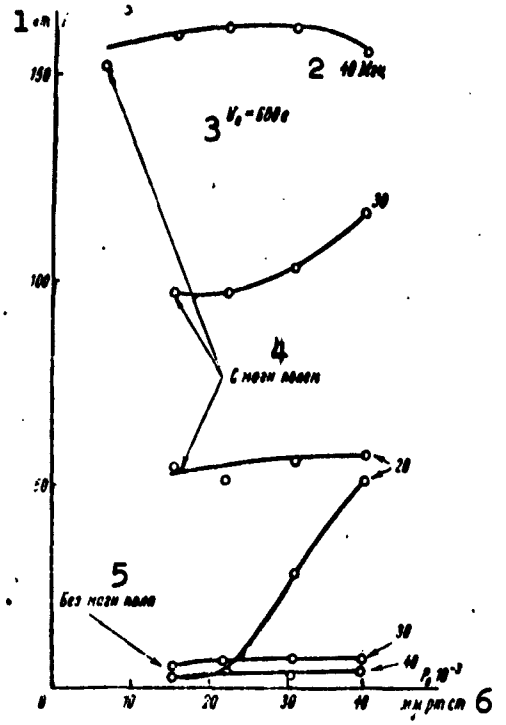

Fig. 4. Absorption of power by an annular discharge with and without magnetic field as a function of initial discharge-chamber pressure for frequencies of 20, 30, 40 Mc and a high-frequency generator anode voltage of 600v. 1) Watts; 2) 40 Mc; 3) U_a = 600 v; 4) with magnetic field; without magnetic field; 6) mm Hg.

In other words, the atomic-hydrogen concentration in the discharge chamber determines the content of the monatomic ion component in the beam.

There exists for each power level an optimum discharge-chamber pressure, at which the content of monatomic ions is at its maximum. In this case, the components H_2^+ and H_3^+ are approximately equal. The H_3^+ content increases with increasing pressure, while that of H_2^+ increases with diminishing pressure.

As the specific power increases, the content of monatomic ions in the beam also increases, but this is accompanied by an increase in optimum pressure. This behavior of the percentage composition makes it possible to establish the optimum pressure in the source on starting the accelerator by mass spectrometry of the beam.

It was found in our investigation of the discharge that a relatively uniform transverse magnetic field sets up a plasma concentration along the magnetic field; this concentration is a red from 10 to 20 mm in diameter. Concentration of the plasma begins after the magnetic field has reached the resonance value and is most distinctly expressed before quenching of the discharge. The state of the discharge is highly unstable in this mode: a samll change in the magnetic field or the amplitude of the high-frequency field results in its extinction.

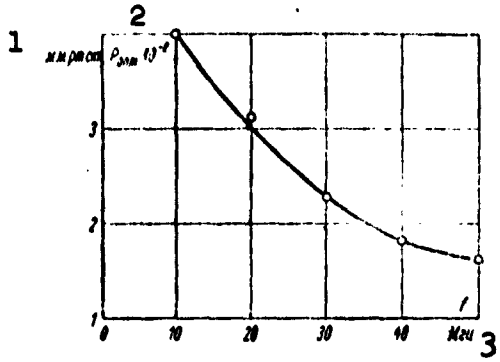

Fig. 5. Variation of optimum gas pressures in discharge chamber in annular discharge in transverse magnetic field as a function of frequency of high-frequency field. Chamber diameter 50 mm. 1) mm Hg; 2) $P_{opt}\ 10^{-2}$; 3) Mc.

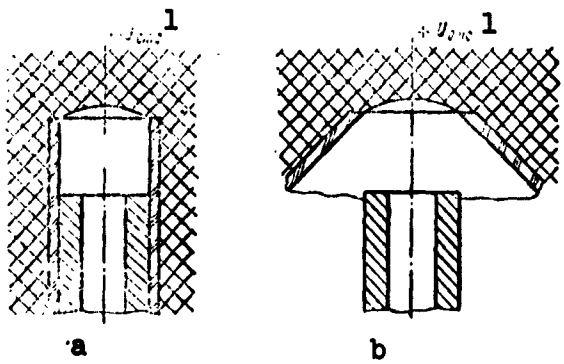

Fig. 6. Diagram of probe scavenging system (a) with insulating cylinder; (b) with insulating diaphragm. 1) U_{ots}.

The second part of the project was devoted to an investigation of the properties of the probe scavenging system (Fig. 6), which has come into extensive use in designs for high-frequency ion sources. This system consists of a scavenging electrode and an insulating cylinder a or diaphragm b, which separates the scavenging electrode from the discharge plasma. The probe is used to apply to the plasma a positive potential with respect to the scavenging electrode, with the result that the boundary of the plasma shifts from the surface of the scavenging electrode and assumes the form shown diagramatically in Fig. 6. Practically all of the scavenging voltage is applied between the surfaces, and this sets up an ion-optical system that focuses the ions into the channel of the scavenging electrodes.

It might be assumed that the focusing properties of this system depend on the propoetions between its dimensions, which are indicated diagramatically in Fig. 7. The influence of the dimensional ratios L/d, D/d and 1/D and the sharpness of focusing was investigated at two levels of power absorbed by the discharge; the focusing criterion was the ratio

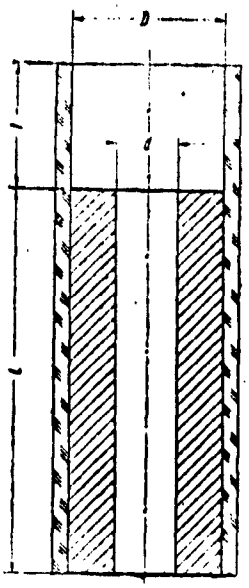

Fig. 7. Designations adopted for dimensions of probe scavenging system.

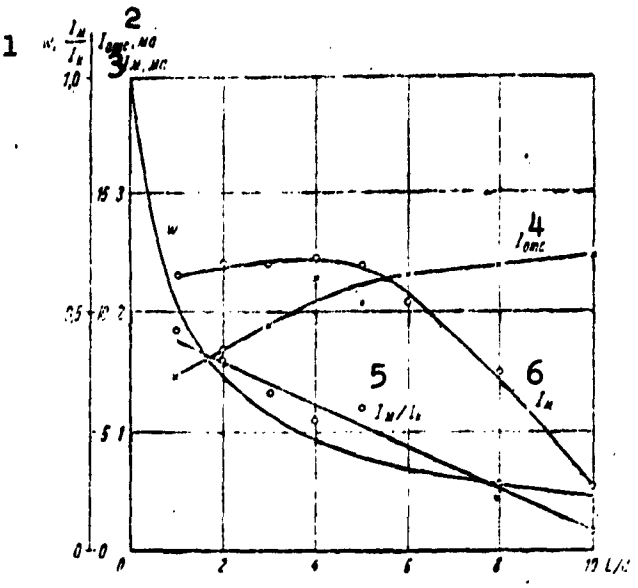

Fig. 8. Influence of ratio L/d on focusing sharpness I_m/I_k, gas flow rate $\underline{w}$, scavenging current I_{ots}, and target current I_m. 1) W, I_m/I_k; 2) I_{ots}, ma; 3) I_m, ma; 4) I_{ots}; 5) I_m/I_k; 6) I_m.

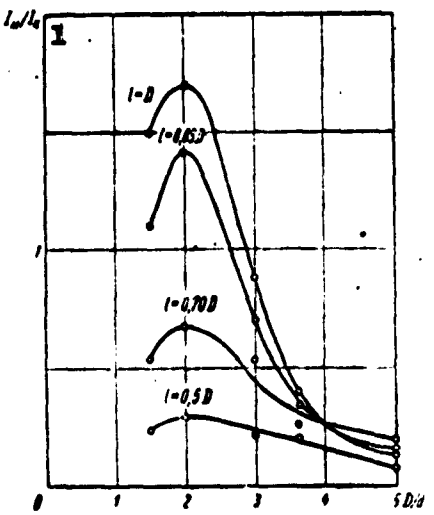

Fig. 9. Sharpness of focusing as a function of ratio D/d for various $\underline{l}$. 1) I_m/I_k.

of the current I_m that had passed through the channel to the current I_k flowing to its walls.

The influence of the channel's length-to-diameter ratio on sharpness of focusing is shown in Fig. 8. To assist comprehension, the variation of the gas flow rate $\underline{W}$, the scavenging current I_{ots} and the target current I_m are also shown here.

It follows from examination of the curves that a relatively sharp increase in gas flow rate begins when the channel length is reduced to less than 4 to 3d. The sharpness of focusing increases almost linearly with diminishing L/d. Clearly, the ratio at which the channel length is 4 to 6 times its diameter will be most favorable for passage of the beam and creation of a pressure gradient.

Figure 9 shows the sharpness of focusing as a function of the ratio between the diameter of the hole in the insulating cylinder and

the channel diameter. The predominance of the insulating cylinder is the parameter. The shape of the curves indicates that a diameter ratio D/d of two is optimal. The following circumstance is worthy of attention: as the ratio D/d diminishes, the optimum scavenging voltage also declines; this facilitates subsequent focusing of the beam considerably. Figure 10 shows the variation of focusing sharpness as a function of scavenging voltage for various ratios D/d. With increasing D/d, the focusing-sharpness maximum is shifted toward higher scavenging voltages.

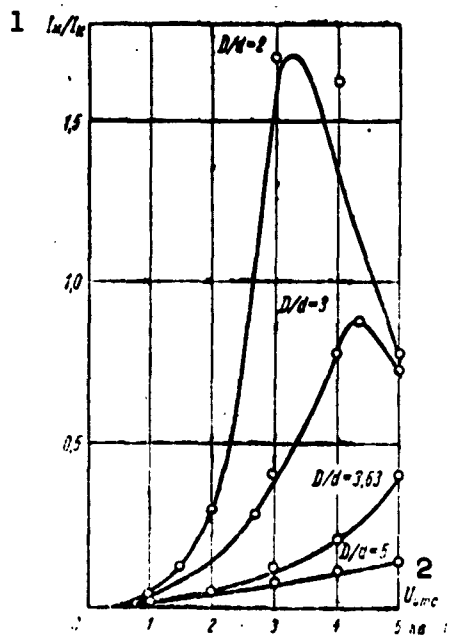

Fig. 10. Variation of focusing sharpness as a function of scavenging voltage for various D/d at a power of 80 watts and $\underline{l}$ = D. 1) I_m/I_k; 2) U_{ots}; 3) kv.

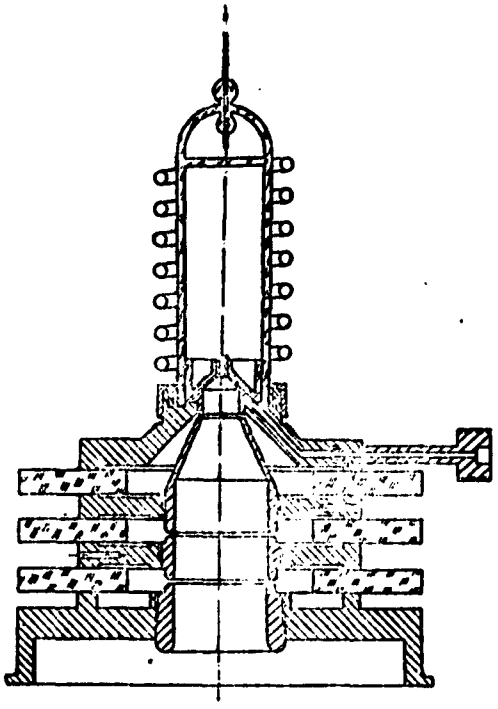

Fig. 11. Design of high-frequency ion source.

The last important ratio – the ratio of the predominance $\underline{l}$ of the insulating cylinder over the plane of the scavenging electrode to the electrode diameter D – is one of the basic factors determining the focusing properties of the system. Focusing properties begin to appear at $\underline{l}$ = 0.5D and increase rapidly as it increases further, but the total

current drops off sharply and the optimum scavenging voltage increases simultaneously. The influence of $\underline{l}$ on the sharpness of focusing is manifested particularily strongly in the region of optimum diameter proportions: at D/d = 2, a change in $\underline{l}$ from 0.5D to D increases the focusing sharpness by a factor of 6. The relationship $\underline{l}$ = D should be taken as the upper limit of the predominance.

Thus, it is necessary to maintain certain dimensional ratios – L/d = 4 to 6, D/d = 2 and $\underline{l}$/D = 0.5 to 1 – in the form of probe scavenging system under consideration.

It is more practicable to reduce the gas flow rate of the source by reducing the diameter of the scavenging electrode, keeping the dimensional ratios optimal.

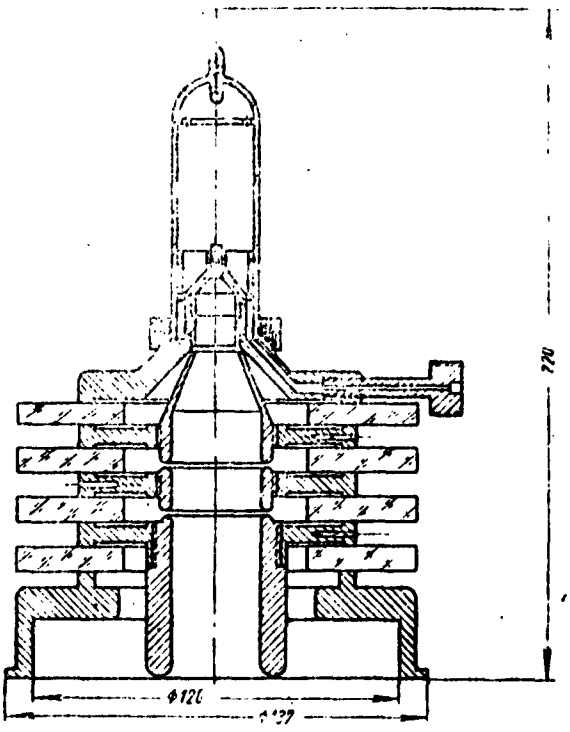

Fig. 12. Design variant of source for EG-2.5.

On the basis of the results obtained, we designed an ion source (Fig. 11) having the optimum proportions for the scavenging-system dimensions and a small discharge chamber. The source is distinguished by the design simplicity of the discharge chamber and the easily exchangeable scavenging system, which makes it possible to use the same source in operation with currents ranging from 100 microamperes to 1 milliampere. The frequency of the high-frequency generator must be no lower than 40 Mc. Like the source designed by V.M. Morozov, the focusing system has a bipolar lens, but it differs from it in that the design provides a strong lens at the scavenging system. Glass disks are used as insulators between the focusing-

Fig. 13. External appearance of source for EG-1.

Fig. 14. External appearance of source for EG-2.5.

system electrodes; this made it possible to reduce the dimensions of the source. The best results obtained with three such scavenging electrodes are assembled in the table.

Figure 12 shows a variant of the electrostatic-generator source design in which the source supply is at the conductor potential. The external appearance of two sources for the EG-2.5 and EG-1 are shown

in Figs. 13 and 14. A special feature of these sources is the increase in electrode-channel length to 8d, as was necessary to reduce the ion current to 100 - 200 microamperes with a power of about 100 watts being absorbed by the discharge. The sources withstood a pressure of 25 atmospheres excess.

TABLE 1

Номер отсасывающего электрода	Диаметр отсасывающего электрода, мм	Диаметр канала, мм	Длина канала, мм	Превышение изолирующего цилиндра над диаметром электрода	Ионный ток, ма	Поглощаемая разрядом мощность, вт	Расход газа при работе источника, см³/ч	Напряжение отсоса, кв	Ток отсоса, ма	Содержание атомарных ионов, %
1	2	1	5	0,65--0,70	0,88	130	4	2,1	2,0	80
2	3	1,5	7,5	0,65—0,70	0,95	126	8,5	2,7	4,0	80
3	4	2	10	0,65—0,70	1,35	125	13	2,7	4,8	80

1 2 3 4 5 6 7 8 9 10 11

1) Number of scavenging electrode; 2) diameter of scavenging electrode, mm; 3) channel diameter, mm; 4) channel length, mm; 5) projection of insulating cylinder above electrode diameter; 6) ion current, ma; 7) power absorbed by discharge, watts; 8) gas flow rate with source in operation, cm^3/hr; 9) scavenging voltage, kv; 10) scavenging current, ma; 11) content of monatomic ions, %.

REFERENCES

1. Gill E.W., Engel A. Proc. Roy. Soc., 197, 107 (1949).
2. Hatch A.J., Williams H.B. J. of Appl. Phys., 25, No. 4, 417 (1954).
3. Kuch B., Neuert H. Zeitschr. fuer Nat. Forsch. [J. Natural Research], Vol. 4a, 456 (1949).

Manuscript page No.

[List of Transliterated Symbols]

49 в = v. Not identified. With letter symbol ω, denotes cyclotron frequency of electron.

51 а = a = anod = anode

53 опт = opt = optimal'nyy = optimum

53 отс = ots = otsos = scavenging

54 м = m = mishen' = target

54 ЭГ = EG = elektrostaticheskiy generator = electrostatic generator

ION SOURCES FOR ELECTROSTATIC GENERATORS IN COMPRESSED GAS

By Ya.M. Fogel', A.M. Markus, V.T. Tolok and Ya.I. Shvarts

GENERAL INFORMATION

The following requirements governed by the needs of various experiments conducted with beams of accelerated particles are set forth for the ion sources of apparatus operating by acceleration of charged particles by a steady-voltage electric field.

1. The ion source must provide for adequate intensity of the accelerated beam at the accelerator output.

2. The ion beam must contain as many monatomic ions as possible in experiments with protons, deuterons, and tritons, or as many doubly-charged helium ions as possible with α-particles.

3. A sufficiently strong ion beam must be formed with a small gas flow into the source.

4. The scattering with respect to energies in the ion beam must be minor.

An electrostatic generator ion source operates in compressed gas under conditions such that the following additional requirements must be set forth for it:

a) long service life,

b) low powering wattage,

c) simplicity of control,

d) small dimensions of the source and its powering system.

These requirements refer to sources operating in the continuous

mode. For sources operating in the pulse mode, these specifications are complemented by the following:

1) the shape of the pulse must be as close as possible to square;

2) the shape and amplitude must be duplicated from pulse to pulse;

3) the pulse duration must be defined.

Three types of sources have hitherto been in use in compressed gas in electrostatic generators: a source with a capillary arc discharge, a magnetic ion source with a cold cathode (Keller and Phillips type) and the high-frequency ion source. The capillary-arc source operates with a hot cathode, so that it has a short service life. This circumstance makes it extremely inconvenient for use in field-type generators. The deficiencies of the capillary-arc source resulted in its going out of service, beginning in the 1950's. Newly built generators are equipped exclusively with Keller or high-frequency sources. In generators built earlier, the arc-type sources are gradually being replaced with sources of these two types. In view of this, the exposition to follow will dwell only on description of the designs and characteristics of the two sources commonly used at the present time – the Keller source and the high-frequency source.

A comparison of the various sources may be made on the basis of the following parameters:

1) the total ionic current;

2) the content of monatomic ions in the beam;

3) the flow of gas into the source;

4) the degree of ionization α of the gas passing through the channel or diaphragm separating the source from the accelerating tube. This quantity may be computed by the formula

$$\alpha = \frac{\gamma}{1+\gamma}, \qquad (1)$$

where

$$\gamma = \frac{M_i}{M_n}, \qquad (2)$$

M_i and M_n are the masses of matter per unit time that have passed through the source channel in the form of the ion beam and the flow of neutral gas.

The quantities M_i and M_n, which are expressed in mg/hr, can be computed by the formulas

$$M_i = 1{,}08 \cdot 10^{15} \frac{m}{e} I, \qquad (3)$$

where m and e are the mass and charge of the ion and I is the magnitude of the ion current in ma, and

$$M_n = 2{,}25 \frac{D^3}{L} P_A \sqrt{\mu}, \qquad (4)$$

where D and L are the diameter and length of the channel in mm, P_A is the gas pressure in the source in units of 10^{-2} mm Hg, and μ is the molecular weight of the gas;

5) the specific supply of power

$$\eta = I/W, \ \mu a/w,$$

where I is the total ion current and W is the supply power to the source;

6) the service life of the source;

7) the energy scattering of the ions in the beam.

The cold-cathode magnetic ion source proposed by Penning and Moubis [1] and improved by Lorrain [2] has been studied in detail in a number of papers by Keller [3-5]. In the Soviet Union, the results of detailed investigation of a source of this type were set forth in a number of surveys by P.S. Markin. The design of the source developed by P.S. Markin has been adopted as the standard for vertical-type electrostatic generators and has been in successful operation for a number of years on the generator of the VG FTI AN UkrSSR. In the USA,

this source is employed in the design developed by Barnett, Evans and Stier [9].

The present authors made certain investigations of a magnetic ion source on a test stand and in a horizontal-type IG-2-410 electrostatic generator and published the results in [10].

A high-frequency ion source was proposed by Tonemann [11], in 1946. From then tc the present time, intensive study of this source has continued on test-stand devices and under the real conditions of accelerator installations. The literature list [12-29] presents only the most detailed studies that have been devoted to this source. We were the first to investigate the performance of a high-frequency ion source under the conditions of the compressed-gas electrostatic generator [21]. A high-frequency, transverse-magnetic-field ion source operating in an ESG in compressed gas was investigated by V.M. Morozov [28]. The foreign literature offers no detailed investigations of the performance of high-frequency ion sources in ESG in compressed gas.

Below we present certain investigations of a cold-cathode magnetic ion source and a high-frequency ion source that were carried out at the FTI AN USSR in 1951-1953.

INVESTIGATION OF COLD-CATHODE MAGNETIC ION SOURCE

Description of Source

A sectional drawing of the source appears in Fig. 1. The discharge chamber is a copper cylinder having an inside diameter of 34 mm, an outside diameter of 40 mm, and a height of 25 mm. An anode in the form of a hollow cylinder is situated inside the chamber. A ring is inserted into the center of this cylinder. The ring and cylinder are at the same voltage and function as the anode. The anode is secured to a copper rod, which serves as the lead-in for the anode

voltage and is insulated from the source housing by a porcelain insulator. The insulator is protected from the atomizing metal by provision of appropriate grooves in the side connecting piece. In addition, the anode cylinder itself serves as an excellent screen for the insulator.

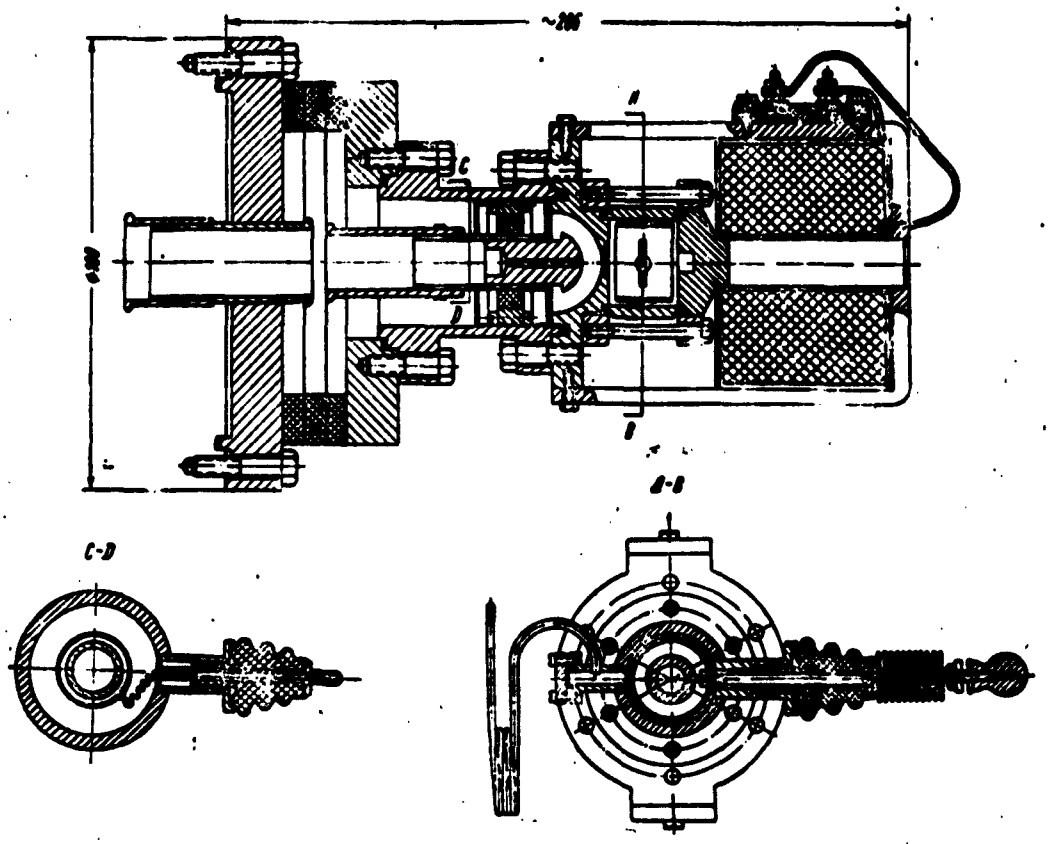

Fig. 1. Sectional drawings of ion source.

The surfaces of the pole pieces of an electromagnet having grooves with the dimensions indicated in Keller's paper [4] serve as the cathodes. The cathode surfaces are lined with Elektron or magnesium. A second side tube brazed into the discharge-chamber wall serves for installation of a manometer tube. The pipeline for supplying gas to the discharge chamber is brazed into this connection piece. The second pole piece has a hole 3 mm in diameter for the emerging ion beam. The drawing electrode has a channel 30 mm long and 3 mm in diameter, the function of which is to provide a pressure drop

between the discharge chamber and the accelerating tube. The surface of the drawing electrode facing the emission hole is made in the form of a hemisphere 12 mm in diameter. The design of the drawing electrode provides for dismantling, so that the gaps can be varied in the necessary range.

The focusing electrode is 5 mm from the drawing electrode and is insulated from it by a short adapter tube cemented together from three porcelain rings. This electrode can also be disassembled and permits varying the corresponding distances.

All elements of the source were fabricated and subsequently assembled in such a way as to maintain coaxiality with the highest possible precision. Particular attention is devoted to coaxiality of the discharge chamber and the drawing-electrode channel. The criterion for proper assembly is free passage of a calibrated three-millimeter rod.

The magnetic field is set up by an electromagnet whose shape and dimensions can be seen from Fig. 1. This electromagnet can be used to produce a magnetic field with strengths up to 600 oersteds in the discharge chamber. If desired, the coil can easily be replaced by a permanent magnet.

Hydrogen is fed into the source through a palladium filter located inside a steel bottle containing hydrogen at a pressure of 6 atm. The bottle contains a quantity of hydrogen such that when it is used at a rate of 10 cm^3/hr, performance of the source is guaranteed for 10 hours each day over a three-month period.

RESULTS OF EXPERIMENTS

The source described in the preceding section was first investigated on the test apparatus whose arrangement is shown in the chapter devoted to the high-frequency source.

TABLE 1

Total Ion Current and Proton Content in Beam as a Function of Gas Pressure

1 Давление, *мм* рт. ст.	$4{,}5 \cdot 10^{-3}$	$9 \cdot 10^{-3}$	$1{,}7 \cdot 10^{-2}$	$2{,}3 \cdot 10^{-2}$	$3{,}5 \cdot 10^{-2}$	$5 \cdot 10^{-2}$	$7{,}5 \cdot 10^{-2}$
2 Поток газа, *см³/ч*	5	10	18	22	42	62	92
3 Общий ток, *мка*	65	115	120	82	72	52	40
4 Содержание протонов, % . . .	14,5	18,6	20,5	24,8	26,6	44	48

1) Pressure, mm Hg; 2) gas flow, cm^3/hr; 3) total current, μa; 4) proton content, %.

TABLE 2

Total Ion Current as a Function of Focusing-Electrode Potential

1 Вытягивающее напряжение, *кэв*	5,4	5,5	5,5
2 Фокусирующее напряжение, *кэв*	0	0,4	0,25
3 Общий ионный ток, *мка*	160	175	180

1) Drawing voltage, kev; 2) focusing voltage, kev; 3) total ion current, μa.

Table 1 lists data illustrating the total ion current and proton content of the beam as functions of the gas pressure in the source and, consequently, of the gas flow.

The data listed in Table 1 were obtained at a magnetic-field strength of 240 oersteds and a drawing-electrode potential of 5-6 ev.

The dependence of total ionic current on the focusing-electrode potential at a magnetic-field strength of 240 oersteds and a gas flow of 10 cm^3/hr is shown in Table 2.

The total ion currents listed in Tables 1 and 2 were measured after the ion beam had been accelerated to an energy of 40 kev. The

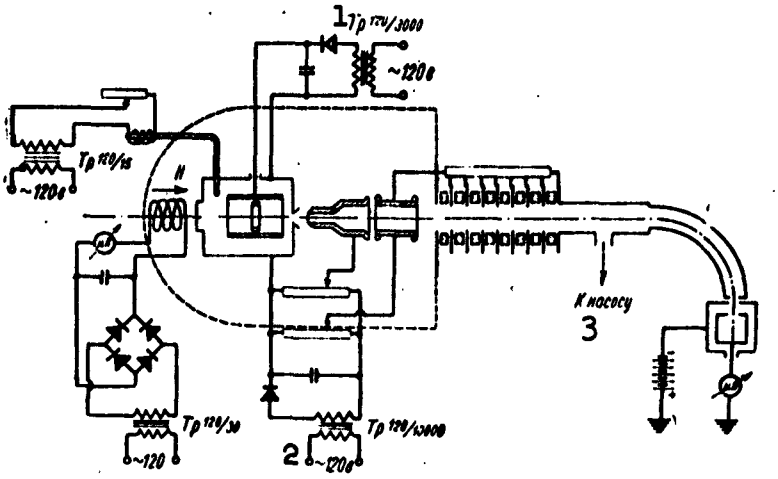

Fig. 2. Electric circuitry of ion source. 1) Tr 120/3000; 2) 120 v AC; 3) to pump.

Fig. 3. Mounting of ion source with adapter tube on accelerating tube of generator.

Faraday cylinder that was used to measure the current was situated at a distance of one meter from the source.

After the source had been tudied on the test apparatus, its performance was investigated in an IG-2-400 horizontal electrostatic generator. The electric circuitry of the source is shown in Fig. 2. The power supply was provided by a polyphase generator with type G-24 permanent magnets that developed an alternating voltage of 135-150 v and a frequency of 500 cycles at 3300 rpm.

Together with the adapter tube for the focusing electrode, the ion source was mounted on the generator's accelerating tube. In view of its low weight, it was simply suspended from the tube (Fig. 3). The accessory apparatus to the source was placed on an aluminum slab secured to the column lugs by three clamps (Fig. 4).

It is necessary to regulate three elements in order to regulate

Fig. 4. Mounting of source apparatus.

the ion-beam parameters: the heating of the palladium filter and the drawing and focusing voltages. We regulated these elements by the use of kapron cords and miniature motors with reducing gearing.

Over a three-month period, the source worked for a total of 300 hours without having to be taken down once. With a gas flow of 8 to 10 cm^3/hr, the total ion current at the accelerating-tube output was 130-140 μa. Focusing of the beam was satisfactory (the diameter of the luminescent spot on the quartz screen was 3-5 mm). A 5-μa proton current can be obtained after the magnetic analyzer at the tube outlet.

INVESTIGATION OF HIGH-FREQUENCY ION SOURCE

Description of Experimental Apparatus

In selecting a high-frequency source for installation in the electrostatic generator, we settled on the source proposed by Tonemann [14], introducing certain modifications into its design. A section of the high-frequency source that we used appears in Fig. 5. The source housing 1 was fabricated from pyrex or quartz. The housing diameter is 30 mm and its length is 200 mm. The plate for applying the drawing potential to the source is the 1-mm tungsten wire 2, which

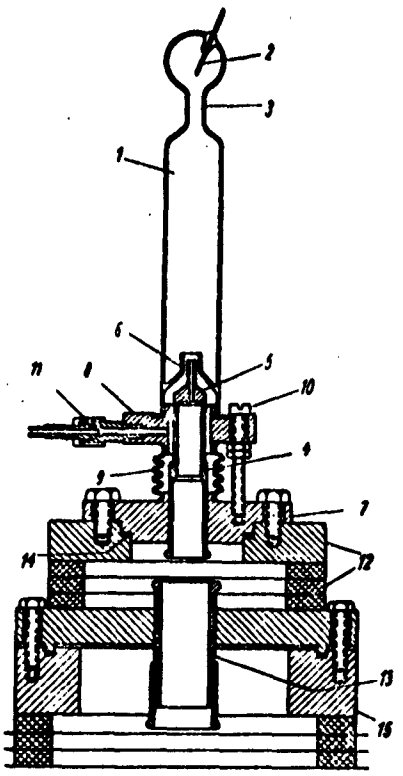

Fig. 5. Construction of high-frequency ion source. 1) Housing; 2) anode; 3) neck; 4) cathode; 5) cathode terminal piece; 6) screen; 7) source flange; 8) upper flange; 9) bellows; 10) adjusting screws; 11) nipple; 12) tube; 13) focusing electrode; 14) gasket; 15) flange.

is sealed directly into the glass when a pyrex bottle is used, and, in the case of the quartz bottle, is welded to a molybdenum strip fused through the quartz. The neck 3 is 20 mm long and 12 mm in diameter. Its purpose is to reduce the flow of hydrogen molecules formed as a result of recombination at the surface of the anode into the discharge space.

The cathode 4 is a copper cylinder with a duralumin terminal piece 5, into which a channel is drilled to set up a pressure gradient between the discharge space and the space for focusing and accelerating the beam. The end of the duralumin cathode adapter is inside the glass screen 6, which has a 6-mm inside diameter. The outside diameter of the adapter is 5 mm.

The cathode is screwed into the lower source flange 7. The source housing is sealed at the upper source flange by a rubber gasket and a pressure ring. The gasketing technique is shown in Fig. 6.

The upper and lower flanges of the source are connected to one another by the bellows 9. The bellows and the three screws 10 are used to regulate the position of the cathode adapter relative to the screen 6, a factor of great importance. Hydrogen is admitted to the source through the nipple 11 in the upper source flange. At its lower flange, the source is seated on the flange of the small tube 12,

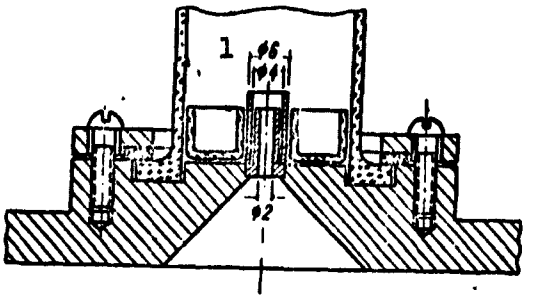

Fig. 6. Method of sealing source housing at upper flange. 1) Diameter 6 [mm].

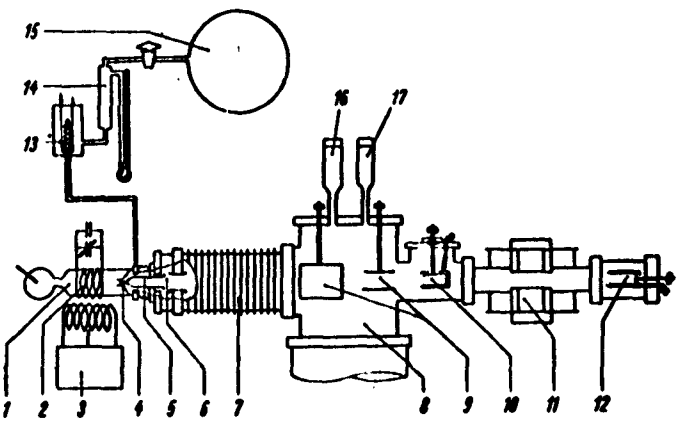

Fig. 7. Diagram of test apparatus. 1) High-frequency source; 2) energizing circuit; 3) high-frequency generator; 4) screen; 5) cathode with channel; 6) focusing lens; 7) accelerating tube; 8) chamber; 9) corrector; 10, 12) Faraday cylinders; 11) magnetic analyzer; 13) palladium filter; 14) instrument for measuring hydrogen flow rate; 15) flask with hydrogen; 16) LT-2 tube; 17) LM-2 tube.

which consists of three porcelain rings and serves as a mount for the focusing electrode 13. Figure 5 shows the adaptation of the entire source system to the flange 15 of the accelerating tube.

During operation, a small fan must be used to blow air over the source bottle.

We studied the performance of the high-frequency source on the test apparatus shown in Fig. 7. This apparatus can be used to determine the total ion current, the proton content in the beam, and the

hydrogen flow rate into the source, as well as for visual observation of beam focusing.

The electric circuit powering the high-frequency source is shown in Fig. 8. An electrodeless discharge was excited in the source by the high-frequency electric field of a coil consisting of four turns of copper tubing 6 mm in diameter. Together with the 30-μμfd capacitor C_1 and the trimmer capacitor C_2, which were connected to it, the coil L_1 forms a tank circuit that is inductively coupled with the coil L_2 (8 turns of six-millimeter copper tubing) of the high-frequency oscillator's tank circuit. After testing several types of high-frequency oscillators, we settled on the oscillator whose circuit is represented in Fig. 8.

This generator is built push-pull around two GI-6-B cermet tubes and is self-exciting. Its wavelength is 15 m. The r.m.s. power in the generator circuit is 150-170 watts. The coil L_3 in the grid circuit consists of five turns of three-millimeter copper wire.

The primary windings of all transformers in the source's supply circuit were fed from a 250-watt, 500-cycle G-24 rotary-magnet polyphase generator. The generator was driven by a motor which was insulated from the generator by a nonconducting V-belt.

Figures 9, 10, and 11 show the test apparatus, the high-frequency source, and the high-frequency oscillator.

RESULTS OF INVESTIGATION OF HIGH-FREQUENCY SOURCE ON TEST APPARATUS

The ion current from a high-frequency ion source as measured by a Faraday cylinder [10] depends (Fig. 7) on:

a) the position of the cylindrical part of the cathode relative to the screen 6 (Fig. 5);

b) the distance of the coil L_1 from the cathode;

c) the hydrogen pressure in the source (or, what is the same

thing, the hydrogen flow admitted into the source);

d) the diameter and length of the channel in the cathode;

e) the magnitude of the drawing and focusing voltage;

f) the magnitude of the r.m.s. power in the coil L_1.

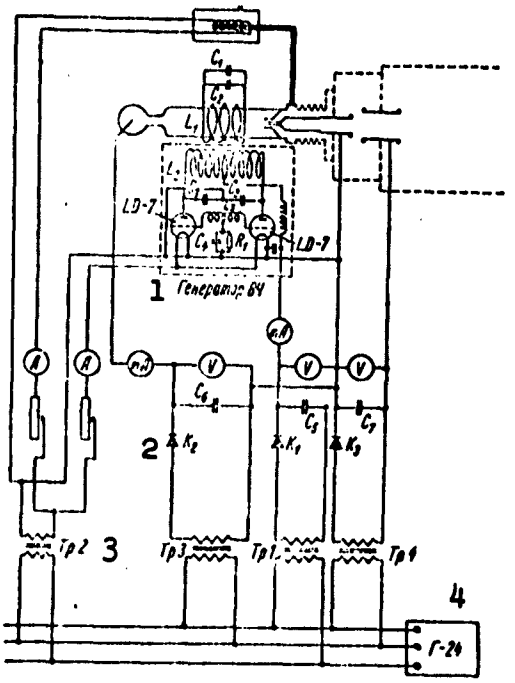

Fig. 8. Electric circuitry powering high-frequency source. 1) High-frequency oscillator; 2) diodes; 3) transformers; 4) G-24.

The composition of the beam depends on the r.m.s. power in the coil L_1, the latter's distance from the cathode, the hydrogen pressure in the source, and the material of the bottle walls.

An important factor determining the magnitude of the total ion current is the position of the cylindrical section of the cathode with respect to the screen. This is not surprising, since the boundary separating the undisturbed plasma from the region of the space charge, the screen, and the face surface of the cathode form an ionic lens that focuses the beam into the cathode channel. Optimum conditions for passage of the beam through the cathode channel prevail when the

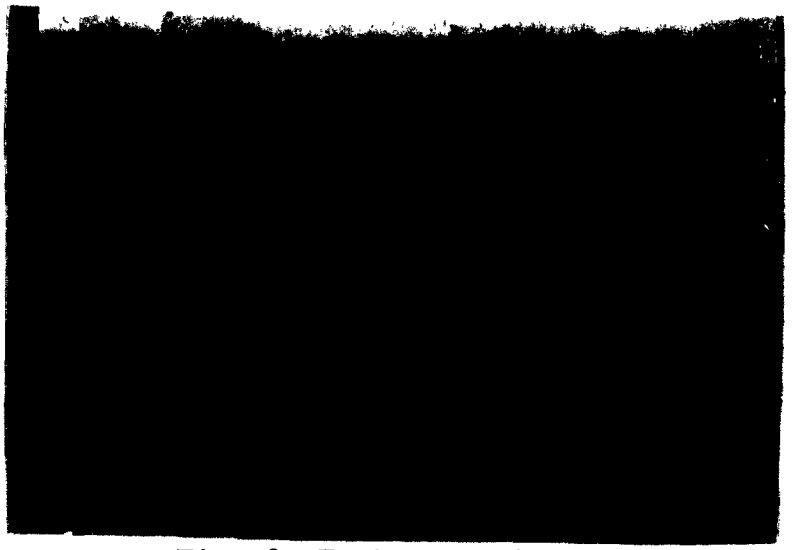

Fig. 9. Test apparatus.

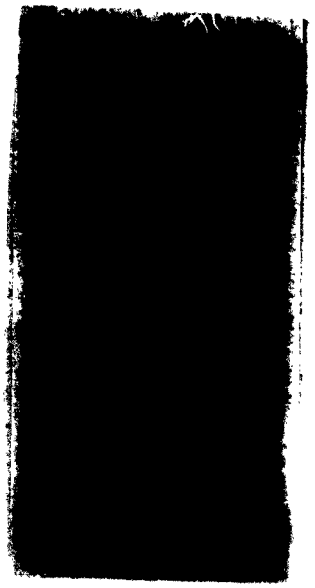

Fig. 10. High-frequency source.

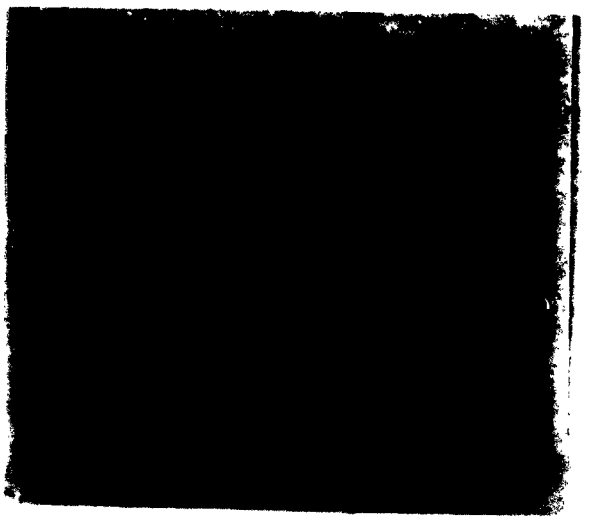

Fig. 11. High-frequency generator.

cathode and screen are rigorously coaxial and when the cathode face plane is at a certain specific distance from the edge of the screen. Normally, the optimum value of this distance is close to the diameter of the channel in the cathode.

It should be noted that if conditions are not adjusted to optimum in the drawing zone, and this situation is characterized by a large discharge current, severe heating of the screen edge (and, if it is made of glass, even melting of the screen) are possibilities; they re-

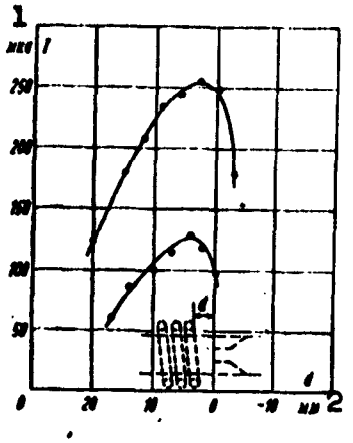

Fig. 12. Total ion current as a function of distance between edge of coil L_1 and edge of cathode. 1) μa; 2) mm.

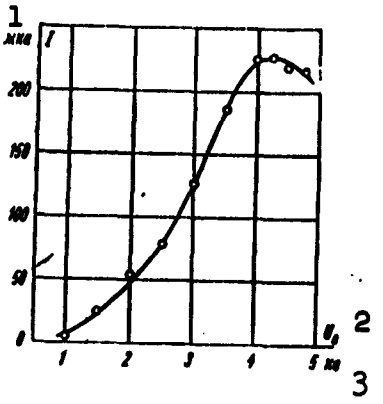

Fig. 13. Total ion current as a function of drawing voltage. 1) μa; 2) U_v; 3) kv.

sult in the source being put out of commission. It follows from this that selection of optimum conditions for drawing ions from the plasma of the high-frequency discharge is extremely important. Only as a result of such selection will the source design provide the possibility of adjusting the position of the cathode with respect to the screen without breaking the vacuum.

Recently, coaxiality between the screen and the cathode channel has been secured by mounting the cathode rigidly and pressing a calibrated quartz tube over it to center the screen mount in the source bottle [17-25]. Such rigid mounting is quite convenient, but requires extremely careful finishing of the surfaces and calibration of all holes in the cathode, quartz tube, and screen and, in the case of unsuccessful fitting, does not offer a possibility of subsequent adjustment during operation.

The total ion current is shown in Fig. 12 as a function of $\underline{d}$ ($\underline{d}$ is the distance between the edge of the coil L_1 and the edge of the cathode); the lower curve is for D = 2 mm and L = 22.5 mm, while the upper curve is for D = 3 mm and L = 22.5 mm (D and L are the

diameter and length of the channel in the cathode).

A typical curve illustrating the total ion current as a function of drawing voltage is shown in Fig. 13.

The total ion current and the beam composition will be seen from the corresponding curves in Fig. 14 as functions of hydrogen pressure.

Figure 15 shows curves of total ion current, discharge current, and the coefficient η as functions of hydrogen flow rate. These curves were obtained for a channel with D = 3 mm and h = 22.5 mm.

Examination of the curves shown in Figs. 14 and 15 permits us to draw the following conclusions:

1) as the hydrogen flow rate increases, the total ion current passes through a maximum, while the discharge current increases monotonically;

2) in this same flow-rate range, the current of H_1^+ ions passes through a shallow maximum, the current of H_2^+ ions diminishes monotonically, and that of H_3^+ ions increases monotonically.

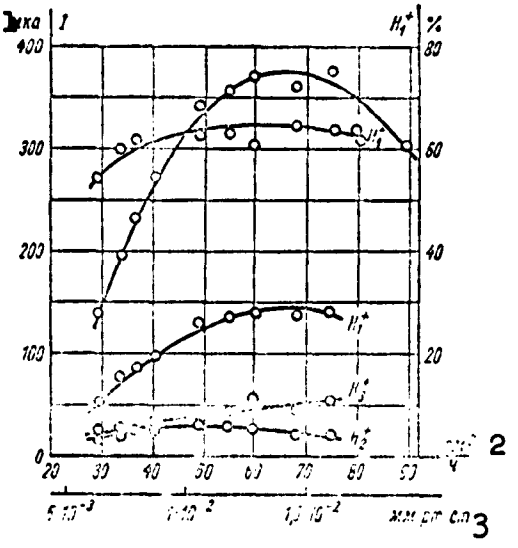

Fig. 14. Total ion current and beam composition as functions of hydrogen pressure. 1) μa; 2) cm^3/hr; 3) mm Hg.

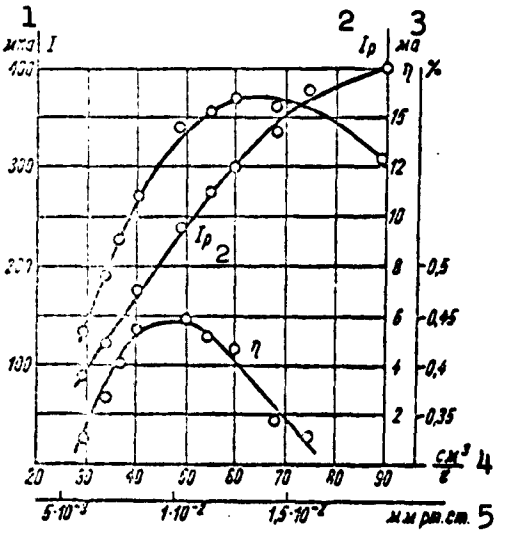

Fig. 15. Total ion current, discharge current, and coefficient η as functions of hydrogen flow rate. 1) μa; 2) I_r; 3) ma; 4) cm^3/hr; 5) mm Hg.

TABLE 3

Working Current as Function of Channel Diameter

1 Номер источника	2 Диаметр канала, мм	3 Максимальный ионный ток, мка	4 Рабочий ионный ток, мка	5 Содержание протонов в пучке, %	6 Рабочий поток, $см^3/ч$	7 Минимальный поток, $см^3/ч$
13	3	375	220	68	36	29,5
14	3	320	220	65	34	27
18	2,6	600	400	77	32	27
20	2	320	200	55	20	14
21	2	330	250	70	20	13
18	2	490	250	65	20	13
22	2	250	200	70	20	13
23	2	690	330	65	21	13,5

1) Source No.; 2) channel diameter, mm; 3) maximum ion current, μa; 4) working ion current, μa; 5) proton content in beam, %; 6) working flow rate, cm^3/hr; 7) minimum flow rate, cm^3/hr.

The continuous increase in discharge current with increasing hydrogen flow rate indicates an increase in the ion concentration in the discharge plasma. The drop observed in the total ionic current is apparently to be accounted for in terms of ion-recharging processes in the channel at high flow rates, the result of which is that an excessive increase of ion concentration in the plasma is countered by a decrease in the number of ions in the ion beam as a result of their recharging in the channel.

The curve shape of Fig. 14 is also observed with other channel diameters, the maximum of the total ionic current shifting toward smaller flow rates with smaller channel diameters.

In an attempt to produce the smallest possible working flow rates, we reduced the channel diameter. It would be expected that the working hydrogen current would be reduced, together with the total ionic current, by a reduction in channel diameter. However, as will be seen from Table 3, the working current was reduced on the reduction in channel diameter, but the total ion current not only did not decrease, but

even increased. This is accounted for by the fact that the electric field focusing the ions into the channel is an extremely important factor. In the case of the reduced-diameter channel, this field was apparently somewhat better matched than in the case of cathodes with larger-diameter channels.

The absence of a heated cathode in the high-frequency ion source enables us to express the hope that its service life will be found quite long. If we disregard the various types of accidental factors, the only effect that might lead to deterioration of the source's performance is cathode sputtering.

Cathode sputtering may be found undesirable for two reasons: a) deposition of the expelled particles on the walls of the bulb may result in an increase in the atomic-hydrogen recombination factor at the walls, and this may have as a consequence a reduction in the number of monatomic ions in the discharge and the beam; b) damage to the surface of the cathode and distortion of its shape may result in deterioration of focusing conditions in the drawing zone and in a drop in ion current.

It should be noted first of all that the rate of cathode atomization depends essentially both on the material of the cathode and on the source's mode of operation.

In our working experience, there were sometimes no traces of cathode atomization in a source that had been working for over 70 hours, while in other cases severe cathode sputtering accompanied by deposition of a metal layer on the source walls was observed even after a few hours of work.

The best materials for the cathode are aluminum and magnesium alloys, and Elektron in particular. The oxide film that forms on the surfaces of these alloys is extremely stable with respect to cathode

sputter.

Since the rate of cathode atomization increases with the speed of the ions bombarding the cathode, it is desirable to work at the smallest possible drawing voltages, consistent, of course, with the necessary ion-current value.

The rate of cathode atomization also increases with increasing mass of the ion. This circumstance must be taken into account in breaking the source in. What happens here is that during the first few hours of operation of the source, its walls evolve considerable quantities of gases. During this stage of the discharge, the plasma contains a considerable number of heavy ions (nitrogen, oxygen, and water-vapor ions and ions of various hydrocarbons), as indicated by data from mass analysis and the presence of banded emission spectra in the emission spectrum of the discharge. In this stage of the breaking-in period, the intensity of the Balmer-series spectral lines of hydrogen is low, and the discharge is pale pink in color. After a few hours of discharge breaking-in, the color of the discharge becomes bright red and the band spectrum fades considerably, while the intensity of the Balmer-series lines rises and mass analysis gives 70% of H_1^+ ions in the ion beam.

While the walls of the source are being broken in by the high-frequency discharge, the drawing voltage should not be applied to them, since bombardment of the cathode by heavy ions of the gases liberated from the walls may result in severe sputtering of the cathode. However, even after elimination of the gas from the source walls, the drawing voltage must be applied with a certain amount of caution, beginning with low drawing voltages and gradually eliminating the gases from the cathode and anode of the source.

The experience at our disposal indicates that deposition of

atomized metal particles on the source walls in the zone of intense high-frequency discharge, i.e., in the region of the walls inside the energizing coil, does not take place. The metal settles on the walls in regions adjoining the zone of intense high-frequency discharge, where the presence of a metallic layer on the walls does not affect either the ion current or the content of monatomic ions in the beam.

It was noted that as the thickness of the atomized-metal deposit on the source walls increases, there is a progressive increase in the working gas flow rate into the source and a certain instability of the current appears.

As concerns damage to the cathode surface as a result of sputtering, this effect was not observed in the overwhelming majority of sources that we investigated in the course of several hours' operation. Only in two sources operating in forced modes (large discharge current, large drawing voltage) was a shallow crater observed on the cathode surface near the entry into the channel. However, we were unable to note any influence of this crater on the performance of the source.

Some of the sources that we studied were put out of commission by melting of the screen. It should be noted on the one hand that this type of melting takes place when focusing conditions in the drawing zone are poor and, on the other hand, that it was observed only in sources with pyrex bulbs. In sealed generators, in which long service life of the source is extremely important, quartz bulbs should be used; melting of the screen was never observed in these sources.

We did not measure the energy scattering of the ions in the beam of the high-frequency source, since such measurements had already been made by Tonemann [14], Neuert [16], and Goodwin [23]. These measurements indicated that the scattering of the ions at a drawing voltage from 3 to 5 kv does not exceed a few tens of volts.

Using the test apparatus, we studied the performance of 40 specimen high-frequency ion sources, taking a large number of measurements. The results of this study enable us to draw the following conclusions:

1. In the steady-state working mode, which can be maintained throughout the working day, the ion source produces ion currents of 250-300 μa with a hydrogen flow of 20-25 cm^3/hr. In a more heavily forced but also stable mode, ion currents of 600-700 μa were obtained with the same hydrogen flow rate.

2. A 60-70% proton content in the beam is reached after a brief running-in period.

3. The results indicated above are obtained with a drawn power of the order of 250-300 watts.

4. Our results indicated the possibility and expediency of setting up the high-frequency ion source in an electrostatic generator under pressure.

Results of Investigation of Performance of High-Frequency Source in Electrostatic Generator Under Pressure

After the high-frequency source had been studied on the test apparatus, it was installed in compressed gas in a horizontal type IG-2-410 electrostatic generator.

The electric circuitry of the source power supply is shown in Fig. 16. It differs from the corresponding circuit on the test apparatus in that the source is powered from two type G-24 generators, thereby eliminating a slight overload observed on the single generator in operation with the test apparatus. In addition, the relay E has been added to the circuit; its function is to cut in the plate voltage of the high-frequency oscillator when a certain time interval (of the order of two minutes) has elapsed after the heat has been thrown into the cathodes of the GI-6-B tubes.

The installation of the source and its power circuit under the conductor of the IG-2 generator are shown in Figs. 17, 18, and 19.

With the source operating under the conductor, four control elements were adjusted from outside: the hydrogen flow rate into the source, the resonance tuning of the circuit exciting the discharge, and the drawing and focusing voltages. All of these elements were regulated by means of kapron cords and miniature motors with reducing gear boxes.

The control system that we adopted required a certain procedure in switching the source on.

1. Before the motor is switched on, the bands of the variac D_1 in the drawing-voltage circuit are pulled out of their zero position; as a result, the contacts p open, the coil circuit of relay E is broken, and, when the conveyor belt is set in motion, the plate-voltage circuit of the high-frequency oscillator is not closed.

2. Setting the conveyor belt in motion switches on the heat to the tube cathodes and the palladium filter.

3. After two minutes, when the tube cathodes have had time to warm up and the hydrogen flow has reached a rate of 20-25 cm^3/hr, the variac D_1 is pulled to zero, the contact p makes and operates the relay E, which closes two contacts simultaneously: the first transmits the plate voltage, while the second shorts the contact p, so that in subsequent adjustment of the drawing voltage, the plate voltage will remain switched on.

Discharge does not always begin at normal gas flow rate when the high-frequency oscillator is switched on. A mirror in the conductor and a periscope system at the control panel make it possible to observe the glow in a neon tube that fires when the high-frequency field appears in the energizing coil, as well as the discharge light in the

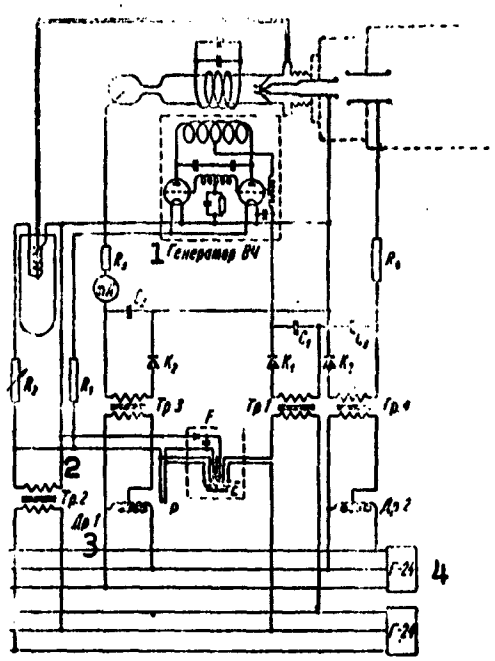

Fig. 16. Electric circuit powering ion source. 1) High-frequency generator; 2) transformer; 3) choke; 4) G-24.

source bulb. If the neon lamp lights up, but the discharge glow is not seen, the hydrogen flow into the source is increased until the discharge is initiated. Then the flow is reduced to its normal value.

4. The discharge is adjusted to maximum intensity by tuning the energizing conductor to resonance.

5. The drawing voltage is switched on. The discharge current is monitored on a milliammeter through an inspection window.

6. The focusing voltage is switched on.

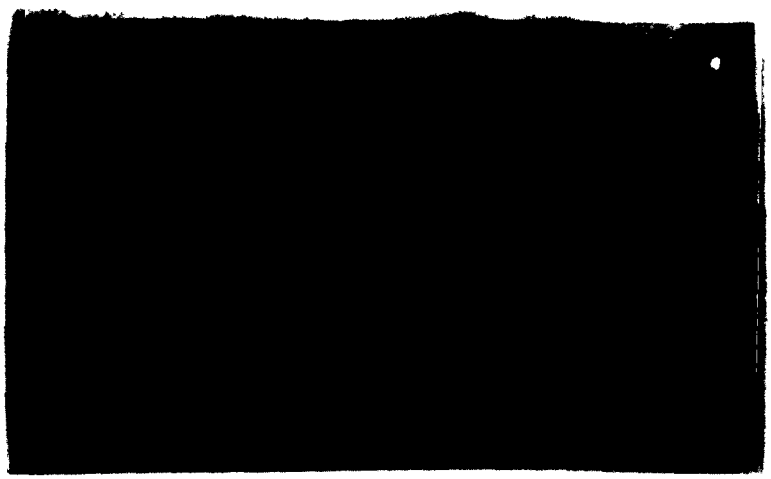

Fig. 17. Installation of high-voltage source.

All these operations require 3-5 minutes, after which the voltage may be fed to the accelerating tube of the electrostatic generator.

An ion source that had previously been thoroughly tested on the test unit was selected for installation in the electrostatic genera-

Fig. 18. Installation of power circuit to high-frequency source under conductor of IG-2 generator.

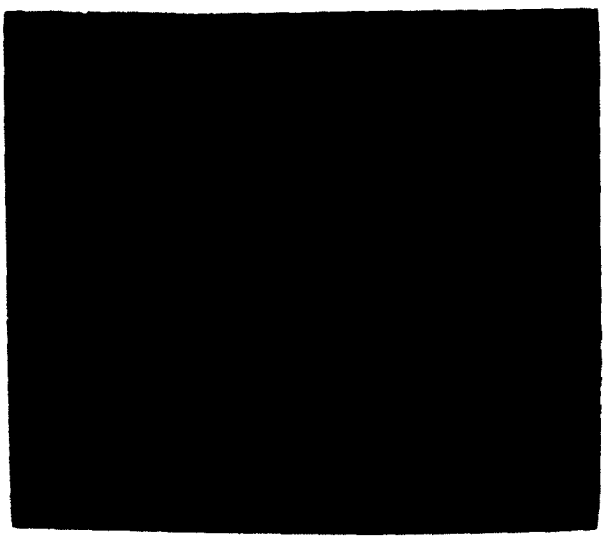

Fig. 19. General appearance of high-frequency source.

TABLE 4

Characteristics of Generator Ion Source

Ионный ток, 1 мка	2 Состав пучка, %				4 Поток водорода, см³/ч
	H_1^+	H_2^+	H_3^+	тяжелые 3 ионы	
600	66,5	15,5	15,5	2,5	23

1) Ion current, μa; 2) beam composition, %; 3) heavy ions; 4) hydrogen flow, cm^2/hr.

tor. Table 4 presents the basic characteristics of this source.

The source and all elements of its power system were first tested in a pressure chamber under a 16-atmosphere pressure.

To measure the total ion current of the accelerated beam, we secured an attachment with a Faraday cylinder 1 (Fig. 20) 50 mm deep and 20 mm in diameter to the exit from the accelerating tube of the generator. The bottom of the Faraday cylinder was cooled with running water. To suppress secondary emission, a 500-v negative potential was applied to the cylinder 2, which was 20 mm in diameter and 20 mm long. The beam entered the Faraday cylinder through the water-cooled diaphragm 3, which was 18 mm in diameter. To determine the position of the beam and study its focusing, the quartz screen 4, which was equipped with crosshairs, was set up before the diaphragm. The screen was watched through the inspection window 8 with the aid of the mirror 9.

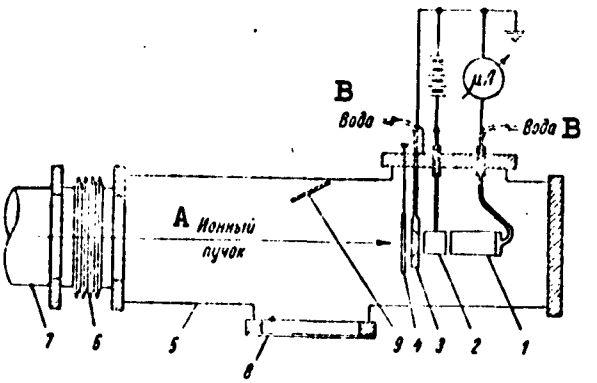

Fig. 20. Diagram showing measurement of ion current. 1) Faraday cylinder; 2) cylinder; 3) diaphragm; 4) quartz screen; 5) diaphragm; 6) guard cylinder; 7) Faraday cylinder; 8) inspection window; 9) mirror. A) Ion beam; B) water.

The results of ion-current measurements made with various generator voltages are shown in Table 5.

The decrease in ion current with increasing generator voltage is

TABLE 5

Results of Ion-Current Measurement at Various Generator-Voltage Levels

1 Ток зарядки, *мка*	2 Ток потенциометра, *мка*	3 Ток короны, *мка*[1]	4 Ионный ток, *мка*	5 Напряжение генератора, *кв*	6 Давление в котле, *атм*
500	30	40	300	600	4,3
460	33	52	235	700	4,3
480	38	125	200	800	6,0
480	49	130	160	1000	6,0

1) Charging current, μa; 2) potentiometer current, μa; 3) corona current, μa;* 4) ion current, μa; 5) generator voltage, kv; 6) pressure in boiler, atmospheres.

TABLE 6

Data from Analysis of Beam as Obtained with Magnetic Corrector

1 Состав пучка, *мка*				1 Состав пучка, %				3 Напряжение генератора, *кв*
H_1^+	H_2^+	H_3^+	2 тяжелые ионы	H_1^+	H_2^+	H_3^+	2 тяжелые ионы	
142,5	35	30,0	5	67,2	16,4	14,1	2,3	700
130,0	35	27,5	2,5	66,7	17,9	14,1	1,3	700

1) Beam composition [sic], μa; 2) heavy ions; 3) generator voltage, kv.

accounted for by deteriorating beam focusing. While it was still possible to focus the beam onto a spot 5-6 mm in diameter with an extremely weak aureole at voltages below 800 kv, focusing deteriorated considerably when the voltage was raised to 1 Mv: the central spot expanded and lost intensity, and the intensity of the aureole increased.

To improve focusing at high voltages, we modified the focusing lens as shown in Fig. 21. This change improved focusing considerably over the entire range of generator voltages.

At voltages below 800 kv, the beam is easily focused into a spot 2 to 2.5 mm in diameter. At voltages of the order of 1 Mv, focusing

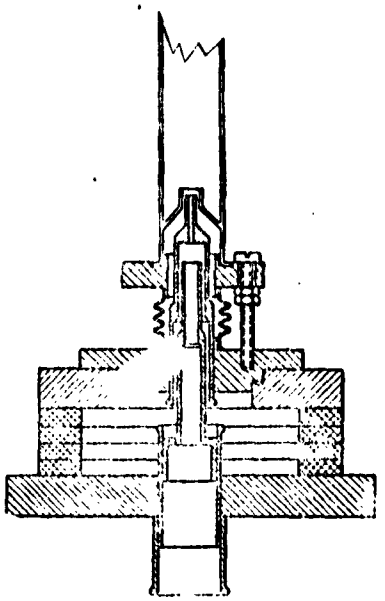

Fig. 21. Design of focusing lens.

deteriorated, but remained satisfactory (central-spot diameter of beam 5 to 6 mm).

To determine the composition of the beam, we employed a double magnetic corrector taking the form of two rigidly secured electromagnets capable of rotating about the tube which served as part of the vacuum line at the output of the accelerating tube. Additional internal pole pieces were set up on rollers inside the tube; these could be turned by the magnetic coupling between them and the external magnetic circuit of the electromagnet. Only one of the corrector electromagnets was used in analyzing the beam. A diagram of the device that we used to determine beam composition is shown in Fig. 22. The magnetic corrector 1 directs

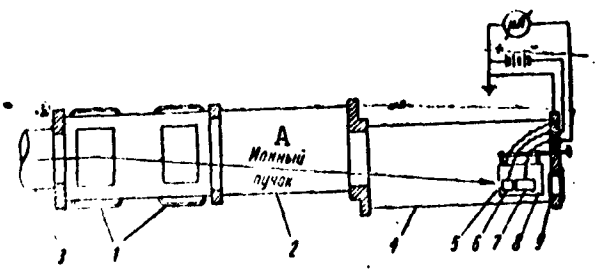

Fig. 22. Diagram of device for determining composition of beam. 1) Magnetic corrector; 2-3) walls of vacuum chamber; 4) chamber; 5) diaphragm; 6) guard cylinder; 7) Faraday cylinder; 8) grounded housing; 9) screen. A) Ion beam.

the deflected beam into the chamber 4. The axis of the measurement system was shifted 10 cm relative to the direction of the undeflected

beam. Basically, the measurement system was the same as that used in measuring total ion current (diaphragm 5, guard cylinder 6, Faraday cylinder 7). Water cooling was not used, since the Faraday cylinder was made from molybdenum. The only essential difference was the fact that the entire system was encased by the grounded housing 8, which served to protect the Faraday cylinder from access of secondary electrons dislodged from the chamber walls. The hole in the housing served as the diaphragm. The entire measurement system was secured to a shaft passing through the bottom of the tube. The entire system could be moved aside by turning it to permit study of beam focusing on the screen 9.

Typical data from beam analysis using the above device are listed in Table 6.

In isolated measurements, the proton current ran as high as 150 μa.

The flow rate of hydrogen into the source was 20-25 cm^3/hr during the measurements. The pressure at the accelerating-tube outlet with the source in operation and with voltage applied to the tube was 6.5 to $7.5 \cdot 10^{-6}$ mm Hg.

This source, with which all experiments on the electrostatic generator were run, operated about 250 hours without showing any deterioration of its characteristics.

Our attention is drawn to the fact that a tube with a uniform field passes a rather well-focused ion beam with a current value as high as 300 μa, while a current of the order of 30 μa passed through the potentiometer.

The results of the present study indicate that

1) the high-frequency ion source can work without trouble for a long time under the conditions of a compressed-gas electrostatic genera-

tor;

2) the use of a high-frequency ion source in the type IG-2-410 electrostatic generator with a uniform-field accelerating tube makes it possible to obtain ion currents up to 300 μa at the generator output with voltages below 1 Mv, together with a proton content of 65% in the ion beam, i.e., proton currents up to 200 μa.

REFERENCES

1. Penning, F.M. and Moubis, J.H.A. Physica 4, 1190 (1937).

2. Lorrain, P. Can. J. of Res. 25, A, 338 (1947).

3. Keller, R. Helv. Phys. Acta 21, 170 (1948).

4. Keller, R. Helv. Phys. Acta 22, 78 (1949).

5. Keller, R. Helv. Phys. Acta 23, 627 (1950).

6. Markin, P.S. Otchet FTI AN USSR [Reports of the Physical-Technical Institute of the Academy of Sciences of the UkrSSR], No. 180, (1950).

7. Markin, P.S. Otchet FTI AN USSR, No. 100 (1951).

8. Markin, P.S. Otchet FTI AN USSR, No. 367 (1952).

9. Barnett, C.F., Stier, P.M. and Evans, G.E. Rev. Sci. Instr., 24, 394 (1953).

10. Fogel', Ya.M. and Markus, A.M., Otchet FTI AN USSR, No. 197 (1951).

11. Tonemann, P.C. Nature 158, 61 (1946).

12. Rutherlen and Cole. Nature 160, 545 (1947).

13. Bayly, J. and Ward, A.G. Can. J. of Res. 26 A, 69 (1948).

14. Tonemann, P.C., Moffatt, J., Roat, D. and Sanders, J.H. Proc. Phys. Soc. 61 A, 483 (1943).

15. Hall, R.N. Rev. Sci. Instr. 19, 905 (1948).

16. Neuert, H. Ztschr. fur Naturforsch. [J. for Natural Research], 4a, 449 (1949).

17. Moak, D., Reese, H. and Guud, W.M. Nucleonics 9, 18 (1951).

18. Fogel', Ya.M., Markus, A.M. and Shvarts, Ya.I., Otchet FTI AN USSR, No. 197 (1951).

19. Fogel', Ya.M., Tolok, V.T. and Shvarts, Ya.I.Otchet FTI AN USSR, No. 247 (1951).

20. Swingle, J.S. and Swann, C.P. Rev. Sci. Instr. 24, 636 (1952).

21. Fogel', Ya.M. and Shvarts, Ya.I. Otchet FTI AN USSR, No. 371 (1952).

22. Fogel', Ya.M., Krupnik, L.I. and Myznikov, K.P. Otchet FTI AN USSR, No. 116 (1953).

23. Goodwin, L.K. Rev. Sci. Instr. 24, 635 (1953).

24. Tonemann, P.C. Progr. Nucl. Phys., Vol. 3, 219 (1953).

25. Reifenschweiler, O. Ann. der Phys. [Annals of Physics], 14, 33 (1954).

26. Banneryee, A.N. Ind. J. Phys. 24, 523 (1953).

27. Eubank, H.P., Peck, R.A., and Truell, R. Rev. Sci. Instr. 25, 989 (1954).

28. Morozov, V.M., Dokl. AN [Proceedings of the Academy of Sciences] 102, 61 (1955).

29. Allan, H.R. and Sarman, N.J. Sci. Instr. 33, 447 (1956).

Manuscript Page No.

[Footnote]

85 *The corona current is the peak current regulating the generator voltage.

Manuscript Page No.

[List of Transliterated Symbols]

62 H = n = neytral'nyy = neutral

63 ВГ = VG [not identified]

63 ФТИ АН УССР = FTI AN USSR = Fiziko-Tekhnicheskiy Institut Akademii Nauk Ukrainskoy SSR = Physical-Technical Institute Acad. Sci. Ukrainian SSR

63 ЭСГ = ESG = elektrostaticheskiy generator = electrostatic generator

67 Тр = Tr = transformator = transformer

SOURCE OF NEGATIVE HYDROGEN IONS FOR AN OVERCHARGING ELECTROSTATIC GENERATOR

By Ya.M. Fogel', L.I. Krupnik, A.G. Koval', and A.D. Timofeyev

INTRODUCTION

The models of negative-hydrogen-ion sources to be described in the present paper are based on the phenomenon in which positive hydrogen ions are converted into negative ions on passage through a supersonic jet of mercury vapor (mercury-jet target). Studies [1, 2], which were carried out earlier in our laboratory and devoted to study of the properties of the supersonic mercury-vapor jet in a vacuum and an investigation of the phenomenon in which positive hydrogen ions were converted into negative ions in this jet, made it possible to approach practical realization of a negative-hydrogen-ion source based on this phenomenon. The basic application in mind in designing this source was its use as a negative-ion injector for an overcharging electrostatic generator. The first model of the injector was designed and built in 1955. Study of this model's characteristics had been basically completed by the end of 1955. On the basis of this investigation, we designed and, by the end of 1956, had built and installed a second model of the injector with a new ion-optical system. Tests of this model had been completed by 1 May 1957.

After familiarizing ourselves with the negative-ion source of Weinman and Cameron [3] (University of Wisconsin), we designed a third injector model. A number of units of this model (positive-ion

source, focusing lens) represent copies of the Weinman-Camoron source. However, we introduced an essential modification in replacing the continuous-flow gaseous target with a vapor-jet target. In this way, we eliminated the necessity of evacuating the source with a high-capacity pump.

FIRST INJECTOR MODEL

Description of Apparatus

Figure 1 shows the construction of the first model of the negative-hydrogen-ion injector. A beam of positive hydrogen ions is created with the aid of an ion gun consisting of the ion source 1 (Fig. 1 shows a cold-cathode Keller-type source), an ion lens 2, and an accelerating tube 3. The ion gun is secured to the flat ground-in joint 4, which makes it possible to shift the ion beam in two mutually perpendicular directions. Thereafter, the ion beam enters the chamber of the electrostatic corrector 5. This chamber houses a pair of crossed plate capacitors that make it possible to deflect the ion beam in two mutually perpendicular directions. The corrector chamber has an inspection window 6, through which it is possible to observe the ion beam by the luminescence that it excites in the residual gas.

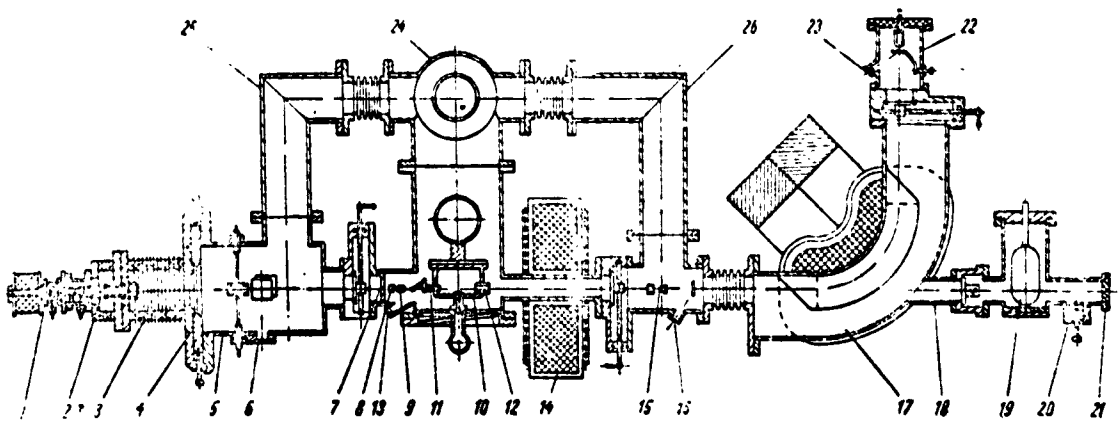

Fig. 1. Construction of negative-ion injector (first model).

Before striking the vapor-jet target, the beam passes through a 9-mm diaphragm 7, and the amperage of the beam is measured by the magnetically controlled Faraday cylinder 9. Secondary electron emission from the Faraday cylinder and from the edges of the diaphragm is suppressed by applying a negative potential (– 300 v) to the cylinder 8. The beam enters the supersonic-jet chamber 10 through the entry channel 11, which is 9 mm in diameter and 30 mm long, and exits from it through channel 12, which is 16 mm in diameter and 40 mm long. The beam diameter can be estimated directly before the entry into the supersonic-jet channel by means of a retractable quartz screen that is visible through the inspection window 13. The axis of the entry and exit channels is at a distance of 6 mm from the exit section of the Laval nozzle. The chamber for the vapor-jet target (Figs. 2 and 3) is described in greater detail in Reference [2].

The ion beam passes through the supersonic mercury-vapor jet and undergoes a certain amount of scattering in the process. The scattered beam is focused by the magnetic lens 14. After passage of [sic] the supersonic stream through [sic] the chamber and the magnetic lens, the beam intensity may be measured with the Faraday cylinder 15. The sharpness with which the beam is focused before entry into the magnetic analyzer 17 may be observed through the inspection window 16. A magnetic analyzer with a radius of 20 cm for the average beam trajectory and a deflection angle of 90° is used to separate a negative-ion beam from the beam that has been transformed on passage of the positive hydrogen ions through the supersonic stream of mercury vapor. In addition, the magnetic analyzer separates the beam of negative hydrogen ions from the beam of mercury atoms that has escaped through the channel 12 of the supersonic-jet chamber. Following rectilinear trajectories, the mercury atoms pass through the side arm 18, which is brazed into

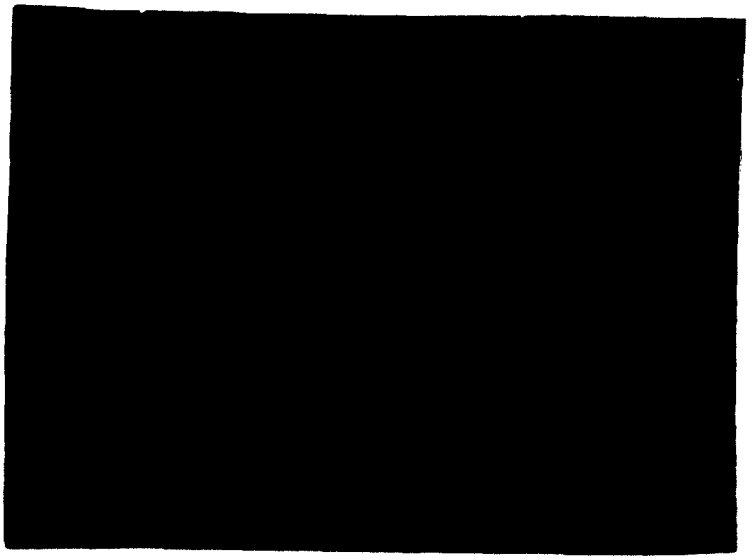

Fig. 2. General appearance of apparatus.

the side wall of the magnetic-analyzer chamber, and condense on the wall of the glass trap 19, which is filled with liquid air. The Faraday cylinder 20 enables us to measure the intensity of the undeflected beam after passage through the sleeve 18. The beam diameter can be estimated by observing the luminescence of the quartz screen through the inspection window 21.

The intensity of the negative-hydrogen-ion beam is measured with the Faraday cylinder 22. The diameter of the beam before entry into the Faraday cylinder may be observed on the quartz screen through the inspection window 23. To permit study of the current and current-density distribution over the section of the negative-ion beam, an externally controlled iris diaphragm (not shown in Fig. 1) is set up in front of the Faraday cylinder. The diameter of the diaphragm can be varied from 3 to 22 mm.

The injector is evacuated by a pump set consisting of type MM-1000, MM-40 and VN-461 pumps through the branch pipe 24, which is connected directly to the MM-1000 pump. To increase the rate of evacuation from the corrector space, accelerating tube, and magnetic-analyzer chamber, these spaces are connected to the side arm 24 by the bypass tubes 25

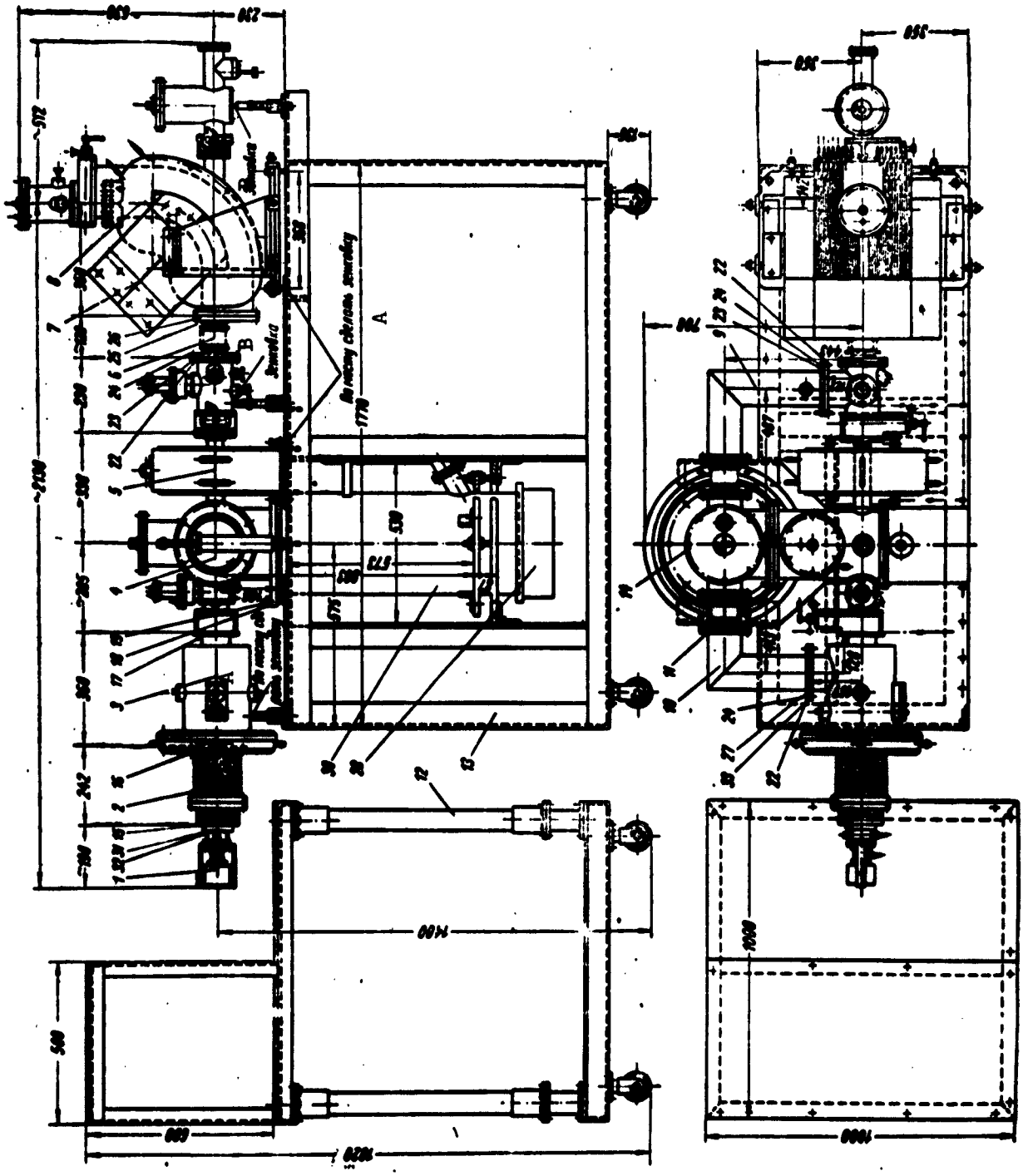

Fig. 3. Diagram of negative-ion source.
A) Countersink to position; B) countersink.

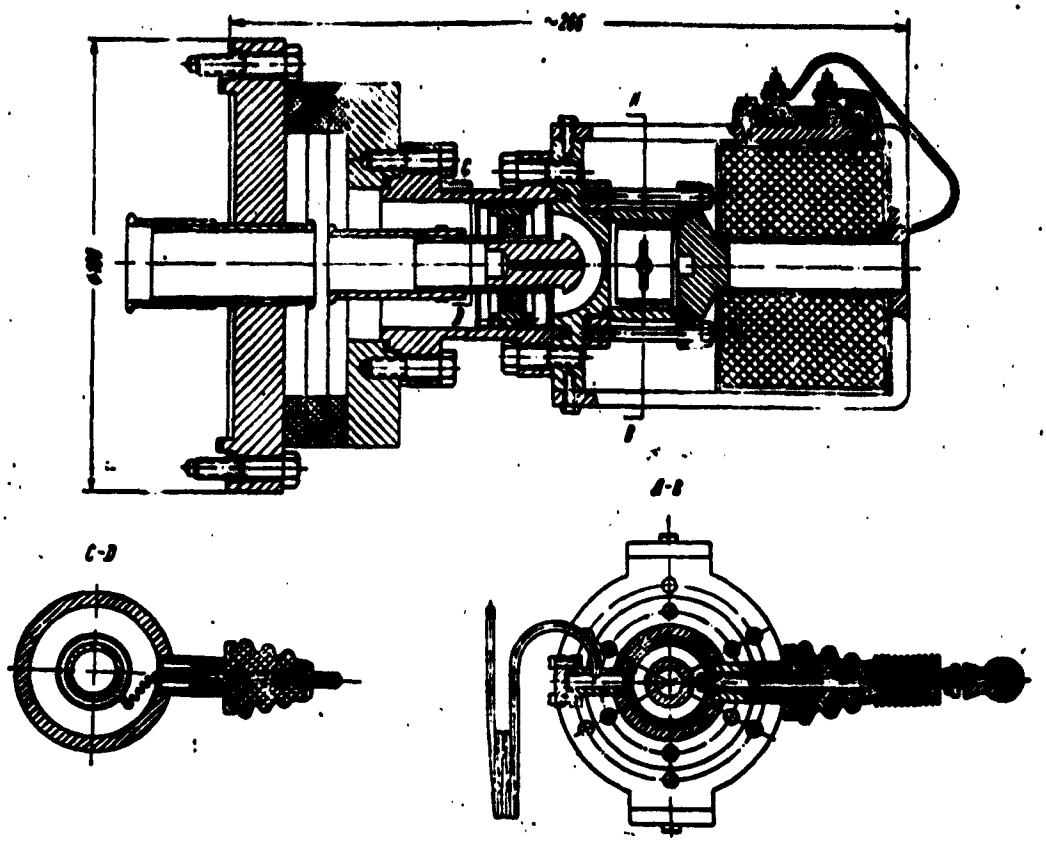

Fig. 4. Magnetic ion source of Keller type with cold cathode.

and 26.

Together with the evacuation system, the injector is mounted on a special stand welded together from angle iron. The dimensions of the apparatus will be seen from Fig. 3, which shows a drawing of the source.

The general appearance of the entire apparatus is shown in Fig. 2.

The apparatus of the system supplying the source with negative ions is situated in a special desk that is insulated from the ground by four isolite cylinders 12 (see Fig. 3).

INVESTIGATION OF CHARACTERISTICS OF FIRST INJECTOR MODEL

Negative-Ion Spectrum

Experiments were carried out on the first model of the negative-

ion injector with three different sources in the ion gun: Keller [4] and Barnett-Evans-Stier [5] cold-cathode magnetic ion sources (sectional drawings of these sources appear in Figs. 4 and 5) and a Reifenschweiler [6] high-voltage source (Fig. 6). An oil-vapor target was used in addition to the mercury-vapor target for conversion of positive into negative ions. The investigation of the oil-vapor target was described in Reference [7]. The relative contents of H_1^+, H_2^+ and H_3^+ ions in the ion beams of these sources are different. Cold-cathode sources produce a beam in which the number of H_2^+ ions is largest; thus, for example, the Keller source produces a beam containing 90% of H_2^+ ions, while the source of Barnett et al produces a beam with 80% of H_2^+ ions. Usually, protons predominate in the beam of the high-frequency ion source (60-70% H_1^+).

In the injector described here, a beam of positive hydrogen ions that have not been resolved with respect to mass enters the vapor-jet target. As a result of this, molecular ions of hydrogen (H_2^+ and H_3^+) can dissociate into atomic particles, some of which can capture electrons to become negative hydrogen ions. As follows from the laws of conservation of energy and impulse, these negative hydrogen ions have an energy equal to one-half and one-third of the energy of the negative hydrogen ions arising from the transformation $H_1^+ \rightarrow H_1^-$.

Figure 6 shows the negative-hydrogen-ion spectrum obtained with the injector's magnetic analyzer during passage of a beam of positive ions from a Keller source through a mercury-vapor target. As will be seen from this figure, three peaks are observed in the negative-ion spectrum: here, the magnetic-field strengths at the maxima of these peaks satisfy the relationship $H_1^2:H_2^2:H_3^2 = 1:\frac{1}{2}:\frac{1}{3}$, i.e., the relationship $E_1:E_2:E_3 = \frac{1}{3}:\frac{1}{2}:1$ prevails for particles with identical values of E^2/m. The peak of the ions with energies E/2 that have arisen from the

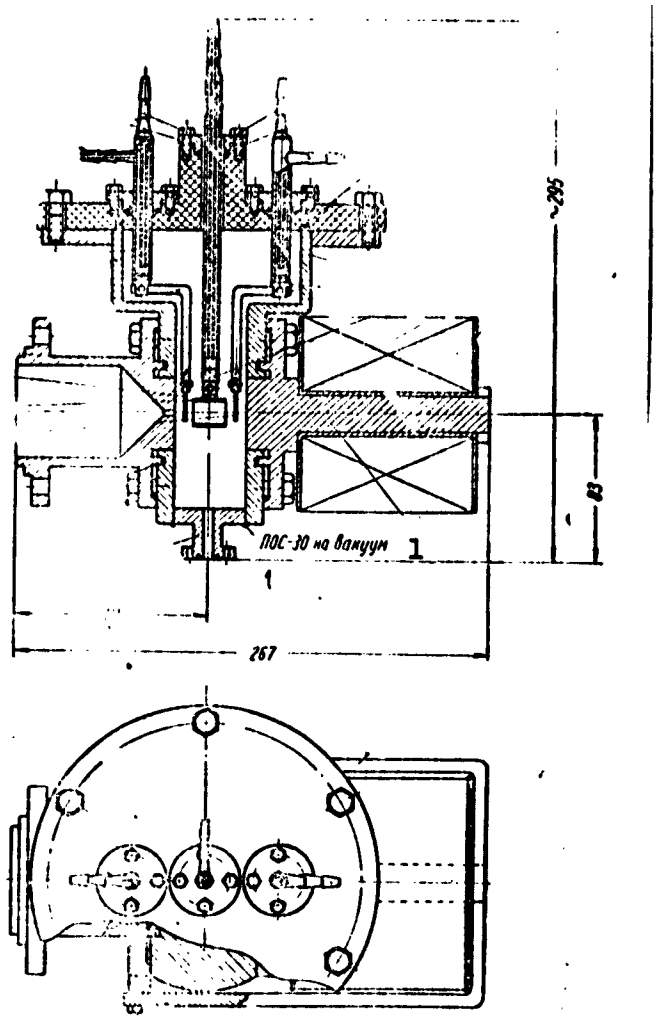

Fig. 5. Evans-Stier-Barnett magnetic ion source.
1) POS-30 for vacuum.

transformation $H_2^+ \rightarrow H_1^-$ is much higher than the peaks with the energies E and E/3, as is readily understood, since the beam of ions from the Keller source consists basically of H_2^+ ions.

The high-frequency source was capable of operating in two modes: in the normal mode, the hydrogen-ion beam contains 60-70% of protons. When the source was fed hydrogen containing impurities, the beam contained 70-80% of H_3^+ ions.

Figure 8 shows the spectrum of negative hydrogen ions obtained on passage of the beam from the high-frequency ion source operating

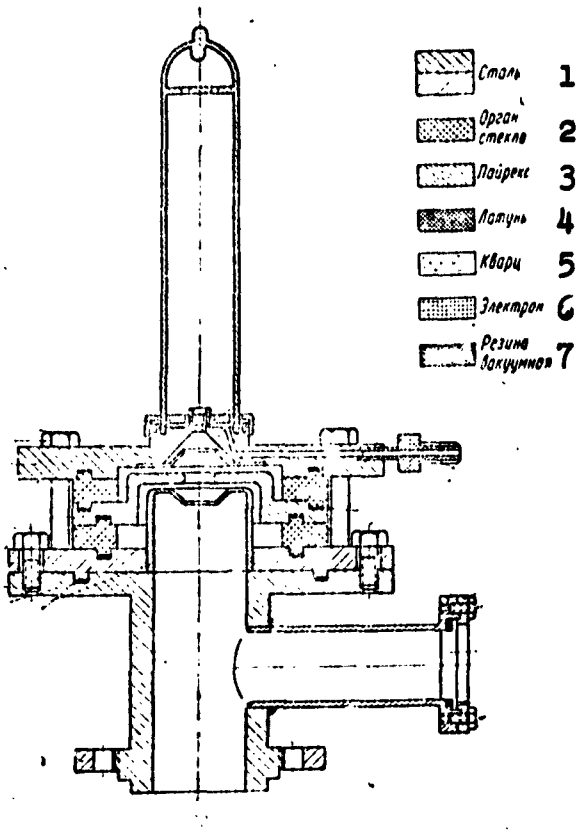

Fig. 6. Reifenschweiler high-frequency source. 1) Steel; 2) organic glass; 3) pyrex; 4) brass; 5) quartz; 6) Elektron; 7) vacuum rubber.

in the normal mode through a jet of vapor from type D1-A vaseline oil. The spectrum of negative ions in the mode with an elevated content of H_3^+ ions (below 70%) is shown in Fig. 9 for passage through a mercury jet. As will be seen from these figures, the largest numbers of negative ions are obtained from the transformation $H_3^+ \rightarrow H_1^-$. Thus, the spectra that we show here indicate that from the viewpoint of producing intense negative-ion beams, the transformation processes $H_2^+ \rightarrow H_1^-$ and $H_3^+ \rightarrow H_1^-$ are more effective, so that we subsequently concentrated our attention on study of these processes.

Conversion Coefficient

A quantity which characterizes the effectiveness with which positive ions have been transformed into negative ions in a given target

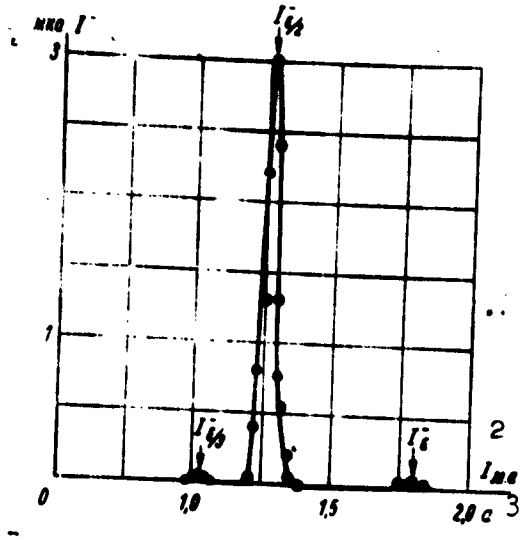

Fig. 7. Spectrum of negative-hydrogen ions as obtained with injector magnetic analyzer on passage of beam of positive ions from Keller source through mercury target. 1) μa; 2) ma; 3) amp.

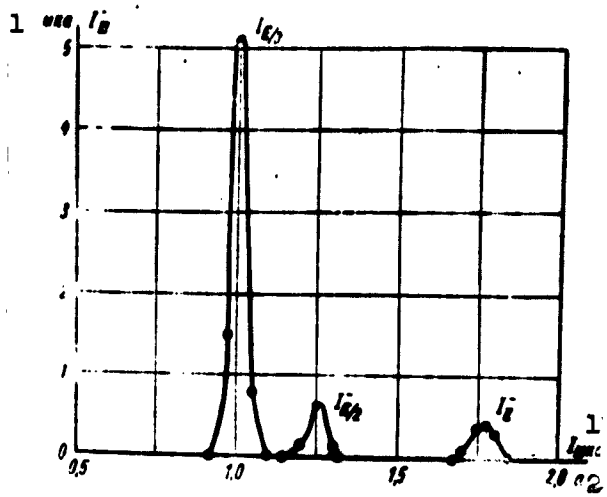

Fig. 8. Spectrum of negative hydrogen ions obtained on passage of beam of positive ions through stream of vapor from type D1-A vaseline oil with source operating in normal mode. 1) μa; 2) amp.

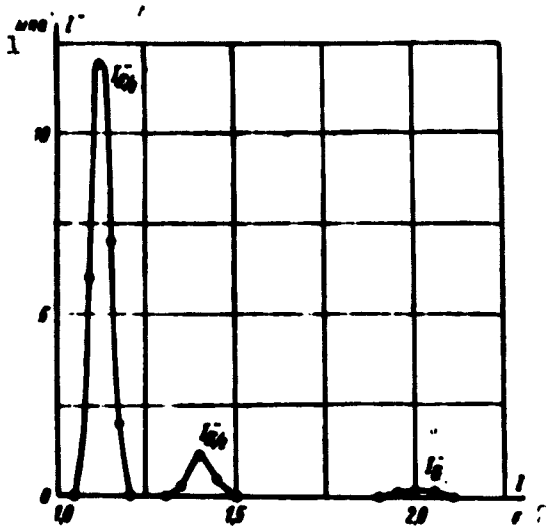

Fig. 9. Spectrum of negative hydrogen ions in mode with elevated content of H_3^+ ions in passage through mercury jet. 1) μa; 2) amp.

is the conversion coefficient, which is defined as the ratio of the number of negative ions in the beam after traversing the target to the number of positive ions that struck the target. As the thickness of the material through which the beam passes is increased, the coefficient of conversion of positive into negative ions increases until an equilibrium composition has been reached in the beam after the target. On reaching a certain target thickness corresponding to the equilibrium composition of the post-target beam, the negative-ion content in it shows its maximum value. Let us denote this coefficient by $(I^-/I^+_{pad})_{max}$. Remembering that

$I^+_{pad} = (I^- + I^0 + I^+ + \ldots + I^{z+})_{prosh}$ ($\underline{z}$ is the ordinal number of the ion), the coefficient of conversion of positive into negative ions may be expressed as

$$\frac{+z! \cdot \cdot \cdot +2!+1!+0!+-1}{-1}$$

Proceeding from these definitions, we may measure the conversion coefficient in either of two ways: 1) by measuring the current of the incident positive-ion beam and the current of the negative component in the beam after the target; 2) by measuring the intensities of all charged components in the beam after the target.

In measuring the conversion coefficient by the first method, it is extremely important that all negative ions that have been formed in the target be focused into the negative-beam receiver. However, the charged particles of the beam are subject to multiple scattering and energy losses on passage through the target. The average scattering angle and energy losses increase with increasing thickness of the target.

These factors, together with certain others (the initial divergence of the beam, the attenuation of the beam as a result of collisions of the ions with residual-gas molecules, etc.) have as a consequence that a number of ions smaller than the number formed in the material enter the negative-ion receiver. In this case, the conversion process is characterized by the real conversion coefficient $(I^-/I^+_{pad})^*$, which depends on the specific experimental conditions. We shall henceforth cite values of the real conversion coefficient as measured by the first method.

With the objective of ascertaining the optimum conditions for the conversion $H^+_2 \rightarrow H^+_1$, we studied the conversion coefficient as a function of the vapor temperature in the boiler, i.e., as a function of the jet thickness. We used Keller and Evans-Barnett-Stier sources to study

this conversion, since the ion beams of these sources consist almost entirely of H_2^+ ions.

Figure 10 shows curves of the conversion coefficient as a function of boiler temperature for various energies in the positive-ion beam. These data were obtained using the Keller-type source.

As will be seen from Fig. 10, the largest conversion coefficient (2.2%) occurs at a boiler temperature of ~160°C (jet thickness $1.4 \cdot 10^{15}$ atoms/cm^2) and at an H_2^+-ion energy of 29.6 kev. The presence of a maximum on the curves of Fig. 10 indicates that we are actually determining the real conversion coefficient, since the true conversion coefficient should be inclined toward saturation as the target thickness is increased. Comparison of the data on the transformation $H_2^+ \rightarrow H_1^+$ with the corresponding data on the transformation $H_1^+ \rightarrow H_1^-$ (see [2]) indicates that the coefficient of the conversion $H_2^+ \rightarrow H_1^-$ is approximately twice the coefficient of the conversion $H_1^+ \rightarrow H_1^-$. This result becomes understandable if we assume that total dissociation of the H_2^+ ions takes place in the jet.

The coefficient of the conversion $H_2^+ \rightarrow H_1^-$ is shown by the curves in Fig. 11 as a function of the energy of the H_2^+ ions for various jet thicknesses. As will be seen from these curves, no dependence of the conversion coefficient on the energy of the H_2^+ ions is observed in the range of energies studied.

A factor of considerable importance for increasing the negative-ion yield is the pressure of the residual gas in that part of the apparatus where the negative ions move, i.e., in the space from the jet chamber to the magnetic-analyzer trap. Figure 12 shows curves of the coefficient of the conversion $H_2^+ \rightarrow H_1^-$ for various residual-gas pressures in the magnetic-analyzer chamber. The lower curve was recorded without the bypass tube 26 (Fig. 1). In this case, the pressure

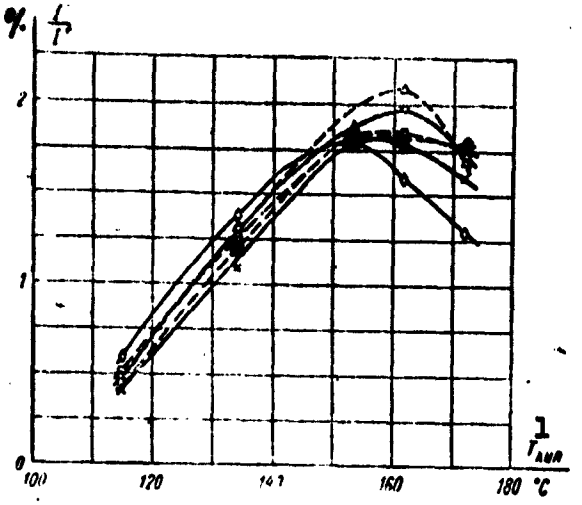

Fig. 10. Conversion coefficient as a function of boiler temperature for various energies of positive-ion beam: ◊) 21.4 kev; □) 26.8 kev; Δ) 29.6 kev; 0) 32.3 kev; ●) 35.3 kev; x) 37.8 kev. 1) T_{kip}.

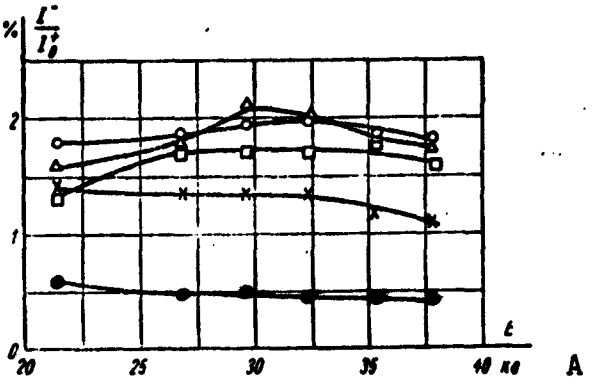

Fig. 11. Coefficient of transformation $H_2^+ \rightarrow H_1^-$ as a function of energy of H_2^+ ions for various jet-thickness values: ●115°C, ×144°C, ○155°C, △161°C, □175°C. A) kv.

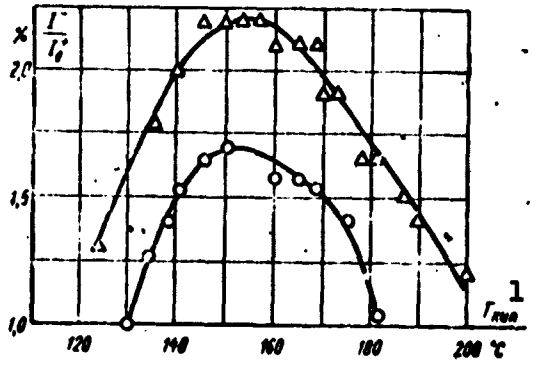

Fig. 12. Dependence of conversion coefficient for various residual-gas pressures in magnetic-analyzer chamber. 1) T_{kip}.

in the magnetic analyzer was 10^{-4} mm Hg. The upper curve was recorded with the bypass tube, and the magnetic-analyzer pressure dropped to $5 \cdot 10^{-5}$ mm Hg. Here, as will be seen from Fig. 12, the yield of negative ions increased by approximately 30%.

The Keller source produced a positive-ion beam with a current of 180-190 μa. Under these conditions, we obtained a stable negative-hydrogen-ion beam with a current of 4 μa.

The curves of Fig. 13 show the coefficient of the transformation $H_2^+ \rightarrow H_1^-$ as a function of the H_2^+-ion energy using the Evans-Stier-Barnett source. The lower curve gives the value of the conversion coefficient defined as the ratio I^-/I_0^+ (I_0^+ is the positive-ion

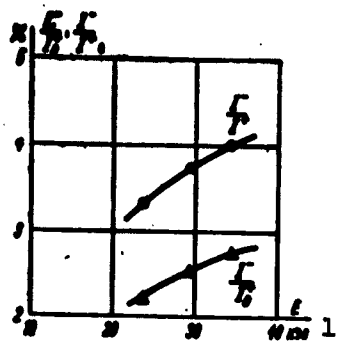

Fig. 13. Coefficient of transformation $H_2^+ \rightarrow H_1^-$ as a function of energy of H_2^+ ions using an Evans-type source. 1) kev.

current to the target). The upper curve gives values of I^-/I^+, where I^+ is the current of H_2^+ ions as measured by the Faraday cylinder 22. This current is determined before the jet is started and after it is shut off. The monitor reading used was the the current I_0^+ incident upon the jet as measured by the Faraday cylinder 9. Since the conversion coefficient I^-/I^+ takes into account the conductivity of the beam of H_2^+ ions between the Faraday cylinders 9 and 22, it is closer to the true value than the conversion coefficient I^+/I_0^+.

The lower curve in Fig. 13 and the corresponding curve in Fig. 11, which was recorded at the same jet thickness, represent slightly different functions of ion energy. This will be understood if we remember that the beam is focused differently in the Keller and Evans-Stier-Barnett sources. Using the latter source, we succeeded in obtaining a positive-ion current as high as 400 μa and, accordingly, a negative-hydrogen-ion current up to 8 μa.

It was shown in Reference [7] that the conversion coefficients in an oil-vapor target are approximately half those observed in a mercury-vapor target, so that we did not study the conversion $H_2^+ \rightarrow H_1^-$ in the oil-vapor target.

The experiments that we carried out confirmed the hypothesis that it is preferable to use the conversion of molecular hydrogen ions to obtain negative ions. From this standpoint, it would be most advantageous to use the conversion $H_3^+ \rightarrow H_1^-$, since in this case the molecular ion dissociates into three monatomic particles. Since cold-cathode magnetic ion sources produce a beam with a very small content of H_3^+ ions, we

used a high-quality Reifenschweiler-type ion source to produce the beam of H_3^+ ions.

We studied the conversion coefficients of H_1^+, H_2^+, and H_3^+ ions as functions of jet thickness and ion energy, using the Reifenschweiler source. Since a hydrogen-ion beam that has not been mass-resolved strikes the vapor-jet target in these experiments, the conversion coefficients for ions of the different masses may be computed if we knew their contents in the beam. The composition of the positive-ion beam was determined before the jet was turned on and then after it was turned off. During the experiment, which took 5-6 hours, the composition of the beam showed little change. We computed the conversion coefficient for a beam composition obtained by averaging the data recorded before and after using the jet.

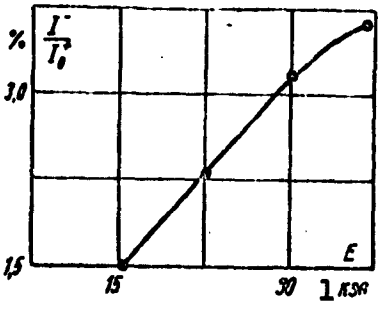

Fig. 14. Coefficient of conversion $H_3^+ \rightarrow H_1^-$ as a function of ion energy with optimum thickness of mercury-vapor target. 1) kev.

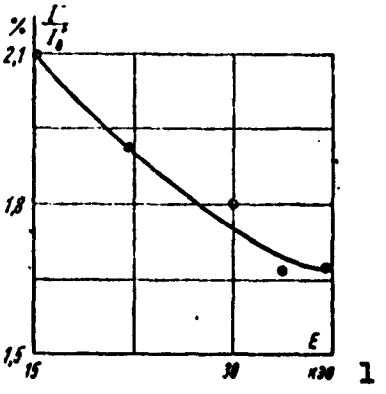

Fig. 15. Coefficient of conversion $H_3^+ \rightarrow H_1^-$ as a function of H_3^+-ion energy during passage of these ions through a stream of type D1-A vaseline-oil vapor. 1) kev.

Despite the relative crudeness of this method, the relationships obtained for the coefficients of the conversions $H_1^+ \rightarrow H_1^-$ and $H_2^+ \rightarrow H_1^-$ as functions of the jet thickness and ion energy agree satisfactorily with the results given in Reference [2].

The coefficient of the transformation $H_1^+ \rightarrow H_3^-$ is shown in Fig. 14

as a function of the ion energy at the optimum mercury-vapor-target thickness. The conversion coefficient increases monotonically up to 37 kev and reaches a value of 4.5% at maximum energy. We were unable to raise the ion energy above 37 kev because of sparkovers in the accelerator tube. Similar experiments were run passing H_3^+ ions through a jet of type D1-1 vaseline-oil vapor. For this case, the curve of the $H_3^+ \rightarrow H_3^-$ conversion coefficient (Fig. 15) is of a completely different nature. We observe an increase in the conversion coefficient with diminishing energy of the H_3^+ ions from 37 to 15 kev. At 15 kev, the conversion coefficient in the oil-vapor jet reaches a value of 2.1%.

We were unable to conduct experiments with beams having energies below 15 kev, since the ion gun did not provide adequate focusing of the beam at these energies.

In the subject experiments on the $H_3^+ \rightarrow H_1^-$ conversion using the Reifenschweiler source operating in the normal mode (20-25% H_3^+), we succeeded in obtaining a maximum H_1^- ion current of 5 μa. In the mode with elevated H_3^+-ion content in the beam, it was possible to produce an H_1^--ion current higher than 12 μa.

The following general conclusions may be drawn from the experiments described here: 1) to produce negative hydrogen ions, it is better to use the transformations $H_3^+ \rightarrow H_1^-$ and $H_2^+ \rightarrow H_1^-$, and not $H_1^+ \rightarrow H_1^-$; 2) the conversion coefficients in a mercury-vapor target are higher than those in an oil-vapor target. In view of the fact that in their normal operating mode, the ion sources produce beams with high contents of either H_1^+ or H_2^+ ions, the most advantageous transformation for producing H_1^- ions is, in the final analysis, the transformation $H_2^+ \rightarrow H_1^-$.

Focusing the Negative-Ion Beam

Visual observation of the luminescence of the quartz screen standing before the Faraday cylinder used to measure the negative-ion current indicates that at the magnetic-analyzer output, the beam of negative hydrogen ions has a diameter of the order of 20 mm. Using the iris diaphragm set up before the Faraday cylinder 22, we made quantitative measurements of the focusing sharpness on the negative-ion beam.

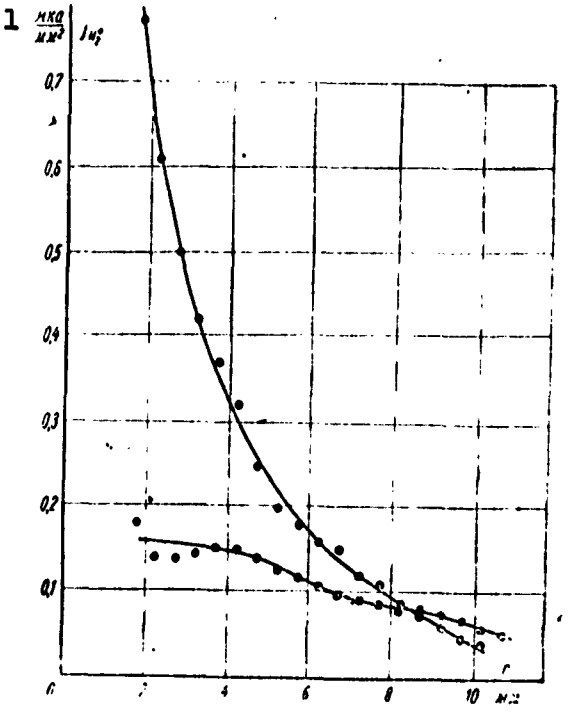

Fig. 16. Relationship $j = f(r)$ for H_2^+ ions with energy of 26 kev obtained from Keller source. 1) $\mu a/mm^2$; 2) mm.

This diaphragm was used to record curves of the H_1^--ion current in the Faraday cylinder as a function of the radius r of the iris diaphragm limiting the beam. Evaluation of these curves by the formula $j = (1/2\pi r)(dI/dr)$ made it possible to ascertain the current-density distribution along the beam radius.

We first conducted experiments to ascertain the influence of the

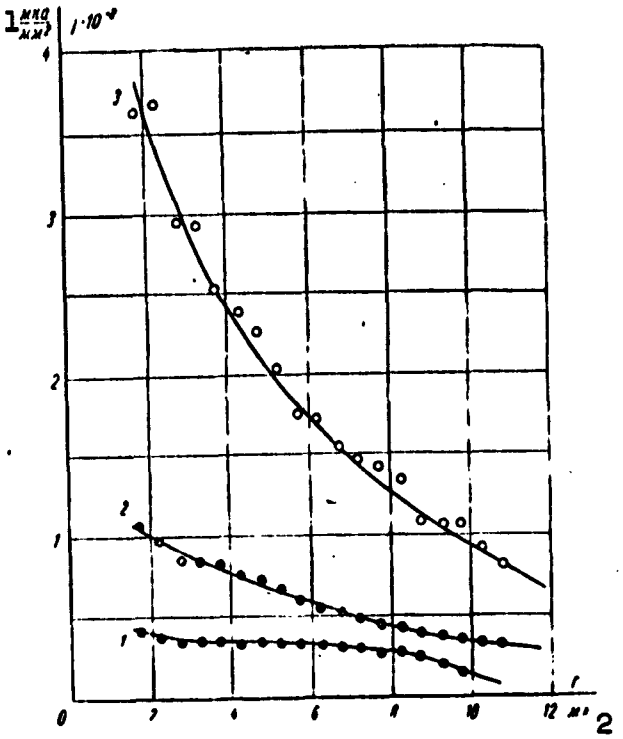

Fig. 17. Relationship j = f(r) for negative hydrogen ions. Curves 1 and 2 represent a beam from the Keller source and curve 3 represents the beam from the Evans source. 1) μa/mm²; 2) mm.

magnetic lens on the focusing of the positive-ion beam. Figure 16 shows curves of the relationship j = f(r) for the H_2^+ ions with energies of 26 kev obtained from the Keller source without passage through the target. In this figure, the lower curve gives the density distribution with the magnetic lens switched off, while the upper curve was recorded with the lens on. It is evident from these curves that the magnetic lens gives adequate focusing for positive-ion beams that have not passed through a target.

Curves of the relationship j = f(r) are shown in Fig. 17 for negative hydrogen ions. The negative ions were obtained by conversion of H_2^+ ions with an energy of 26 kev in a mercury-vapor target of the optimum thickness. Curves 1 and 2 were recorded with the beam from the

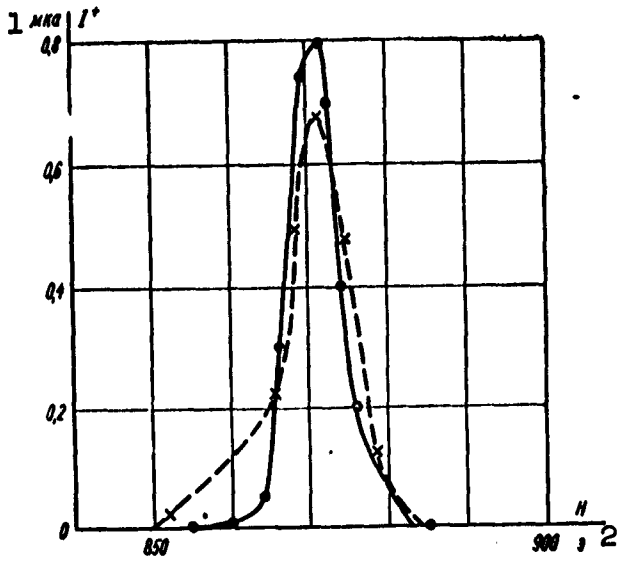

Fig. 18. Current of protons with 19-kev energy as a function of field strength at jet thickness of $1.7 \cdot 10^{15}$ atoms/cm, which is optimal for the conversion $H_1^+ \rightarrow H_1^-$. 1) μa; 2) oersteds.

Keller source, while curve 3 was obtained with an Evans-Stier-Barnett source. The magnetic lens was cut in when curves 2 and 3 were recorded.

As will be seen from Fig. 17, the magnetic lens performs more poorly in focusing a beam of negative ions than when focusing a positive-ion beam. Focusing of the beam produced with the Evans-Stier-Barnett source was much better than that of the Keller-source beam. Even in this case, however, focusing of the negative-ion beam cannot be regarded as satisfactory. The lack of good focusing for a beam of negative ions formed in the target may be accounted for by the wide extent of the zone in which the negative ions are formed (the jet), which serves as the "light source" for the magnetic lens.

Loss of Energy by Ions in Jet

In view of the fact that the negative hydrogen ions obtained with the present injector are formed after passage of positive ions through a mercury-vapor target, it was of interest to ascertain the magnitude

of the ion-energy loss in the mercury-vapor jet, as well as the resulting energy scattering in the beam after passage through the jet.

For this purpose, we set up diaphragms 4 mm in diameter at the entry and exit of the magnetic analyzer and recorded curves of proton current in the Faraday cylinder after the exit diaphragm as a function of magnetic-field strength in the analyzer chamber with and without a jet on the path of the beam. Figure 18 shows curves of proton current (energy 19 kev) as a function of field strength at the optimum jet thickness, which was $1.7 \cdot 10^{15}$ atoms/cm for the $H_1^+ \rightarrow H_1^-$ transformation. As will be seen from this figure, the maxima of the curves coincide within the limits of the measurement error; this testifies to a highly insignificant energy scattering when the protons pass through the mercury-vapor jet. Thus, the energy scattering in the beam due to energy losses in the jet is very small.

SECOND INJECTOR MODEL

Construction of Injector

The results of investigation of the first negative-hydrogen-ion injector model, as cited in the foregoing section, indicated the possibility of employing the positive-to-negative transformation in a mercury-vapor target to produce a beam of H_1^- ions with a current as high as 8 μa. Such a beam intensity would be adequate for further acceleration of the beam in an overcharging electrostatic generator. However, focusing of the negative-ion beam at the injector output was found to be unsatisfactory. Moreover, since the entry into the accelerating tube of the overcharging generator is an aperture lens with a focal length that is a function of the generator voltage, it was necessary to provide a device to regulate the beam focus before entry into the tube in such a way that the beam would be focused on the overcharging device in the generator conductor. It was also necessary to

provide for correcting the beam before entry into the tube so as to make it possible to pass the beam along the axis of the gaseous target in the overcharging unit of the generator.

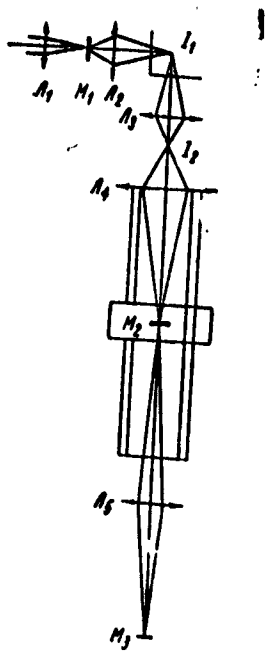

Fig. 19. Ion-optical system of second injector model. Л) L.

A second model of the negative-ion injector was designed, built, and installed to solve these problems. A diagram of the ion-optical system of this model is shown in Fig. 19.

The beam of positive ions emerging from the source is focused by the first electrostatic quadrupole lens L_1 in such a way that the focus of the ion beam will fall onto the mercury-vapor target. The second quadrupole lens L_2 focuses the negative-ion beam onto the entry to the magnetic analyzer after it has experienced a certain amount of scattering in the jet. After the magnetic analyzer the negative-ion beam is focused by a third quadrupole lens L_3. By means of this lens, the ion-beam focus is adjusted in such a way before the entry into the accelerating tube as to make it coincide with the focus of the entry aperture lens of the tube.

A diagram of the second injector model with its new ion optics is shown in Fig. 20. As will be seen from this figure, the second injector model differs from the first by the addition of the two quadrupole electrostatic lenses 5 and 16 before the vapor-jet target and after the magnetic analyzer, and in that the magnetic lens after the vapor-jet target has been replaced by the quadrupole lens 8. Other additions are the electrostatic beam corrector 18 to direct the beam into the overcharging unit and the type MM-1000 pump 19 for evacuation of the first tube in the overcharging generator.

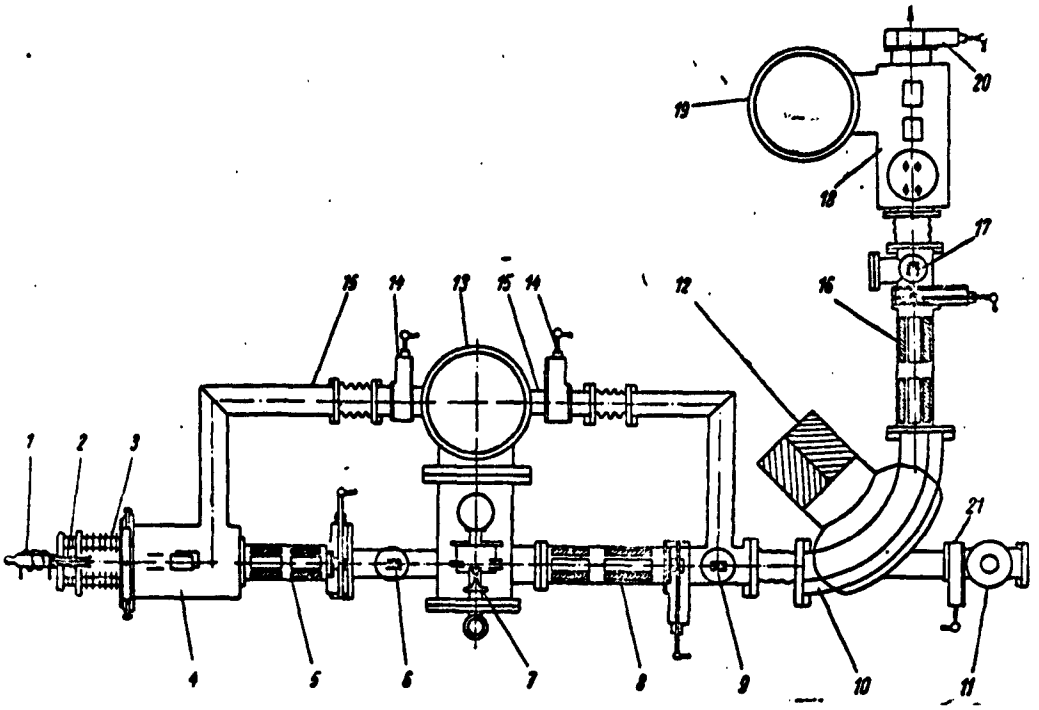

Fig. 20. Diagram of second injector model with new stronger optical system.

Six Faraday cylinders were installed to investigate the passage of the beam through the injector: the first (current I_0) directly after the source ion lens (not shown in Fig. 20), the second (current I_I) in front of the vapor-jet-target chamber, the third (current I_{II}) behind the second lens, the fourth (current I_{III}) at the direct exit from the magnetic analyzer, the fifth (current I_{IV}) behind the third lens, and the sixth (current I_V) after the electrostatic corrector.

Iris diaphragms whose diameters could be varied from 3 to 21 mm were set up before the Faraday cylinders used to measure the currents I_{III}, I_{IV}, and I_V. Using these diaphragms, we recorded curves of the currents I_{III}, I_{IV}, and I_V as functions of the radius r of the iris diaphragm limiting the beam. Evaluation of these curves by the formula $j = (1/2\pi r)(dI/dr)$ made it possible to ascertain the distribution of current density along the beam radius. For visual observation of the beam, retractable quarts screens were set up ahead of the Faraday

cylinders.

Investigation of Characteristics of High-Voltage Ion Source

In the second injector model, the positive-ion beam was created by an ion gun consisting of a high-frequency source, an ion lens, and an accelerating tube with flat electrodes.

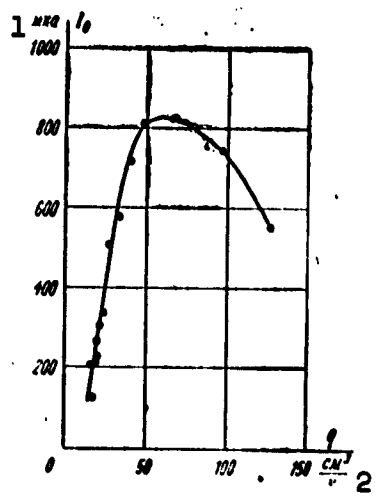

Fig. 21. I_0 as a function of gas flow rate. 1) μa; 2) cm^3/hr.

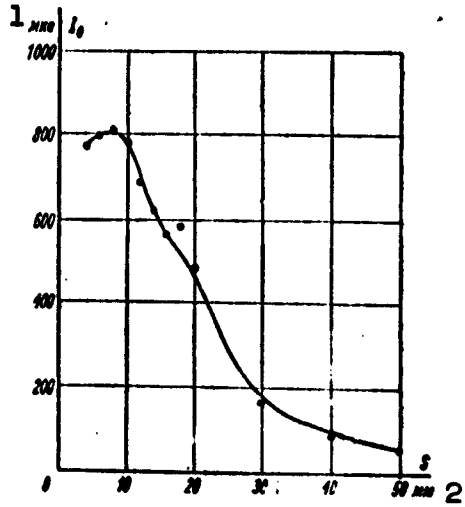

Fig. 22. I_0 as a function of distance between edge of coil and face surface of probe. 1) μa; 2) mm.

We settled on the design proposed by Reifenschweiler [6] for the high-frequency source. In this design, a three-electrode lens similar to that studied by Johannson and Scherzer [8] is used for primary focusing of the beam. The construction of this source and the three-electrode lens are shown in Fig. 6. We inserted a Faraday cylinder with an aperture diameter of 24 mm into the side tube 5 to measure the ion current I_0 drawn from the source. Using the source shown in Fig. 6, we conducted a number of measurements with the objective of ascertaining the current as a function of the various parameters.

First we ascertained the optimum dimensions of the probe and the quartz tube pressed on over it. These dimensions were found to be as follows: diameter and length of channel in probe, 2.3 and 10 mm; out-

side diameter of probe 4.3 mm; distance from end plane of quartz tube to face plane of probe, 2.3 mm. Under these conditions, we studied the current I_0 as a function of gas flow rate into the source, drawing voltage, power dissipated at the plates of the high-frequency oscillator tubes,* and the position of the coil exciting the discharge relative to the probe.

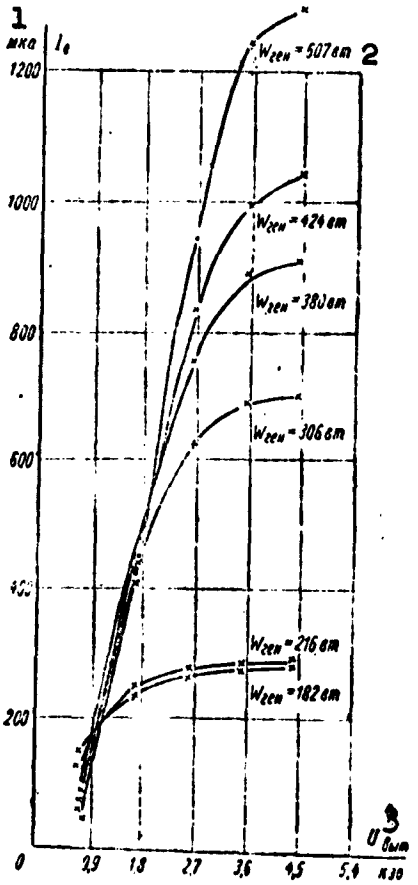

Fig. 23. I_0 as a function of U_{vyt} for various generator powers. 1) μa; 2) W_{gen} = 507 watts; 3) U_{vyt}, kev.

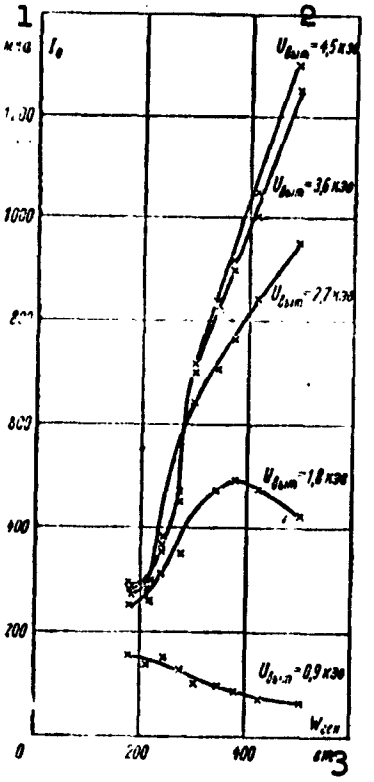

Fig. 24. I_0 as a function of generator power for various values of U_{vyt}. 1) μa; 2) U_{vyt} = 4.5 kev; 3) W_{gen}, watts.

Figure 21 shows a curve of I_0 as a function of gas flow rate. As will be seen from this curve, we observe a sharp increase in I_0 with increasing flow in the flow-rate region from 10 to 45 cm^3/hr, after which the current begins to drop after reaching a maximum in the

region of 60 cm^3/hr. This curve is typical and only shifts along the flow-rate axis for probe channels with different diffusion resistances.

Figure 22 shows a curve of I_0 as a function of the distance from the edge of the coil to the probe face plane. As will be seen from this curve, the current I_0 reaches a maximum at s = 6 to 10 mm.

The family of curves in Fig. 23 characterizes I_0 as a function of the drawing voltage for various generator powers.

A family of curves for I_0 as a function of generator power with various drawing-voltage values is shown in Fig. 24.

To resolve the question as to what part of the current I_0 can be focused, we registered the current I going to the Faraday cylinder in front of the vapor-jet target chamber as a function of drawing voltage for various accelerating-tube voltages. For each value of the drawing voltage, we selected the optimum focusing voltage.

Figure 25 shows curves of $I_I = f(U_{vyt})$ for voltages of 12.2, 18.3, 24.4, and 30.5 kv. The broken line on the same figure shows the curve of $I_0 = f(U_{vyt})$. As will be seen from this figure, all of the current I_0 is focused into the Faraday cylinder before the vapor-jet target chamber at voltages above 24 kv.*

We conducted further investigations in the following mode: q = = 30 to 40 cm^3/hr, s = 6 mm, W_{gen} = 300 watts and U = 2 to 3 kv. Under these conditions, the current I_0 was 350-400 μa. However, as will be seen from the characteristics of the high-voltage source, currents I_0 two to three times larger can be produced in a somewhat forced mode (large values of U_{vyt} and W_{gen}).

Conduction of Positive-Ion Current

We adopted the ratio $\Sigma I_V/I_0$ as the quantity characterizing the beam conduction; here, ΣI_V is the sum of the ions of all components of the beam as measured by the sixth Faraday cylinder, and I_0 is the

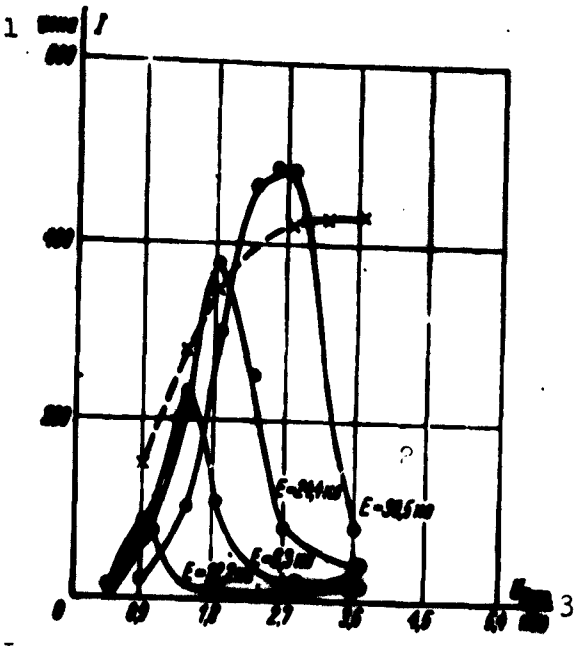

Fig. 25. Relationship $I_I = f(U_{vyt})$ for various optimum focusing voltages. 1) μa; 2) E = 30.5 kv; 3) U_{vyt}, kev.

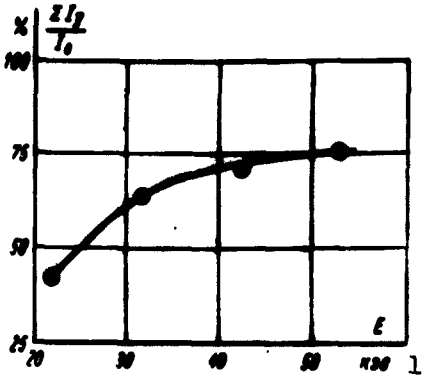

Fig. 26. Beam conduction as a function of ion energy. 1) kev.

current measured by the first Faraday cylinder.

The measurements of beam conductivity through the entire apparatus were preceded by measurements of its conduction through the individual units. It was found that conduction of the beam depends on the ion energies. Beam conduction is shown in Fig. 26 as a function of ion energy. As will be seen from this figure, the beam conduction increases with energy more rapidly in the energy range from 22 to 32 kev (43-63%) and more slowly in the range from 32 to 53 kev (63-75%).

The size of the beam does not change when the channels are taken out of the jet chamber. These modifications, and all subsequent ones, were made at a current I_0 = 350 to 400 μa.

We adjusted the potentials on the electrodes of the three quadrupole lenses (these potentials were in the range from 0.25 to 2 kev) as well as the potential difference across the source ion lens (this potential difference varied in the range from 1.8 to 2.6 kev) in order to reach the highest conduction. At an energy of 22 kev, the highest conduction was achieved by shorting 6 to 8 ring electrodes of the

accelerating tube to the ground.

Focusing of Positive Ions

Before proceeding to a study of negative-ion focusing at the output of the negative-ion source, we made certain investigations of positive-ion focusing.

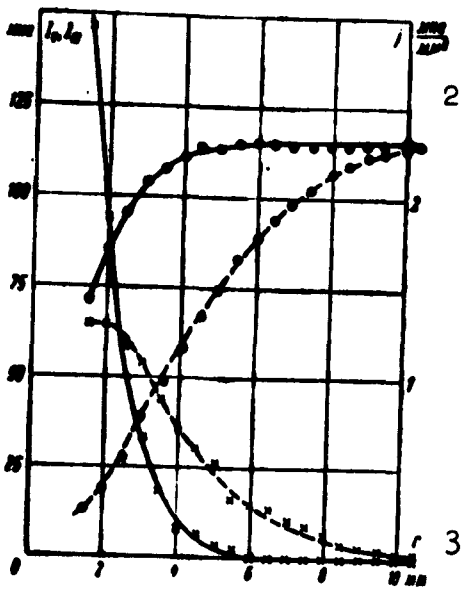

Fig. 27. Relationships I = = f(r) and j = φ(r) for beam of protons with 32.4 kev energy:...) I; xxx) j; ———) near position; – – –) far position. 1) μa; 2) μa/mm^2; 3) mm.

A detailed investigation of positive-ion focusing was carried out in two positions at distances of 45 and 100 cm from the central plane of the third lens, using the fifth and sixth Faraday cylinders with the adjustable diaphragm.

Figure 27 shows curves of I = f(r) and j = φ(r) for a proton beam with an energy of 32.4 kev. Figure 28 presents curves of j/j_{maks} for this same case. As will be seen from these curves, focusing of the beam at a shorter distance from the third lens is better than at the longer distance; this is confirmed by both the shape of the curves in Figs. 27 and 28 and by the following figures: the beam diameter in the near position was 12 mm, while in the far position it was over 21 mm, and the current density is already 22.5% of the maximum with the 12-mm beam diameter.

A beam with a 70-μa current enters the fifth Faraday cylinder through a 3-mm diaphragm, while the beam entering the sixth carries only 13 μa. Better focusing of the beam in the near position is observed in all other cases that we investigated, i.e., for H_2^+ and H_3^+

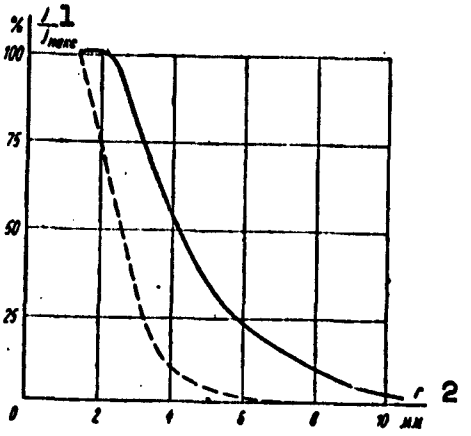

Fig. 28. Relationship j/j_{maks} = = f(r) for proton beam with e energy of 32.4 kev. – – –) near position; ———) far position. 1) j/j_{maks}; 2) r, mm.

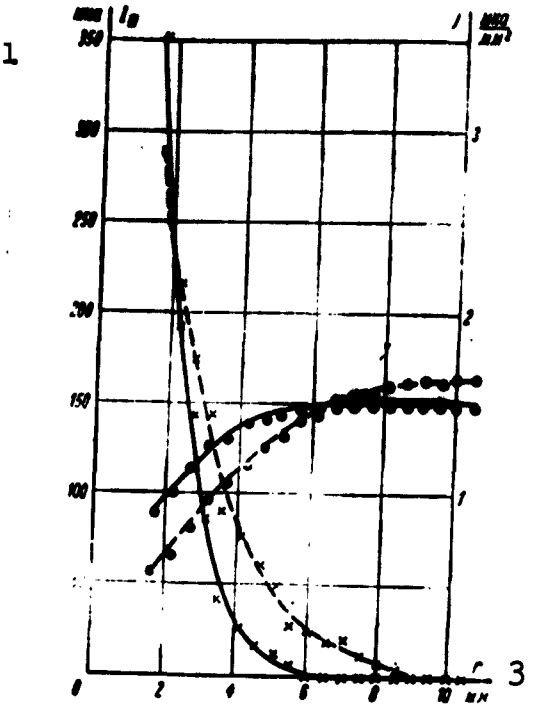

Fig. 29. Curves of I(r) and j for beam of protons with energy of 43 kev; ...) I; xxx) j; ———) focusing onto 3-mm aperture; – – –) focusing on 21-mm aperture. 1) μa; 2) $\mu a/mm^2$; 3) r, mm.

ions and for other energies.

We achieved optimum focusing in the plane of the diaphragm in front of the Faraday cylinder by two methods: by regulating the potentials on the lenses, we achieved the ion-current maximum in the Faraday cylinder at the smallest diaphragm diameter (3 mm) in the first case and at the largest diaphragm diameter (21 mm) in the second case.

Figure 29 shows curves of I = f(r) and j = φ(r) for a beam of protons with an energy of 43 kev; it will be evident from these that focusing the beam onto a narrow diaphragm gives somewhat better results than focusing on a wide diaphragm, although the maximum current value is somewhat larger in the second case.

The investigations that we carried out indicated that the current-density distribution in the beam for the H_1^+, H_2^+, and H_3^+ ions in the

energy range from 22 to 43 kev does not depend – within the limits of measurement error – either on the type of ion or on its energy. In all of these cases, no less than 90% of the ions in the beam passed through a diaphragm 8 mm in diameter.

Conversion Coefficient

Before proceeding to our study of negative-ion focusing, we investigated the real conversion coefficient of positive hydrogen ions into negative as a function of the thickness of the vapor-jet target (boiler temperature) and of ion energy.

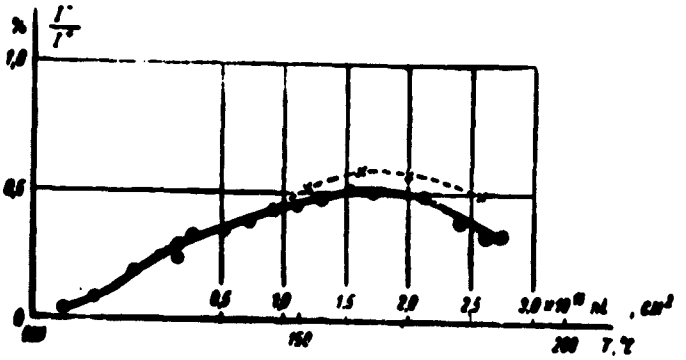

Fig. 30. Coefficient of conversion $H_1^+ \rightarrow H_1^-$ as a function of thickness of vapor-jet target for protons with 30-kev energy.

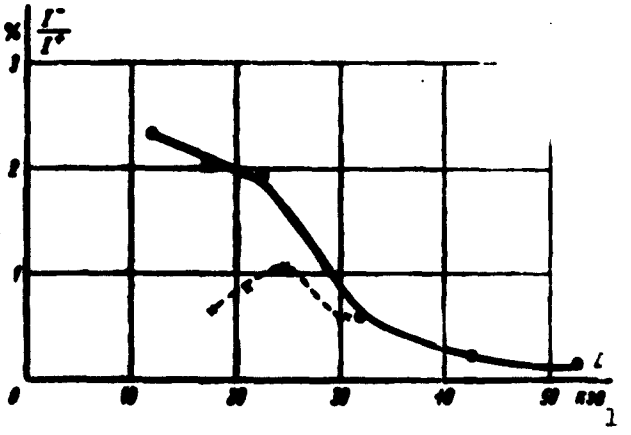

Fig. 31. Comparison of curves of coefficient of conversion $H_1^+ \rightarrow H_1^-$ as a function of proton energy. 1) kev.

Figure 30 shows the coefficient of the conversion $H_1^+ \rightarrow H_1^-$ as a

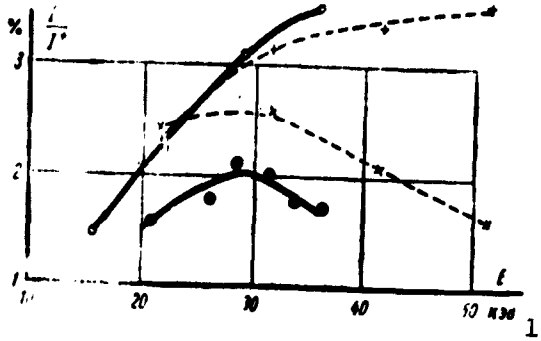

Fig. 32. Conversion coefficient as a function of positive hydrogen-ion energy. ———) Data from present study; – – –) data of L.I.Krupnik (dissertation); 0,+) conversion $H_3^+ \rightarrow H_1^-$; 0,x) conversion $H_2^+ \rightarrow H_1^-$.

function of the thickness of the vapor-jet target for protons with an energy of 30 kev. The solid curve was obtained on the second model of the negative-ion source, and the broken-line curve on the first model.

As will be seen from Fig. 30, neither the position of the maximum ($t = 170^\circ C$, $nL = 2 \cdot 10^{15}$ atoms/cm^3) nor the value of the conversion coefficient has undergone any essential change in the present measurements as compared with the previous ones.

Figure 31 presents a comparison of the curves of the conversion coefficient for $H_1^+ \rightarrow H_1^-$ as a function of proton energy: that obtained in Reference [2] (broken curve) and in the present study (solid curve). As will be seen from the comparison, the shape of the conversion-coefficient curve as a function of energy and its magnitude in the region of energies smaller than 25 kev differs between them. This fact is not surprising, since the value of the real conversion coefficient depends heavily on the ion-optical properties of the system [6]. In view of the fact that negative-ion focusing was improved in the present model (see below) over the focusing in the first injector model, it may be assumed that the values obtained in the present study for

the real conversion coefficient are closer to the values of the true conversion coefficient than the values that we obtained earlier.

As will be seen from Fig. 32, we do not observe such large differences for the conversion coefficients of $H_2^+ \rightarrow H_1^-$ and $H_3^+ \rightarrow H_1^-$ obtained in the present study and in our earlier study [1] as for the conversion $H_1^+ \rightarrow H_1^-$.

Negative-Ion Focusing

An investigation of negative-ion focusing was carried out on the same premises as the investigation of positive-ion focusing.

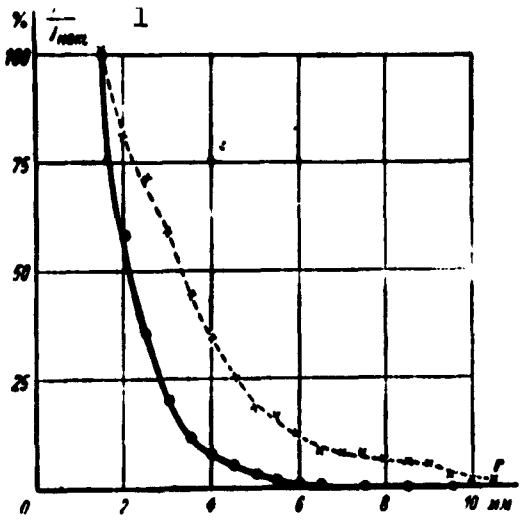

Fig. 33. Dependence of j/j_{maks} = = f(r) for H_1^- ions with energy of 22.4 kev. 1) j/j_{maks}.

As in the case of positive ions, focusing of the negative-ion beam at a shorter distance from the third lens was found to be preferable to a longer distance, as is illustrated by the curves (Fig. 33) of j/j_{maks} = = f(r) for H_1^- ions with an energy of 22.4 kev. A similar situation also obtains for H_1^- ions with other energies, a fact characterized by the data of Table 1, which lists values of j/j_{maks} and I/I_{maks} for a diaphragm 8 mm in diameter.

It will be seen from Table 1 that with a given positive-ion energy, H_1^- ions from the conversion $H_1^+ \rightarrow H_1^-$ focus better than those from the conversion $H_3^+ \rightarrow H_1^-$. This difference is more noticeable in the far position than in the near position.

Focusing of a beam of H_1^- ions of approximately equal energies but obtained by conversion of different positive ions are the same within the limits of measurement error, as will be seen from Figs. 34 and 35.

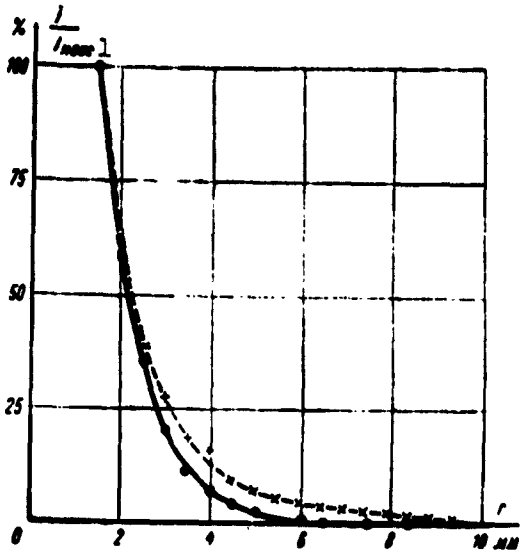

Fig. 34. Focusing of ion beam in near position; ———) conversion $H_1^+ \rightarrow H_1^-$, $E_{H_1^+}$ = 22.4 kev; – – –) conversion $H_3^+ \rightarrow H_1^-$, $E_{H_3^+}$ = 53.3 kev. 1) j/j_{maks}.

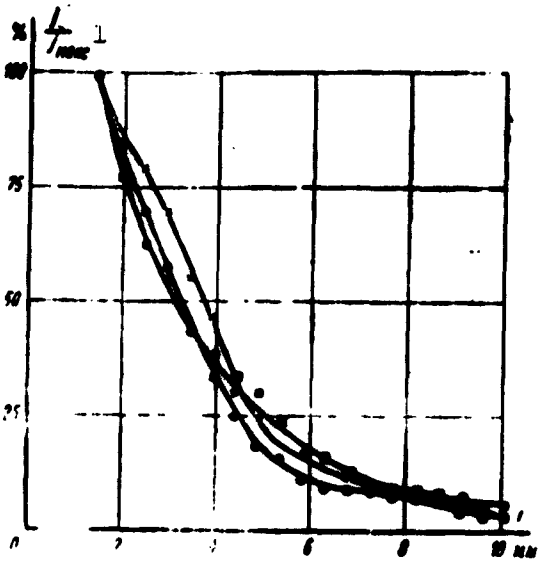

Fig. 35. Focusing of ion beam in far position. ...) conversion $H_1^+ \rightarrow H_1^-$, $E_{H_1^+}$ = 22.4 kev; ●●●) conversion $H_1^+ \rightarrow H_1^-$, $E_{H_2^+}$ = 43 kev; xxx) conversion $H_3^+ \rightarrow H_1^-$, $E_{H_3^+}$ = 53.3 kev. 1) j/j_{maks}.

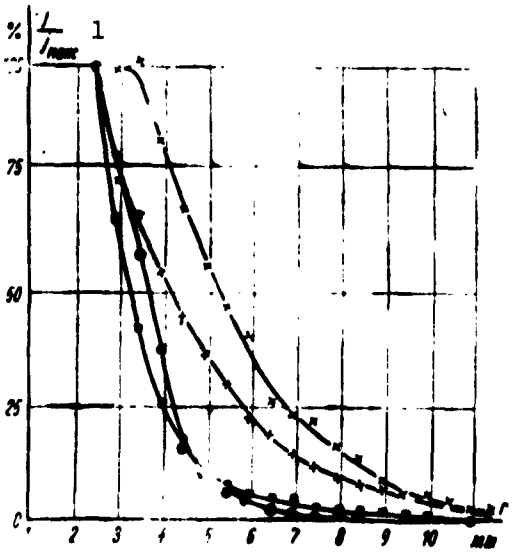

Fig. 36. Curves of $j/j_{maks} = f(r)$ in different focusing positions. ●●● H_1^- and ... H_1^+) in near position; +++ H_1^- and xxx H_1^+) in far position. 1) j/j_{maks}.

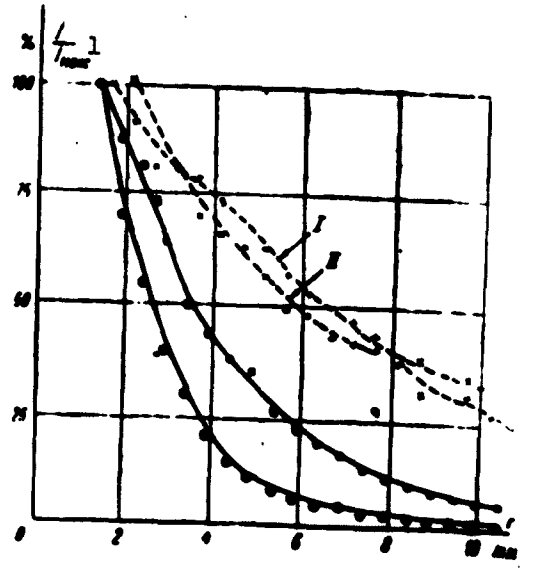

Fig. 37. Comparison of negative-ion beam focusing by first (I) and second (II) injector models. – – –) data of first model; ———) data for second model; ...) near position; ●●●) far position. 1) j/j_{maks}.

TABLE 1

Ratios j/j_{maks} and I/I_{maks} for Diaphragm 8 mm in Diameter

1 Энергия положительных ионов*	2 Преобразование	3 $j/j_{макс}$		4 $I/I_{макс}$	
		5 в ближнем положении	6 в дальнем положении	5 в ближнем положении	6 в дальнем положении
22,4	$H_1^+ \rightarrow H_1^-$	0,075	0,35	0,92	0,56
32,4	$H_1^+ \rightarrow H_1^-$	0,12	0,37	0,80	0,53
32,4	$H_1^+ \rightarrow H_1^-$	0,21	0,68	0,73	0,29
43,0	$H_1^+ \rightarrow H_1^-$	0,21	0,43	0,71	0,34
53,0	$H_1^+ \rightarrow H_1^-$	0,14	0,39	0,75	0,34

1) Positive-ion energy; 2) conversion; 3) j/j_{maks}; 4) I/I_{maks}; 5) in near position; 6) in far position.

The curves of $j/j_{maks} = f(r)$ given in Fig. 36 enable us to compare focusing of the positive and negative ions in the injector model that we studied. As will be seen from this figure, focusing of positive and negative ions is practically the same in the near position, while in the far position focusing of negative ions is better than that of positive ions.

Figure 37 shows curves of $j/j_{maks} = f(r)$, which permit comparison of the focusing of negative-ion beams of approximately the same energy in the first and second injector models. In the first model, the H_1^- ions were obtained from the conversion $H_2^+ \rightarrow H_1^-$. Beams of H_2^+ ions with energies of 26 and 28.4 kev were obtained from cold-cathode Keller [4] (curve I) and Barnett-Stier-Evans [5] (curve II) magnetic ion sources. In the second model, the H_1^- ions were obtained by the conversion $H_3^+ \rightarrow H_1^-$ applied to H_3^+ ions with energies of 43 kev.

As will be seen from Fig. 37, focusing of the beam of H_1^- ions is much better in the second injector model than in the first.

Table 2 presents values of the ratios $I_{d=3}/I_{maks}$ and $I_{d=8}/I_{maks}$; these indicate what part of the maximum current entering the Faraday cylinder through a 21-mm-aperture diaphragm can pass through diaphragms

TABLE 2

Ratios $I_{d=3}/I_{maks}$ and $I_{d=8}/I_{maks}$ for Various Source Models

1 Источник	$I_{d=3}/I_{макс}$ 2	$I_{d=8}/I_{макс}$
3 Модель I, источник Келлера	0,03	0,24
4 Модель I, источник Барнетта и др.	0,01	0,22
5 Модель II, дальнее положение	0,13	0,52
6 Модель II, ближнее положение	0,18	0,58

1) Source; 2) maks; 3) model I, Keller source; 4) model I, Barnett et al source; 5) model II, far position; 6) model II, near position.

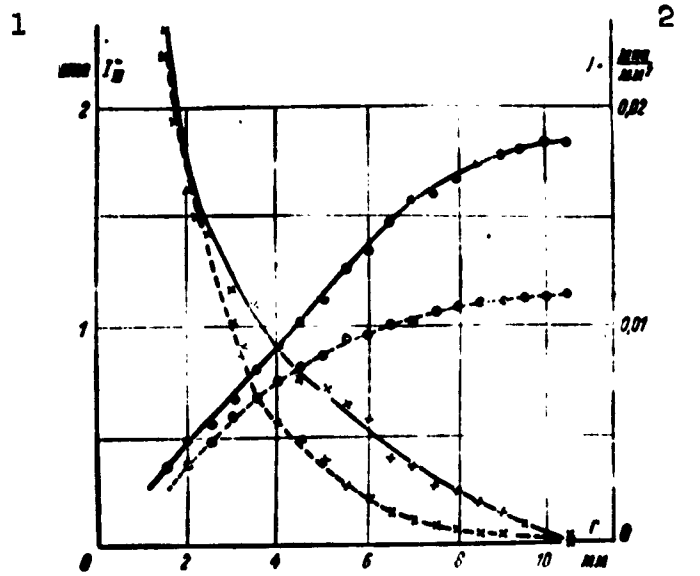

Fig. 38. I_{III} and $\underline{f}$ as function of focusing position in transformation $H_1^+ \rightarrow H_1^-$: ●●●) I; xxx) j; ———) $E_{H_1^+}$ = 22.4 kev; – – –) $E_{H_2^+}$ = 32.4 kev. 1) μa; 2) μa/mm^2.

3 and 8 mm in diameter.

The absolute values of the current and current density of the negative-ion beam as contained in the present experiments are characterized by the curves of I = f(r) and j = φ(r) shown in Figs. 38 and 39. As will be seen from these figures, the maximum current of H_1^- ions obtained from the transformation $H_1^+ \rightarrow H_1^-$ is 1.6 μa while the

maximum current from the transformation $H_2^+ \rightarrow H_1^-$ reaches 7.4 μa. Thus, the negative-ion currents obtained in the present study are of the same order of magnitude as the currents obtained in the first injector model. However, it is necessary to remember that the experiments described here were conducted at a current I_0 = 350-400 μa. As follows from the data presented in the section devoted to the high-frequency ion source, currents I_0 exceeding those used in the measurements described above can be obtained in a slightly forced operating mode of the source.

The following conclusions may be drawn on the basis of comparison of the results obtained in investigation of the characteristics of the first and second injector models:

1. Focusing of the negative-ion beam is much better in the second model than in the first.

2. The magnitude of the current in the negative-ion beam is the same for both models (1.5 to 2 μa for the transformation $H_1^+ \rightarrow H_1^-$ and 7-8 μa for the transformation $H_3^+ \rightarrow H_1^-$).

3. In a slightly forced regime of the high-frequency source, it is possible to obtain 3-5 μa from the transformation $H^+ \rightarrow H_1^-$ and 15-20 μa from the transformation $H^+ \rightarrow H_1^-$.

THIRD INJECTOR MODEL

The negative-hydrogen-ion source built by Weinman and Cameron [3] at the University of Wisconsin has excellent characteristics. It produces a H_1^--ion beam with a current of 25-30 μa in a diameter of 3-6 mm. The major deficiency of this source consists in the fact that a continuously flowing gaseous target is employed to convert the positive hydrogen ions into negative ions. As a result, it is necessary to evacuate the source with a high-power pump at a rate as high as 7000 liters/sec, and even under these conditions the pressure in the

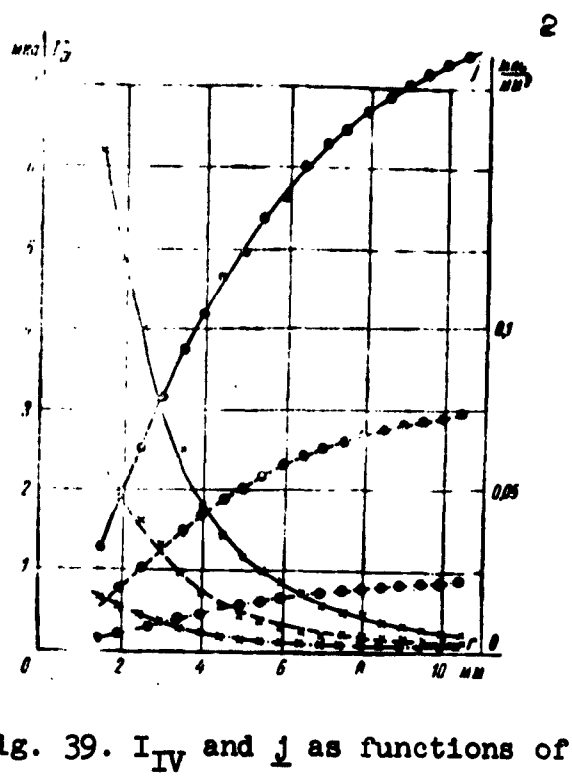

Fig. 39. I_{IV} and j as functions of focusing position in transformation $H_3^+ \rightarrow H_1^-$; ●●●) I; xxx) j; ———) $E_{H_3^+}$ = 53.3 kev; – – –) $E_{H_3^+}$ = 43 kev; –·–·–) $E_{H_3^+}$ = 32.4 kev. 1) μa; 2) μa/mm^2.

source chamber reaches 10^{-4} mm Hg. Careful examination of the Weinman-Cameron source showed that it can be reworked in such a way as to permit replacing the running gaseous target with a vapor-jet target. The structure of a third injector model based on this idea is shown in Fig. 40. The positive-ion source used is a hot-cathode Kistermaker-Dekker source 1 [9], a detailed description of which is given in a paper by these authors. The entire positive-ion source is mounted on the flange 2 and insulated from the injector housing by the plexiglas ring 3. In turn, the injector housing is insulated from the MM-1000 pump by the porcelain insulator 4. The drawing electrode 5, which shapes the positive-ion beam, functions simultaneously as the entry channel 6 of the vapor-jet target. The negative hydrogen

ions coming out through the exit channel 7 of the vapor-jet target are focused by a three-electrode lens whose middle and last electrodes are insulated from the housing by the plexiglas insulator 8 and the porcelain insulator 9.

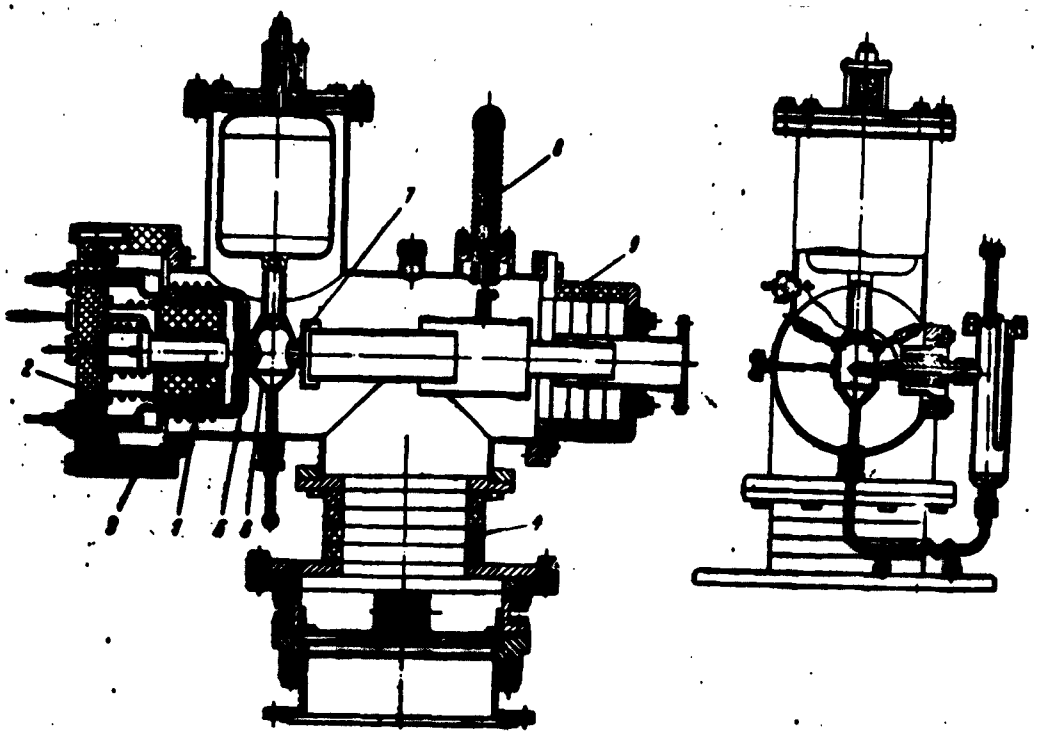

Fig. 40. Structure of third injector model.

The device, which is shown in Fig. 40, is connected via a bellows to the magnetic analyzer and an output unit of the same type as was used in the second model.

Investigation of the third model of the negative-ion source has not yet been completed, but certain preliminary results, which we shall presently describe, will set forth the potential of this model.

Before attempting to investigate the conversion of positive into negative ions, we conducted experiments with the objective of finding the optimum operating conditions for the positive ion source and evaluating the influence of the size of the positive-ion current passing through the channel in the drawing electrode.

The positive-ion current was measured as follows. The output of the middle electrode was capped and this electrode was used as a Faraday cylinder to measure the positive-ion current. Secondary electron emission from the Faraday cylinder was suppressed by applying a 400-volt negative potential to the first electrode of the lens. It was established by special experiments that the positive-ion beam did not strike the walls of this electrode.

We studied the positive-ion current as a function of hydrogen flow rate into the source, magnetic field strength, discharge voltage and current, the distance of the cathode from the emission aperture, the distance of the drawing electrode from the emission aperture, and the drawing potential difference.

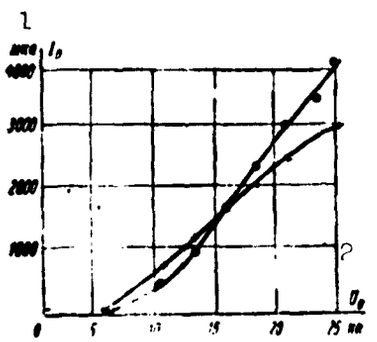

Fig. 41. Positive-ion current as a function of drawing potential difference for two discharge-current values. xxx) I_{raz} = 1 amp; ...) I_{raz} = 1.5 amp. 1) μa; 2) U_v, kv.

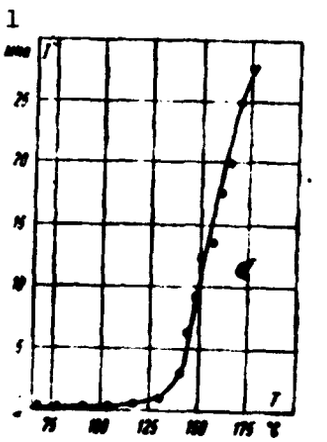

Fig. 42. Current of H_1^- ions as a function of boiler temperature. 1) μa.

Figure 41 presents curves showing the positive-ion current as a function of drawing potential difference for two values of the discharge current. As will be seen from these curves, a beam of positive ions with a current value as high as 4 ma can be passed through the vapor-jet target. A magnetic analysis of the beam carried out using the unit's magnetic analyzer indicated that the positive-ion beam contained 45%

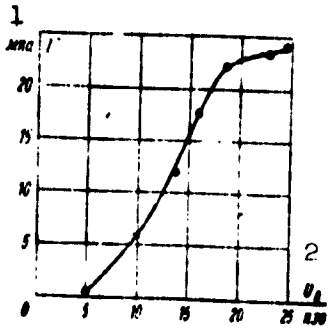

Fig. 43. Negative-hydrogen-ion current as a function of drawing potential at T = = 180°C. 1) μa; 2) U_v, kev.

of H_2^+ ions.

In the very first experiments on conversion of positive into negative ions in the vapor-jet target, we ran up against ... beginning with ... [Translator's note: One or two sticks of type dropped from Russian original, page 181]. These difficulties consisted in the fact that, beginning with a certain jet thickness, discharges arose in the space between the emission aperture of the ion source and the drawing electrode and in the acceleration space of the negative ions, i.e., between the chamber of the vapor-jet target and the first electrode of the focusing lens. It was established that these discharges take place as a result of penetration of secondary electrons into these spaces after they arise on interaction of the beam ions with atoms of the jet. To eliminate the discharges, we set up an electric field to block exit of secondary electrons from the vapor-jet target chamber. This succeeded in eliminating the discharges in the acceleration space of the positive and negative ions to some extent, and enabled us to begin our study of conversion of positive hydrogens into negative ions in the vapor-jet target. The transformation $H_2^+ \rightarrow H_1^-$ was the subject of investigation, since it produced the largest number of H_1^- ions.

Figure 42 shows a curve of the H_1^--ion current as a function of boiler temperature. The current was measured with the Faraday cylinder 17 (see Fig. 20), which was set up behind the quadrupole lens. The measurements were made at a constant drawing voltage of 21 kev.

The negative-hydrogen-ion current is shown by the curve in Fig. 43 as a function of drawing potential for a constant boiler tempera-

ture of 180°C.

As will be seen from the curves of Figs. 42 and 43, H_1^--ion currents in excess of 20 μa were obtained in the very first experiments with the third model, i.e., currents significantly larger than those obtained with the first and second models.

Additional and more detailed studies of the properties of the third model are being continued.

REFERENCES

1. Fogel', Ya.M., Lisochkin, G.A. and Stepanova, G.I., ZhTF [J. Tech. Phys.], XXV, 1944 (1955).

2. Fogel', Ya.M. Krupnik. L.I. and Ankudinov, V.A., ZhTF, XXVI, 1208 (1956).

3. Weinman, J.A. and Cameron, J.K. Rev. Sci. Instr., 27, 288 (1956).

4. Keller, R. Helv. Phys. Acta. XXII, 78 (1949).

5. Barnett, C.F., Stier, P.M. and Evans, G.E. Rev. Sci. Instr., 24, 394 (1953).

6. Reifenschweiler, O. Ann. der Phys. [Annals of Physics], 14, 33 (1954).

7. Fogel', Ya.M., Krupnik, L.I. and Slabospitskiy, R.P., ZhTF, XXVII, 981 (1957).

8. Johannson W. and Scherzer, O. Ztschr. f. Phys. [J. Phys.], 80, 193 (1935).

9. Kistermaker, J. and Dekker, H.L. Physica, XVI, 198 (1950).

Manuscript Page No.

[Footnotes]

113 *To excite the high-frequency discharge, we employed a generator assembled in a push-pull circuit and based on

Manuscript Page No.

[Footnotes]

two GI-6B cermet triodes.

114 *The fact that the maxima of the curves of $I_I = f(U_{vyt})$ lie above the curve of $I_0 = F(U_{vyt})$ at 24.4 kv and 30.5 kv indicates that the beam diameter at entry into the Faraday cylinder measuring the current I_0 is larger than 24 mm.

Manuscript Page No.

[List of Transliterated Symbols]

97 ПОС = POS [= posadka = fit?]
99 пад = pad = padayushchiy = incident
100 прош = prosh = proshedshiy = passed
113 выт = vyt = vytagivayushchiy = drawing
113 ген = gen = generator = generator
116 макс = maks = maksimal'nyy = maximum
127 раз = raz = razryadnyy = discharge
127 в = v vytyagivayushchiy = drawing

DISTRIBUTION LIST

DEPARTMENT OF DEFENSE	Nr. Copies
HEADQUARTERS USAF	
AFCIN-3D2	1
ARL (ARB)	1
OTHER AGENCIES	
CIA	1
NSA	6
AID	2
OTS	2
AEC	2
PWS	1
NASA	1
RAND	1
SPECTRUM	1

MAJOR AIR COMMANDS	Nr. Copies
AFSC	
SCFTR	1
AEDC (AEY)	1
ASTIA	25
TD-Bla	5
TD-Blb	3
SSD (SSF)	2
APGC (PGF)	1
ESD (ESY)	1
RADC (RAY)	1
BSD (BSF)	1
AFSWC (SWF)	1
AFMTC (MTW)	1
TD-B2	1